



National Library
of Canada

Canadian Theses Service

Ottawa, Canada
K1A 0N4

Bibliothèque nationale
du Canada

Services des thèses canadiennes

CANADIAN THESES

NOTICE

The quality of this microfiche is heavily dependent upon the quality of the original thesis submitted for microfilming. Every effort has been made to ensure the highest quality of reproduction possible.

If pages are missing, contact the university which granted the degree.

Some pages may have indistinct print especially if the original pages were typed with a poor typewriter ribbon or if the university sent us an inferior photocopy.

Previously copyrighted materials (journal articles, published tests, etc.) are not filmed.

Reproduction in full or in part of this film is governed by the Canadian Copyright Act, R.S.C. 1970, c. C-30.

**THIS DISSERTATION
HAS BEEN MICROFILMED
EXACTLY AS RECEIVED**

THÈSES CANADIENNES

AVIS

La qualité de cette microfiche dépend grandement de la qualité de la thèse soumise au microfilmage. Nous avons tout fait pour assurer une qualité supérieure de reproduction.

S'il manque des pages, veuillez communiquer avec l'université qui a conféré le grade.

La qualité d'impression de certaines pages peut laisser à désirer, surtout si les pages originales ont été dactylographiées à l'aide d'un ruban usé ou si l'université nous a fait parvenir une photocopie de qualité inférieure.

Les documents qui font déjà l'objet d'un droit d'auteur (articles de revue, examens publiés, etc.) ne sont pas microfilmés.

La reproduction, même partielle, de ce microfilm est soumise à la Loi canadienne sur le droit d'auteur, SRC 1970, c. C-30.

**LA THÈSE A ÉTÉ
MICROFILMÉE TELLE QUE
NOUS L'AVONS REÇUE**

**A Critical Review of the
Process of Fretting Fatigue**

Yousri El Borai

A Major Technical Report

in

The Department

of

Mechanical Engineering

**Presented in Partial Fulfillment of the Requirements
for the Degree of Master of Engineering at
Concordia University
Montréal, Québec, Canada**

September 1986

©Yousri El Borai, 1986

Permission has been granted to the National Library of Canada to microfilm this thesis and to lend or sell copies of the film.

The author (copyright owner) has reserved other publication rights, and neither the thesis nor extensive extracts from it may be printed or otherwise reproduced without his/her written permission.

L'autorisation a été accordée à la Bibliothèque nationale du Canada de microfilmer cette thèse et de prêter ou de vendre des exemplaires du film.

L'auteur (titulaire du droit d'auteur) se réserve les autres droits de publication; ni la thèse ni de longs extraits de celle-ci ne doivent être imprimés ou autrement reproduits sans son autorisation écrite.

ISBN 0-315-35527-1

ABSTRACT

A Critical Review Of Fretting Fatigue Process

Yousri El Borai

In this report an attempt has been made to present a broad spectrum, the complex interactions, nature and influence of major factors that basically affect the material fretting fatigue under the repeated displacement between surfaces in contact. It was necessary to define and differentiate between fretting fatigue and fretting corrosion(wear), their theories and their fretting mechanisms. In light of the foregoing it was desirable to take a close analytical look at the distribution of stress in the vicinity of the contact area which leads to fatigue cracking and consequently a reduction in fatigue strength. Some general guidelines for design are presented, but the importance of dealing with each fretting fatigue situation is emphasized through the current literature for which the application and concepts are elucidated towards the specific design conditions.

ACKNOWLEDGEMENT

The author wishes to express his gratitude and indebtedness to his faculty advisor, Dr. M. O. M. Osman for the valuable discussions and guidance received during the preparation of this study.

Grateful appreciation is also accorded to Dr. M. H. Attia for guidance and encouragement throughout all phases of this report.

Finally, the author wishes to acknowledge the year of understanding and unselfish encouragement afforded him by his wife Laila throughout this undertaking.

Table of Contents

	PAGE
Title Page	1
Signature Page	11
Abstract	111
Acknowledgement	1v
Table of Contents	v
List of Figures and Tables	x
List of principal symbols used	xvii
CHAPTER 1	
<u>INTRODUCTION</u>	
1. 1 Background	1
1. 2 Scope of the investigation	1
1. 3 Parameters influencing the formulation of fretting fatigue/wear process	2
CHAPTER 2	
<u>BASIC CONCEPTS IN FRETTING FATIGUE/WEAR PROCESS</u>	
2. 1 Definition of fretting, fretting fatigue and fretting wear	8
2. 2 Fretting fatigue	8
2. 2. 1 Mechanisms of fretting fatigue	9
2. 2. 2 Microscopic observation	9

	PAGE
2.2.3 Theories of fretting fatigue mechanisms	11
2.2.4 Effect of the main variables on fretting fatigue, amplitude of motion, number of cycles, frequency, environment and temperature	18
2.3 Fretting Wear	24
2.3.1 Mechanisms of fretting wear	25
2.3.2 Theories of fretting wear mechanisms	25
2.3.3 Effect of the main variables on fretting wear amplitude of motion, number of cycles, frequency, environment and temperature	30

CHAPTER 3

THE ROLE OF ELASTIC STRESS ANALYSIS IN THE INTERPRETATION OF FRETTING FATIGUE FAILURES.

INTRODUCTION	37
Theoretical modeling	38
3.1.1 Contact of spheres model	38
3.1.1.1 Sphere to sphere contact	38
3.1.1.2 Sphere on flat	43
3.1.2 Cylindrical on flat surface model	46
3.1.3 Cylinder on cylinder contact model	48
3.1.4 Flat circular contact model	52

	PAGE
3. 1. 5 Flat on flat model	59
3. 2 Justification of theoretical model	70
3. 2. 1 Sphere on sphere model experiment	70
3. 2. 2 Sphere on flat model experiment	73
3. 2. 3 Circular flat contact model experiment	74
 CHAPTER 4	
<u>FRACTURE MECHANICS FOR PREDICTING FATIGUE</u>	
4. 1 Introduction	77
4. 2 The S-log N curve	81
4. 3 The stress intensity factor	83
4. 4 The fracture mechanics model	85
4. 4. 1 Stress intensity factor due to line loads	85
4. 4. 2 Stress intensity factor due to distributed loads	88
4. 4. 3 mean and alternating stress intensity factor under fretting conditions	89
4. 5 Calculation of crack rates	90
4. 6 Fracture mechanics predictions	91
4. 6. 1 Effect of initial flaw size and length correction on predicted life	91
4. 6. 2 Predicted and measured crack propagation curves	96

	PAGE
4.6.3 Effect of assumed distribution of pad load on fatigue life	99
4.6.4 Prediction for the range of pad spans	100
4.6.5 prediction at two pad loads	102
 <u>CHAPTER 5</u>	
<u>PRACTICAL APPLICATION</u>	
5.0 INTRODUCTION	104
5.1 The identification of fretting fatigue failure	104
5.2 Examples of fretting fatigue failure in practice	105
5.3 Design approach to prevent fretting fatigue	108
 <u>CHAPTER 6</u>	
<u>CONCLUSION AND RECOMMENDATION FOR FURTHER WORK</u>	
6.1 Conclusions related to the main parameters influencing the formulation of fretting fatigue/wear process	112
6.2 Conclusions to the mechanism of fretting fatigue/wear	112
6.3 Conclusions to the elastic stress analysis in the interpretation of fretting fatigue failures	114
6.4 Conclusions related to application of fracture mechanics for prediction fretting fatigue	115

	PAGE
6.5 Conclusions related to practical applications interpretation of fretting fatigue.	115
6.6 Further work	116
BIBLIOGRAPHY	117

List of Figures and Tables

<u>FIGURES</u>	<u>TITLE</u>	<u>PAGE</u>
1	System diagram illustrating numerous factors in fretting fatigue	7
2	Areas of local welding on fretted surface	10
3	Smearred material on fretted surface	10
4	Delamination on fretted surface	10
5	Fatigue crack in boundary between slip and non-slip region on fretted surface	10
6	Delamination and associated fatigue crack on fretted surface	12
7	Fretting fatigue crack initial in surface	12
8	Site of fretting fatigue failure on a press- fitted steel shaft	12
9	Site of fretting fatigue failure on a press- fitted steel shaft at higher magnification	12
10	Schematic representation of contact between two asperities	14
11	Areas of slip and non-slip in the contact of a cylinder with a plane	16
12	Effect of amplitude of slip on the fretting fatigue strength of induction hardened carbon steel specimens	16

<u>FIGURE</u>	<u>TITLE</u>	<u>PAGE</u>
13	Schematic representation of fatigue limit versus slip amplitude	19
14	Fretting fatigue experiments for T1. 6A. 4V and 304 stainless steel	23
15	Schematic representation of initiation and spreading of fretting damage	26
16	Uhlig's model of fretting on an oxide covered metal surface	28
17	Fretting wear volume versus amplitude for AISI 9310 steel	32
18	Fretting wear volume versus number of fretting cycles for AISI 9310 steel	34
19	Fretting wear volume of various metal combina- tion in dry air and in an inert environment	36
20	Fretting wear volume versus temperature	36
21	Contact of elastic spheres under normal and tangential forces	39
22	Spherical surfaces in contact subjected to oscillating force and torsional couple	42
23	Frictional energy dissipation at the contact of steel sphere and plate	45
24	Stress concentration at the edge of a micro-slip region	47

<u>FIGURE</u>	<u>TITLE</u>	<u>PAGE</u>
25	Contact of cylindrical solids separated by a thin elastic film	50
26	Arrangement of flat circular contact pressed by a normal load and subjected to either a tangential shear force or twisting couple	54
27	Distribution of shear traction on flat circular contact subject to a twisting moment M	58
28	Distribution of shear traction on flat circular contact subject to tangential force T	58
29	Distribution of normal pressure on flat circular contact	58
30	Physical system analyzed. Flat on flat model	60
31	Load used in flat on flat model	60
32	Distribution of contact loads	63
33	Classical solution	63
34	Stress and strain contour lines	66
35	Stress contour lines	68
36	Stress contour lines	69
37	Annular region of micro-slip showing fretting damage at the contact of a steel spheres	72
38	Variation of tangential compliance of flat circular contact with film thickness	75

<u>FIGURE</u>	<u>TITLE</u>	<u>PAGE</u>
39	Variation of torsional compliance of flat circular contact with film thickness	75
40	Possible mechanisms for the formation of persistent slip bands on the surface of a test-piece	78
41	Dislocation arrangements near the surface and within the material in a face centred cubic metal as a function of stacking fault energy	78
42	Stage I and stage II development of a propagation crack	80
43	Typical crack growth curve indicating a threshold value of stress intensity factor	80
44	Schematic representation of the S-log N curve	82
45	Effect of fretting on the fatigue behaviour of an austenitic steel	82
46	Assumed distribution of frictional and normal pad loads	84
47	Stress intensity factors for different distribution of frictional pad load	86
48	Stress intensity factors for different distribution of normal pad load	86

<u>FIGURE</u>	<u>TITLE</u>	<u>PAGE</u>
49	Crack plate subjected to contact forces	87
50	Crack plate subjected to distribution contact stresses	87
51	Fretted specimen assembly	92
52	Effect of initial flaw size on predicted life-constant amplitude loading	94
53	Effect of initial flaw size on predicted life-variable amplitude, no length correction	94
54	Effect of initial flaw size on predicted life-variable amplitude, length correction used	95
55	Effect of initial flaw size on predicted life-no pads; variable amplitude; length correction used	95
56	Peak stress intensity factors for a range of pad load distribution	95
57	Predicted and measured curves-constant amplitude loading	97
58	Predicted and measured curves-variable amplitude loading	97
59	Predicted lives for a range of pad load distributions-constant amplitude	97
60	Predicted lives for a range of pad load distributions-variable amplitude	97

<u>FIGURE</u>	<u>TITLE</u>	<u>PAGE</u>
61	Predicted and achieved lives for a range of pad spans-constant amplitude	101
62	Predicted and achieved lives for a range of pad spans-variable amplitude	101
63	Predicted and achieved lives for two pad loads-pad span=16.5mm; constant amplitude	101
64	Predicted and achieved lives for two pad loads-pad span = 16.5mm; variable amplitude	101
65	Schematic diagrams of thin sheet joints illustrating commonly occurring fretting points	107
66	Schematic diagram illustrating how drilling burrs cause fretting points	107
67	An anodised and painted aluminum alloy surface where fretting abrasion has penetrated to cause metal-to-metal contact	107
68	Schematic diagram illustrating the positions of frequency observed fretting damage	107
69	Schematic diagram illustrating how misalignment of a fork end fitting can cause fretting fatigue problems	107
70	Front elevation of single pinned joint and slide elevation of single pinned joint	107

<u>TABLE</u>	<u>TITLE</u>	<u>PAGE</u>
1	Effect of varying the frequency level in particular environment on the fatigue characteristic of several material	20
2	Wear rates under fretting and unidirectional sliding conditions	31

LIST OF PRINCIPLE SYMBOLS USED

A	=	Cross section area of specimen
A_n	=	Coefficient determine the film deformation
a	=	Radius of a plane circular area
a_0	=	Maximum radius of no slip region
a'	=	Minimum radius of no slip region
a''	=	Crack length
b	=	Flat on flat contact length
b'	=	Distance from crack site to concentrated force point
c	=	Half width of contact between cylinder on flat
c'	=	Diameter of the asperity
d	=	Variable adhesive width
E	=	Energy dissipated
e	=	Fretting scare width
F_a''	=	Semi-range alternating stress intensity factor
F_f	=	Maximum frictional force in stress cycles on each pad foot
F_n	=	Normal force on each pad foot
f	=	Frequency
G	=	Shear modulus of material
G_f	=	Film modulus rigidity
G_s	=	Modulus of rigidity of the cylindrical block of steel

H	=	Hardness of the bridge material
H ₀	=	Overall height of the plate
h	=	Outstanding height of the fretting pad
I	=	Moment of inertia
J _n (x)	=	Bessels function
K _d	=	Length correction stress intensity factor
K	=	Stress intensity factor
K _a	=) Alternating stress intensity factor
K _m	=	
K _{fp}	=	Stress intensity factor due to frictional load
K _{fp1}	=	As K _{fp} but without component due to reacting stresses
K _{fp2}	=	Component of K _{fp} due to reacting stresses
K _{np}	=	Stress intensity factor due to normal load
K _I , K _{II}	=	Mode I and mode II stress intensity factor
L ₀	=	Overall length of the plate
M	=	Twisting moment
M ^o	=	Oscillating twisting couple
M'	=	Defined by equation 3.1.5.2
N	=	Local normal force
N ^o	=	Normal force per unit length
N ₀	=	Steady normal force
N'	=	Total number of cycles
P	=	Hertzian pressure (stress)

P	=	Normal contact stress in the asperities
P_0	=	The maximum Hertzian pressure (stress)
P^*	=	Oscillating inclined force
P'	=	Alternating normal force
Q	=	Axial force
Q_0	=	Alternating axial force. (cyclic loading)
q	=	Surface shear traction
q_M'	=	Stress distributed due to moment
q_N'	=	Stress distributed due to normal load
q_0	=	Initial shear traction
$\bar{q}(\xi)$	=	Hankel inversion theorem
r	=	Variable radius
S	=	Friction stress distribution
S_{max}	=	Maximum shear stress in the specimen
S_{alt}	=	Alternating shear stress in the specimen
s	=	Spacing between asperities
T	=	Tangential force
T'	=	Distributed tangential load
T^*	=	Alternating shearing force
$2t$	=	Elastic film thickness
v_f, v_s	=	Displacement condition for no slip
u_f	=	Tangential displacement of a point on the surface on bottom cylinder

- u_x = Tangential displacement of a point on the surface on top cylinder
- W = Weight losses due to fretting
- x = Variable
- α = Amplitude of slip
- α_m = Relative amplitude of slip
- β = Oblique angle defined in Fig. 23.
- β' = Relative angle of twist
- ϕ = Pad span
- ν = Poissons ratio of material
- δ = Relative tangential displacement
- σ = Stress
- σ^a = Stress outside contact area for cylinder on flat
- σ^i = Stress inside contact area for cylinder on flat
- σ_a = Semi-range alternating body stress
- σ_{alt} = Alternating stress
- σ_m = Mean stress
- σ_r = Root square of alternating stress
- τ_{xy} = Distribution of surface shear traction
- ρ = Ratio = $\frac{r}{a}$
- μ = Coefficient of friction

CHAPTER 1

INTRODUCTION

1.1 HISTORICAL BACKGROUND

The earliest reference to fretting in the published literature was a paper by Eden, Rose, and Cunningham (1) in 1911. They referred to the phenomenon of fretting in the grips of fatigue testing machines. Tomlinson(2) in 1927 published the results of an experimental testing program which was probably the first serious attempt to explore the fundamental nature of the fretting phenomenon. Fink et al. (3) in 1929 began publishing a series of papers describing their investigations of what they experienced " Reiboxidation ". Through the decade from the early thirties to the early forties, the effort devoted to fretting investigations accelerated. During the fifties and sixties extensive details and theories to the status of knowledge in the field of fretting was developed by Uhlig, Feng, Tierney and McClellan(4), Waterhouse(5), Nishioka and Hirakawa(6). In the seventies and eighties clear definition was obtained to differentiate between the fretting wear and fretting fatigue. Other investigations have made important studies in defining the basic mechanism of fretting. These include Godfrey(7, 8) Bailey(7), Uhlig(9), Feng and Rightmire(10, 11) and Bill(12).

1.2 SCOPE OF INVESTIGATION

This work will be concerned mainly with the brief presentation of various parameters that affect the fretting process and also with some of the major theories that have been presented by recent researchers on the subject. Emphasis will be laid most on the mechanics of the fretting process, the role of elastic stress analysis in the interpretation of the fretting fatigue failures and the fracture mechanics for predicting the fretting fatigue, with critical appraisal of the various theories and models available on the subject, from the point of view of suitability for use and the establishment of parameters leading to the design and choice of equipment for a specific process. A typical occurrence of fretting fatigue failures in practice will be described and also the techniques used for avoidance of fretting fatigue failures.

1.3 PARAMETERS INFLUENCING THE FRETTING FATIGUE/WEAR PROCESS

The main objectives of the fretting fatigue/wear theories are the prediction of the manner in which the fretting initiate cracks on material, the derivation of formulae for the calculation of forces involved, the establishment of control factors of product geometry and quality, and providing a basis for the appraisal of the prediction of the life of a structure component as a function of all pertinent operational parameters with a

statistical significance. Such objectives are not easily attainable when the phenomenon under study is as complex as fretting fatigue. The main factors that influence the mechanics of the fretting fatigue process may be listed as given below :

1. The amplitude of relative motion between the surfaces being fretted
2. The amplitude and distribution of pressure between the two surfaces being fretted
3. The state of stress, including magnitude, direction and variation with respect to time, in the region of the surface of each of the two members being fretted
4. The number of cycles of fretting
5. The material of each of the two members being fretted
6. The cyclic frequency of relative motion between the two members being fretted
7. The temperature in the region of the two surfaces being fretted
8. The atmospheric environment surrounding the surfaces being fretted

The complete list of 55 variables includes(13):

1. Material of the mating parts
2. Heat treatment of materials
3. Hardness of materials
4. Normal load distribution

5. Coefficient of friction
6. Thermal conductivity
7. Contact pressure distribution
8. Magnitude and position of maximum pressure
9. Relative position of mating parts in the electromotive series
10. Chemical reactivity and combinativity
11. Ambient atmospheric composition
12. Humidity
13. Ambient temperature
14. Interface temperature
15. Ability of material to form oxides
16. Size of oxide particles
17. Shape of oxide particles
18. Hardness of oxide particles
19. Weldability of the combination of materials
20. Melting temperatures of materials
21. Recrystallization temperatures of materials
22. Recovery rates of materials
23. Amplitude of motion
24. Direction of motion, especially with respect to stress field
25. Cyclic form of motion pattern
26. Magnitude, direction, and type of applied stress field
27. Magnitude, direction and type of residual stress field due to heat treatment, shot-peening, cold-rolling or other treatment

28. Surface roughness or waviness
29. Notch sensitivity
30. Fracture strengths of materials
31. Yield stress
32. Endurance limit stress
33. Moduli of elasticity of materials
34. Type of forming or machining process used to fabricate parts
35. Directions and type of surface markings
36. Stability of the oxide
37. Wear properties
38. Geometry of the mating parts
39. size of the contact area
40. Type of fit at contact area, i. e., press fit, loose fit, etc.
41. Speed of oscillation
42. Continuous or intermittent service
43. Dry, lubricated or contaminated mating surfaces
44. Weight change or rate of weight change during fretting
45. Dimensional change or rate of dimensional change during fretting
46. Change or rate of change of contact area
47. Damping capacity of materials
48. Natural vibration characteristics of parts involved
49. Self-excited vibration due to stick-slip action

50. Normal contact stress
51. Poisson's ratio effects
52. Ductility and malleability of materials involved
53. Time or duration of fretting contact
54. Depth of residual stress field
55. Crystal lattice structure of material

Fig(1) summarizes in chart form the primary factors to be considered in fretting fatigue(14). The diagram represents the actual physical/chemical process. The materials, stress environment chemistry and temperature, frequency, wave form, and contact stress must all be considered in both the mechanism of fretting fatigue and structural behaviour in fretting fatigue resistance.

FRETTING-FATIGUE

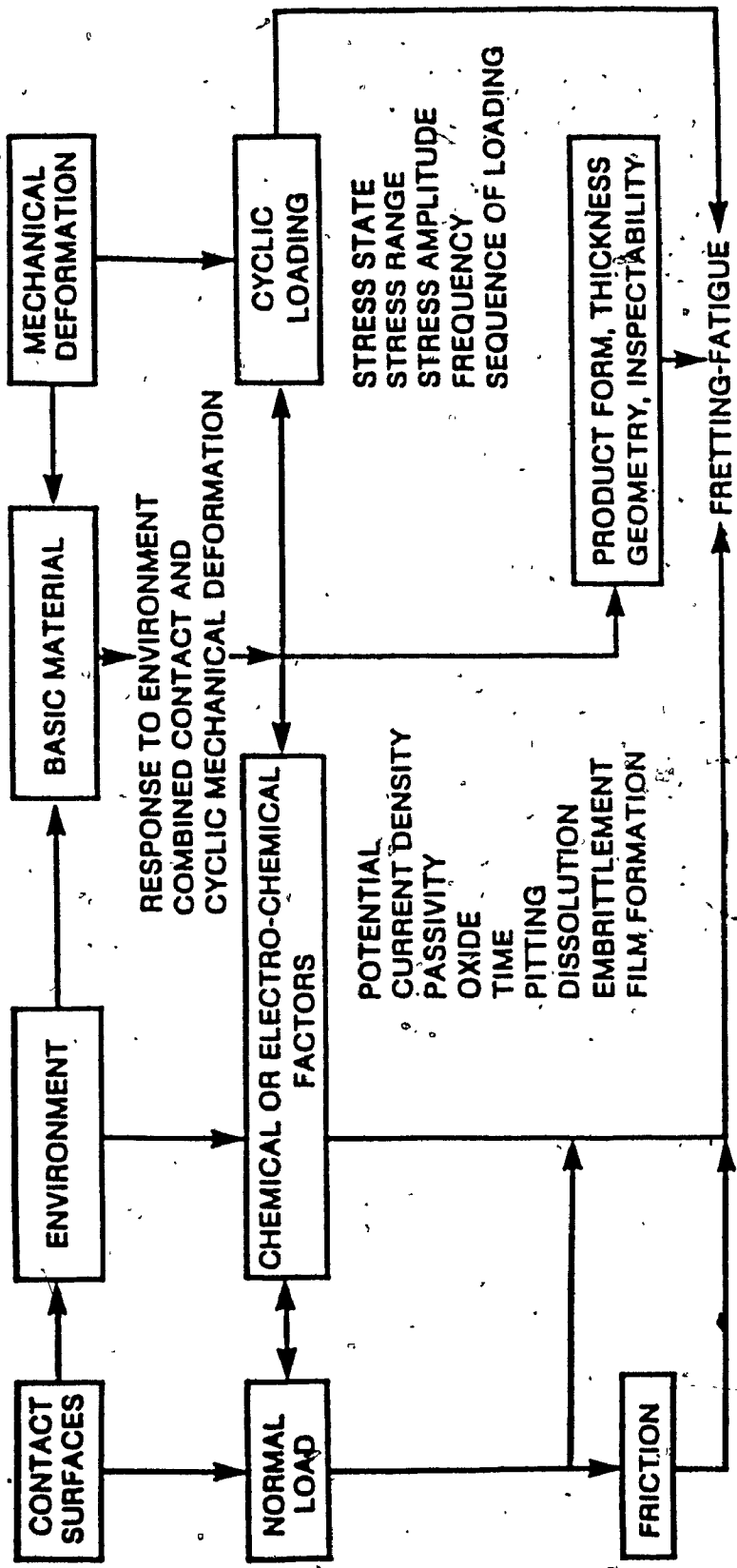


Fig .1. System Diagram Illustrating Numerous Factors in Fretting Fatigue.

After Hoepfner(14)

CHAPTER 2

BASIC CONCEPTS IN FRETTING FATIGUE/WEAR PROCESS

INTRODUCTION

The objective of this chapter is to summarize from the fundamental aspects of fretting, fretting fatigue, fretting wear; the theories and the effects of the experimental parameters on the fretting wear and fretting fatigue and to determine whether common grounds can be established.

2.1 DEFINITION

Many attempts were made to differentiate between fretting wear and fretting fatigue. Chives's (15) attempt indicated that fretting wear and fretting fatigue phenomena are in general likely to occur in somewhat different situations, the fretting wear related to the material removal while fretting fatigue relates to only induced stress. Bill (16) had established a clear definition which is as follows:

Fretting is the surface damage caused by low amplitude oscillation of two sliding surfaces in contact.

Fretting Wear is the removal of material from contacting surfaces through fretting action.

Fretting Fatigue is the reduction in the material fatigue endurance due to fretting surface damage.

2.2 Fretting Fatigue

Observations were made indicating that fretting failures are consistently occurring in the areas showing surface damage often near the edges of contact areas or near slip/non-slip boundaries (17, 18), accompanied by crack initiation and propagation and a bulk alternating stress in one of the contacting bodies

2.2.1 MECHANISMS OF FRETTING FATIGUE

2.2.1.1 Atomic scale The movement of atoms under the influence of the applied alternating shear stress causes the atoms to form either edge or screw dislocations which is in general terms the start or the initiation of a crack. If the surfaces of the crack were to slide over each other in a direction perpendicular to the leading edge of the crack, this would constitute an edge dislocation (mode I of edge crack). The formation of screw dislocation leads to the subsurface crack and would constitute mode III crack (further explanation will be presented in section 4.1 for cracks initiation related to fracture machines).

2.2.1.2 MICROSCOPIC OBSERVATION

Waterhouse (19) illustrated the pattern of fretting fatigue process with the scanning electron microscope as shown in figures (2-9). As it can be seen, observations of the damage on mild steel indicated that at the early stages, local welds occurred causing considerable roughening of the surface (Fig. 2.). This was followed by smearing of material and a reduction in the surface roughness (Fig. 3.). eventually, material was removed from



Fig. (2) Areas of local welding on fretted surface of 0.2C steel after 500 cycles of fretting. After Waterhouse(19).



Fig. (3) Smeared material on fretted surface of 0.2C steel after 500 cycles of fretting. After Waterhouse(19).



Fig. (4) Delamination on fretted surface of 0.7C steel after 10 cycles of fretting. After Waterhouse (19).



Fig. (5) Fatigue crack in boundary between slip and non-slip region on fretted surface of 0.7C steel. After Waterhouse(19).

the surface by delamination process producing plate-like particles of debris (Fig. 4.). At this stage, the debris consists of thin oxide-covered metal particles. Development of debris can cause the boundary between the region of slip/non-slip to move and is thought to be the reason for the generation of multiple cracks which is a feature of fretting fatigue failure (Fig. 5.). The sub-surface cracks, which are a feature of delamination process crack could change direction and become propagating fatigue cracks, progressing into the bulk of the material (Fig. 6.) Cracks, once initiated, follow a course at an angle to the surface, but when the crack is caused by the fretting action, it changes direction, becoming perpendicular to the principal alternating stress. Figure 7 illustrates another form of fretting fatigue crack and the initial oblique portion of the crack is opened due to the stress concentration at this point in the surface. On the final fractured surface, the oblique part of the crack appears as a tongue on one surface and a matching chip on the other one. Fig 8 and 9 show such a tongue on a fatigue fracture of a steel shaft with a press fitted collar. In addition to the main crack, which caused the failure, numerous other cracks are visible (Fig. 9.).

2. 2. 3 THEORIES OF FRETTING FATIGUE MECHANISMS

The observation made previously applies to the initial stage in the development of a fatigue crack which ultimately



Fig.(6) Delamination and associated fatigue cracks on fretted surface of Ti-6Al-4V, After 3×10^5 cycles of fretting. After Waterhouse (19).



Fig(7) Fretting Fatigue crack initiated in surface of aged AL-4Cu alloy. After Waterhouse (19).



Fig.(8) Site of fretting fatigue failure on a press-fitted steel shaft showing typical tongue. After Waterhouse (19).



Fig.(9) Site of fretting fatigue failure on a press-fitted steel shaft at higher magnification showing subsidiary cracks. After Waterhouse (19).

produces a fretting fatigue failure. Most investigation e.g (20) have been concerned with the alternating shear stress produced in contact region. The magnitude of these shear stresses depends on the degree of adhesion or the coefficient of friction between the surfaces. Liu, et al. (21) have completed the analysis based on the forces acting on an infinitesimally small element of material near the interface of a microweld as shown in Fig. 10. The following terminology was used:

S_{max} = maximum shear stress in the asperities of gripping pad

P = normal contact stress in the asperities

μ = coefficient of friction

P_0 = yield pressure of the weaker material

H = hardness of the gripping pad material

S_{alt} = alternating shear stress in specimen due to alternating bending stress and frictional shear stress

σ_{alt} = alternating normal stress due to bending of specimen

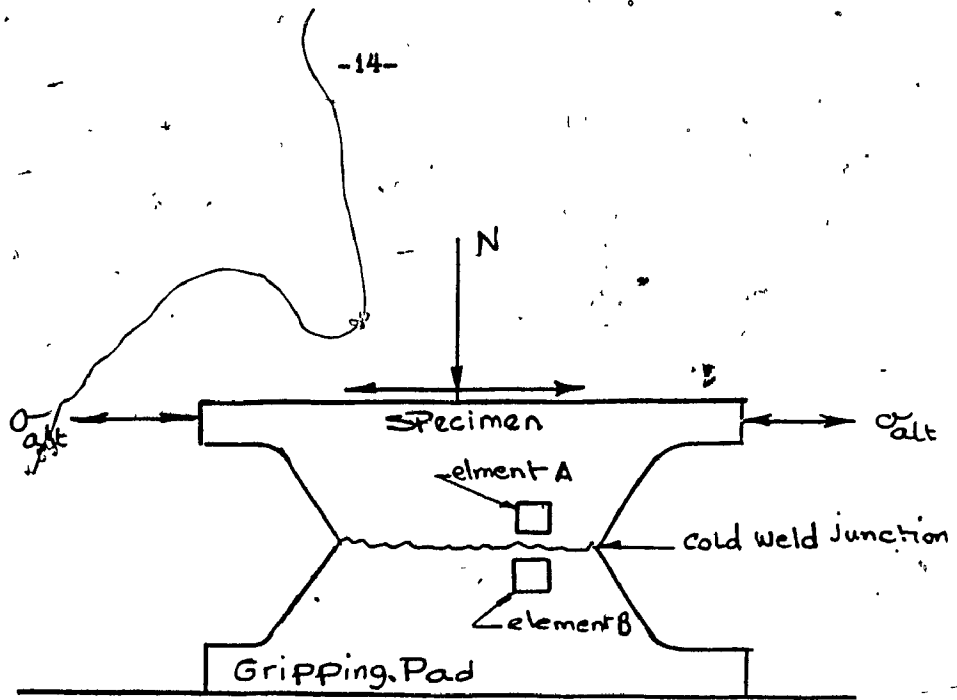
σ_y = yield strength in the weaker material

assuming $P_0 = 3\sigma_y$ and $\sigma_y = K.H$ and that the asperity is subjected to a shear stress S , the maximum pressure that the asperity on the gripping pad can sustain is given by :

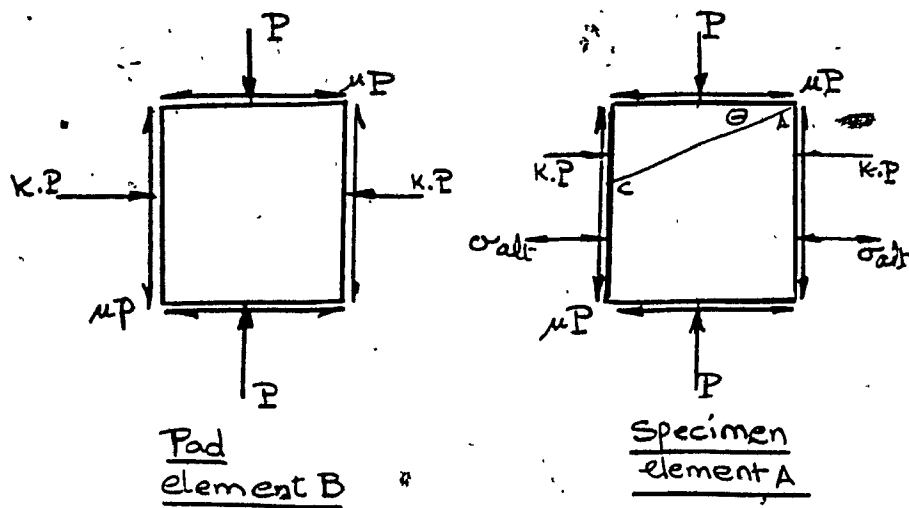
$$P^2 = \frac{k_1 \cdot H^2}{k_2 + 4 \mu^2}$$

where k_1, k_2 = constants

The maximum alternating shear stress in the element due to the



(a)



(b)

Fig. 10. Schematic representation of contact between two asperities.

(a) Element of material near interface.

(b) Stresses on elements of material.

After Corten (21)

oscillating motion relative to the gripping pad at the interface (Fig. 10. a.) is :

$$S_{alt} = \frac{1}{2} (4\mu^2 P^2 + \sigma_{alt}^2)^{1/2}$$

When S_{alt} reaches the fatigue endurance of the material in shear a fatigue crack is initiated. Their assumption was based on the fatigue endurance in shear is half the value of the normal fatigue endurance which gives this critical value of the alternating normal stress. (Maximum shear stress failure theory).

$$\begin{aligned} \sigma_{alt} &= (4 S_{alt}^2 - 4 \mu^2 \frac{k_1 H^2}{k_2 + 4\mu^2})^{1/2} \\ &= 2 (S_{alt}^2 - \mu^2 P^2)^{1/2} = 2 (S_{alt}^2 - \frac{\mu^2 k_1 H^2}{k_2 + 4\mu^2})^{1/2} \end{aligned}$$

Agreement with the experimental results is found to be reasonably good. Nishioka and Kirakawa(22) have applied similar analysis to the case of a cylindrical surface fretting against a flat specimen where the motion is at right angle to the line of contact. The relation between the fraction of the area over which slip does not occur and the applied normal load N , the tangential force T and the coefficient of friction μ (Fig. 11.) is :

$$\frac{d}{c} = \left[1 - \left(\frac{T}{\mu N} \right) \right]^{1/2} \quad 2.2.3.1$$

where : c = half width of contact between cylinder on a flat

d = variable adhesive width

The relation between the relative slip α^N and these quantities is given by :

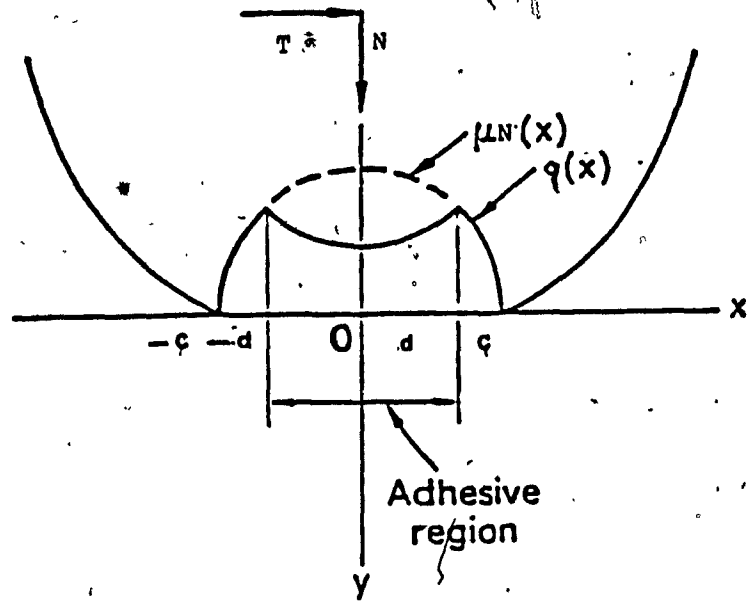


Fig. 11. Areas of slip and non-slip in the contact of a cylinder with a plane. (K.Nishioka and K.Hirakawa, Bull.Jap. Soc.Mech.Engrs. 12,693 (1969).)

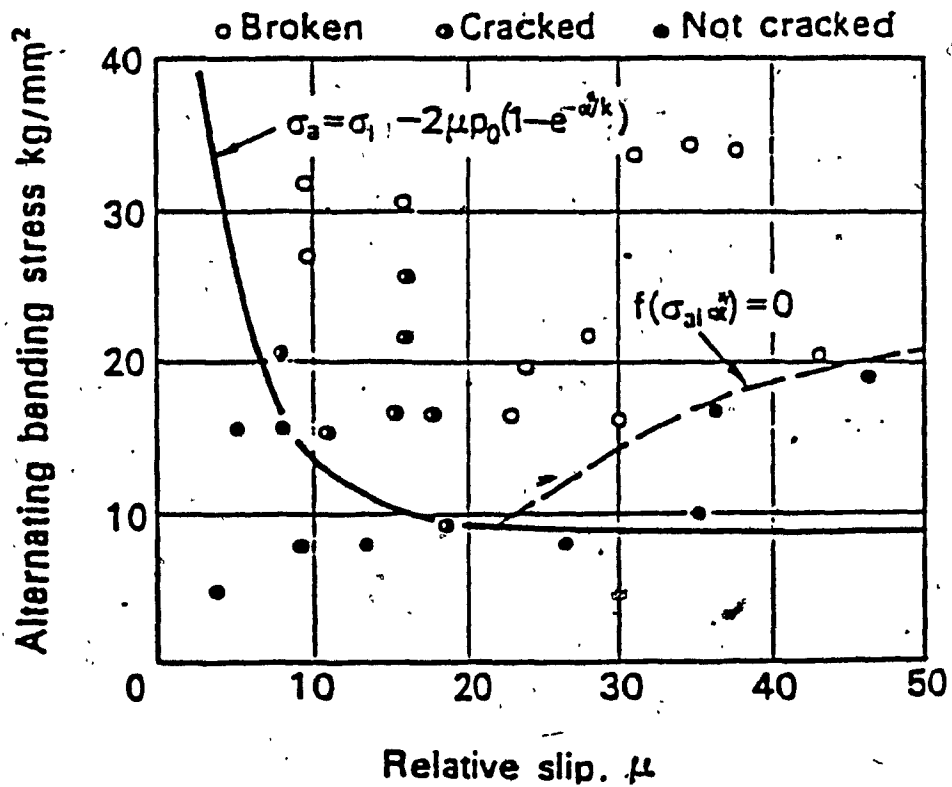


Fig. 12. Effect of amplitude of slip on the fretting fatigue endurance of induction hardened carbon steel specimens. (K.Nishioka and K. Hirakawa, Bull.Jap.Soc.Mech.Engrs. 12,696 (1969).)

$$\alpha^* = -k \ln \left(1 - \frac{T}{\mu N} \right) \quad 2.2.3.2$$

The direct stress at a distance x from the centre line within the region where slip is occurring i.e. $c > x > d$ is given by :

$$\sigma_x = -2 \mu \bar{p} \frac{d}{c} \left[(x/d)^2 - 1 \right]^{1/2} - \bar{p} \left[1 - (x/c)^2 \right]^{1/2} \quad 2.2.3.3$$

Where \bar{p} is the mean pressure over the contact area (Hertzian stress). This is maximum when $x = c$ so that :

$$\sigma_{\max} = 2 \mu \bar{p} \left[1 - (d/c)^2 \right] \quad 2.2.3.4$$

substitution of 2.2.3.4 in eqn. 2.2.3.1 yields:

$$\sigma_{\max} = 2 \mu \bar{p} (T/\mu N) \quad 2.2.3.5$$

The maximum alternating direct stress in the fretted region is the applied alternating stress $\sigma_a + \sigma_{\max}$ (where σ_a is a semi-range alternating body stress). If the alternating stress to initiate a fatigue crack is σ_1 then for the fretting to initiate a crack.

$$\sigma_a + \sigma_{\max} \geq \sigma_1 \quad 2.2.3.6$$

$$\sigma_a \geq \sigma_1 - 2 \mu \bar{p} (T/\mu N) \quad 2.2.3.7$$

Substituting of 2.2.3.7 in eqn. 2.2.3.2

$$\sigma_a \geq \sigma_1 - 2 \mu \bar{p} \left[1 - \exp \left(-\alpha^*/k \right) \right] \quad 2.2.3.8$$

This expression is represented in fig. 12 and is shown to agree well with the experimental results at lower values of the amplitude of slip. The greater than expected survival rate at high

valued of slip is attributed to the removal of crack nuclei by excessive wear before they have the opportunity to propagate

2.2.4 EFFECT OF THE MAIN VARIABLES ON FRETTING FATIGUE

2.2.4.1 AMPLITUDE OF MOTION

It appears that there is no minimum surface slip amplitude below which fretting will not occur. At low amplitude, most of the debris are retained in the contact area where is at high amplitudes debris are forced from the contact area and concentrated in a ring around the fretted surface. The fretting fatigue endurance versus slip amplitude is presented semi-quantitatively in Fig. 13. Fretting fatigue endurance (or limit) decreases with increasing amplitude up to about 8 μm , but is shown here to be relatively insensitive to further increases in amplitude.

2.2.4.2 FREQUENCY

Researchers have investigated the effects of varying the frequency level, in particular effects of environment on the fatigue characteristics of several materials. The result of these investigations are summarized by Hoepfner et al. (25) in table(1). Several investigators found that there is no effect of environment on crack growth rates at high frequency levels. Endo et al. (83), observed that fatigue life increased with increasing frequency up to 50Hz in fretting fatigue experiment on carbon steel. Increases in crack propagation rates were found with decrease in frequency at lower frequency levels in corrosive environments.

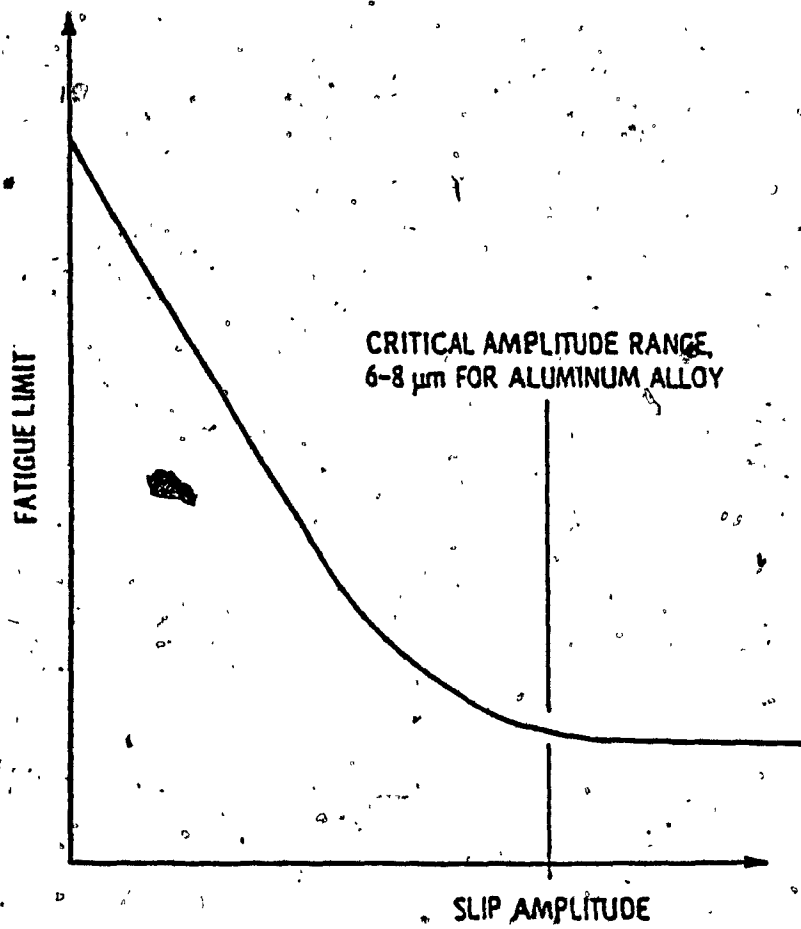


Fig. 13. Schematic representation of Fatigue Limit versus slip amplitude. After Bill (27)

TABLE (1) Effect of varying the frequency level in particular environment on the fatigue characteristic of several material. After Hoepfner (25).

RESEARCH ON FREQUENCY AND ENVIRONMENT

Author(s)	Material	Frequency	Environment	Results
Mager, Landes, Moon;	533B-1 steel	10 cpm 1 cpm 0.5cpm	Reactor water @ 550° F	Crack growth rates in environment are the same as in air for 10cpm and higher
McLaughlin				Growth rates increase as frequency is decreased for 1cpm and lower
Kondo, Kikuyama, Makajima, Shindo	533B-1 steel	100cpm 10 cpm 1 cpm 0.3cpm	Reactor water @ 500° F Growth	Results agreed with Mager. No effect of environment above 10cpm over air tests rates increase as frequency
Kondo, Kikuyama, Makajima, Shindo, Nagasaki	A-302B steel	100cpm 10 cpm 1 cpm	Reactor water @ 500° F	Fatigue life in water environment is shorter than in air Growth rates increase as frequency is decreased Saturation frequency observed below 1cpm
James, Williams	533B-1 steel	600cpm 1 cpm	Air @ 75° 550° F	No effect of frequency in an air environment
Solomon	A286	90cpm to 0.0042cpm	Air @ 1100° F	Increase in crack growth rate for a decrease in frequency. Saturation frequency at 0.05cpm
Gerber, Heald, Kiss	SA508- C12 steel	30cpm to 0.037cpm	Air @ room temp & 550° F high purity water @ 550° F	Growth rates in water are 4-8 times faster than in air @ 550° F. Growth rates in water are 8-15 times for faster than air @ room temperature. Very little difference in growth rates between 0.37 and 0.037cpm (possible saturation frequency)
Gallagher, Sinclair	4340 steel	1cps and 0.002cps	Distilled water	Significant difference in growth rates between frequencies
Vosikovsky	X-65 steel	10 Hertz to 0.01 Hertz	Air, Distill- ed water, 3.5% NaCl solution	No frequency effect in air increase in growth rates as frequency is decreased in environments No difference in growth rates between distilled water and 3.5% NaCl

TABLE 1. (Cont'd)

Author(s)	Material	Frequency	Environment	Results
Yokobori, Sato	2024-T3 Al SM-50 steel	8400cpm 7200cpm 6cpm 1cpm	Air @ room temp	Increase in growth rates for a decrease in frequency for both materials Increase in striation spacing for decrease in frequency
Nakasa, Takai	SNCMB steel	800 to 1 cpm	Distilled water 5-80°C	Increase in growth rates with decrease in frequency
Cavel, Pineau	Alloy 718 (nickel base)	20 Hertz to 0.005 Hertz	Air @ 298°K and 823°K	Increase in growth rates with decrease in frequency
Amzallag, Rabbe, Desestret	Austenitic and ferritic stainless steel	20 Hertz to 0.5 Hertz	Air and 3% NaCl	No effect of environment over air at high frequency (20Hz) Increase in growth rates as frequency is decreased
Ryder, Krupp, Pettit, Hoepfner	Ti-6Al- 4V	20 Hertz to 0.5 Hertz	Air, 3.5% NaCl, sump- tank water	Increase of 4-10 times in growth rates as frequency is decreased
Vosikovskiy	HY130 steel	10 Hertz 1 Hertz 0.1 Hertz 0.01 Hertz	Air, 3.5% NaCl	No effect of environment over air at 10 Hertz Increase in growth rates as frequency is decreased
Braun	SA533B-1 steel	10 Hertz 1.0 Hertz	Air, distilled water	No effect of frequency in air No effect of environment over air at 10 Hertz

The explanations given for the acceleration of the fatigue crack propagation rates as a function of frequency, and environment ranged from hydrogen embrittlement mechanism to an acceleration of the corrosion process at the crack tip.

2.2.4.3 NUMBER OF FRETTING CYCLES

Hoeppner and Goss(26) conducted the fretting fatigue studies on titanium alloys. They found that below a threshold when the number of fretting cycles applied simultaneously with fatigue cycling, the fatigue endurance was not reduced. If after application of a critical number of fretting cycles the fretting reduction in fatigue endurance was significant. However, no further reduction in fatigue endurance occurs if fretting is allowed to continue beyond the critical or "Threshold" number of cycles. Hoeppner results indicated at least for one alternating stress level for Ti-6Al-4V and 7075-T6 Aluminum alloy, that roughly 50,000 (10^4 to 10^5) fretting cycles correspond to the "damage threshold". Bill(27) showed that a similar threshold number of fretting cycles exist for 304 stainless steel as well as for Ti-6Al-4V(Fig. 14.). It is expected that the local effective alternating stress near contacting asperities under fretting condition would be in the order of the yield point of the softer of the two materials. Bill suggested that local low cycle fatigue damage at or near the surface, caused by fretting is the precursor to both rapid fretting wear and fretting fatigue failure.

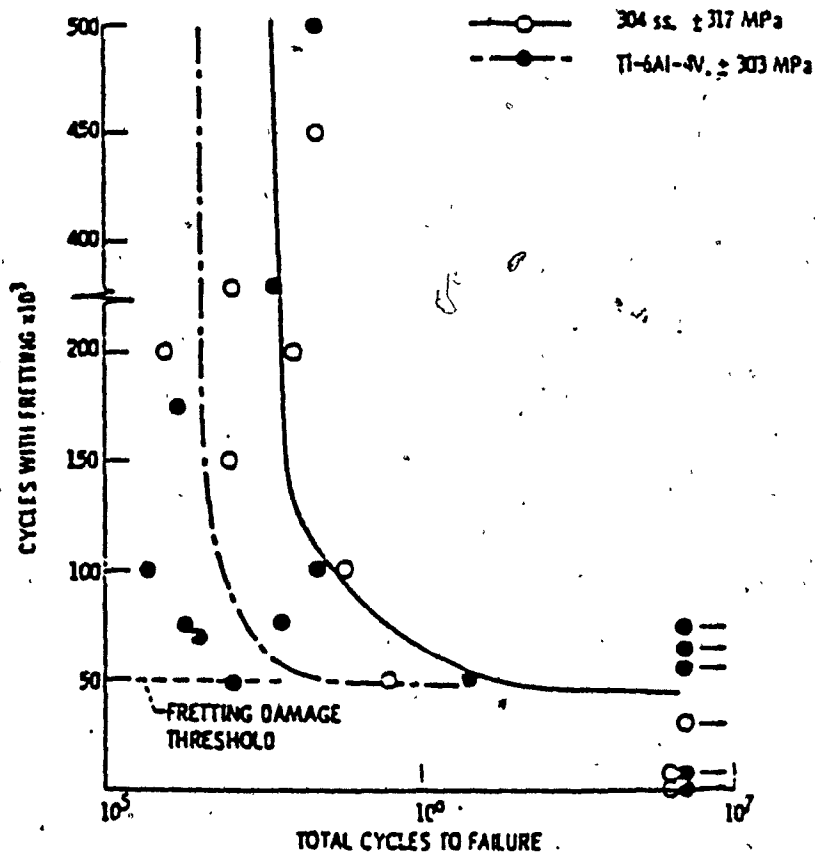


Fig. 14 . Fretting Fatigue experiments for Ti₆Al₄V and 304 stainless steel . After Bill(27) .

2.2.4.5 EFFECT OF ENVIRONMENT

Fretting fatigue experimental results are known to be sensitive to the chemical activity of the environment. Pook and Hoepfner (28) concluded that for some materials the chemical or corrosive contribution to fretting fatigue could be dominant compared to the mechanical contribution alone. (see Table 1). Waterhouse made the general observation that fretting was particularly detrimental to fatigue endurance in a corrosive environment in the case of alloys that depend on protective surface oxide film for corrosion resistance.

2.2.4.6 EFFECT OF TEMPERATURE

Fretting fatigue experiments reported by Hamdy and Waterhouse (29) for Ti-6Al-4V and Inconel 718 showed longer fretting fatigue lives at elevated temperature of up to 600°C than at room temperature. The rapid development of thick surface oxide films was proposed by Waterhouse as being the reason for the extended fretting fatigue lives at elevated temperatures. The formation of surface oxide generally results in reduced adhesion and friction- (30) and therefore a reduced probability of surface crack initiation and growth.

2.3 FRETTING WEAR

Observations made by different investigators indicated that the fretting wear is consistently accompanied by a loss of intermetallic contact and the formation of oxide debris between the

surface together with crack initiation and a microspall event.

2. 3. 1 MECHANISM OF FRETTING WEAR

Feng and Rightmire(31) presented the mechanism of fretting wear as a sequence of event shown in Fig. 15.

It consisted on four stages :

- (a) Initial stage
- (b) Transition period
- (c) Declining stage
- (d) Steady-state stage

The process they visualised consisted basically of the breakaway of particles, subsequent oxidation and abrasion. This process, they believed reached a steady-state (saturation) level when the oxide layer became very thick. Godfrey et al(32-36) employed optical microscopy in attempting to characterise the nature of fretting and establish its mechanism. They concluded that adhesion resulted from contact, and extremely fine particles were subsequently broken loose and oxidised;

subsequently broken loose and oxidised, and surface fatigue was not a factor based on the fact that fretting occurred in less than one cycle.

2. 3. 2 THEORIES OF FRETTING WEAR MECHANISM

Unlig(37-38) points out that any theory of fretting must take account of the following facts:

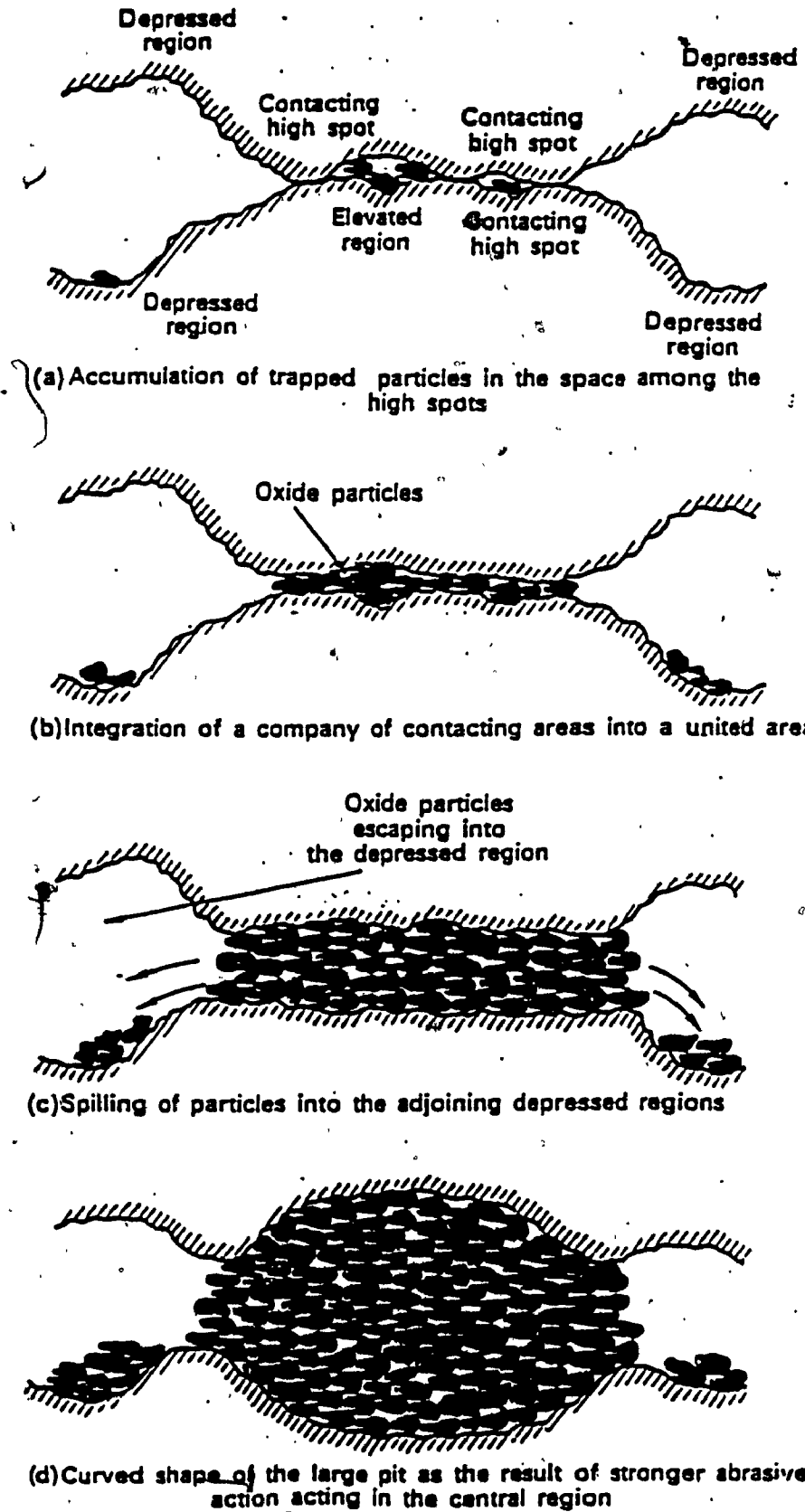


FIG. 15. Schematic representation of initiation and spreading of fretting damage. (I. M. Feng and B. G. Rightmire, *Proc. Instn. Mech. Engrs.* 170, 1056 (1956).)

- (a) Fretting damage is reduced in vacuum or inert atmosphere
- (b) Debris formed by fretting of iron is largely of the composition $Fe_2 O_3$
- (c) Greater damage occurs at low frequencies for a given number of cycles than at high frequencies
- (d) Metal loss increases with load and relative slip
- (e) Greater damage occurs at temperature below room temperature than at temperature above room temperature
- (f) Damage is greater in dry air than in moist air

In explaining these facts he had produced a theory based on model shown in Fig. 16 in which it is assumed that the damage is caused by a regular array of asperities which wipe off the oxide film, which immediately begins to form again to be wiped off again in the next cycle. The contribution of this action to the damage is calculated assuming a logarithmic growth law for the oxide film. He has assumed also that the asperities plough into the metal surface and remove metal directly. The weight loss per cycle due to the scraping off the oxide film is given by:

$$W_{\text{corr}} = 2 n l c k \ln \left[\frac{s}{2 l f \tau} + 1 \right] \quad 2.3.2.1$$

where n = number of circular asperities per unit area.

l = distance moved by an asperity in half a cycle, i. e. the amplitude of slip.

c = diameter of the asperity.

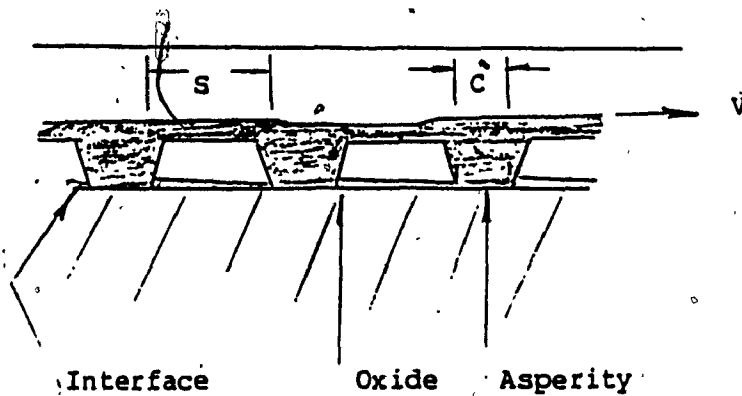


Fig. 16. Uhlig's model of fretting on an oxide covered metal surface (H.H. Uhlig, J. Appl. Mech., 34, 402 (1954)).

s = spacing of the asperities.

f = frequency.

τ, k, k_0 = constants.

The weight loss per cycle due to the ploughing action is given by:

$$W_{\text{mech}} = \frac{2k' \ell \cdot N}{P_0} = k_2 \ell \cdot N \quad 2.3.2.2$$

where N = normal load

P_0 = yield pressure.

k' and k_2 = constants.

Uhlig expands the log. term in eqn(2.3.2.1) and ignores all but the first term, so he is in fact assuming a linear oxidation rate. This reduces eqn. (2.3.2.1) to :

$$W_{\text{corr}} = \frac{nck_s}{f \tau} \quad 2.3.2.3$$

Since the spacing of asperities is $s \approx n^{-1/2}$, and the total real area of contact is $n \pi (c/2)^2$ 2.3.2.3 becomes :

$$W_{\text{corr}} = k_0 N^{1/2} / f - k_1 N / f \quad 2.3.2.4$$

where:

$$k_0 = \frac{2}{\sqrt{P_0 \pi}} \cdot \frac{k}{\tau} \quad \text{and} \quad k_1 = \frac{4}{P_0 \pi} \cdot \frac{k}{\tau}$$

combining eqn. (2.3.2.4) and (2.3.2.2) give:

$$W_{\text{total}} = (k_0 N^{1/2} - k_1 N) N' / f + k_2 \ell N N' \quad 2.3.2.5$$

where N' is the total number of cycles.

W_{total} = the specimen weight-loss.

Equation 2.3.2.5 predicts the fretting weight-loss in hyperbolic function of frequency. Halliday and Hirst(39) made a comparison of mild wear on a steel and fretting at various amplitudes on the same type of steel. These results are shown in Table 2. The rates are similar at large amplitude, but at small amplitude the fretting wear rate becomes very small in comparison with the wear produced in unidirectional motion after sliding for the same distance under the same load. They concluded according to their observation that welding of the surface occurs, and the degree of relative slip influences the result. They showed that fretting was not dependent on the formation of oxide. Waterhouse theory (40) was build on the concept that fretting was much like wear with regard to the adhesion, the breaking of the welds and the metal transfer occurrence. In special cases oxide play an important role in the process.

2.3.3 EFFECT OF THE MAIN VARIABLES ON FRETTING WEAR

2.3.3.1 AMPLITUDE OF MOTION

It is universally agreed that fretting wear increases with increasing amplitude. Tomlinson et al. (2) concluded that slip amplitudes as small as $0.025 \mu\text{m}$ (10^{-6} inch) are sufficient to initiate fretting damage. The effect of the amplitude on fretting wear is shown in Fig. 17 which shows results, obtained for 9310 steel(16). At low amplitude, most of the debris were located in the contact area, whereas at high amplitude debris were forced from the

Table (2)

Wear rates under fretting and unidirectional sliding conditions. After Hailiday (39)

Load (kg)	Amplitude (μm)	Wear Rates (cm^3/cm)	
		Fretting	Unidirectional
70	420	1.18×10^{-7}	1.2×10^{-7}
50	300	8.23×10^{-8}	8.0×10^{-8}
19	20	initial 1.6×10^{-8}	2.2×10^{-8}
		final 1.9×10^{-12}	

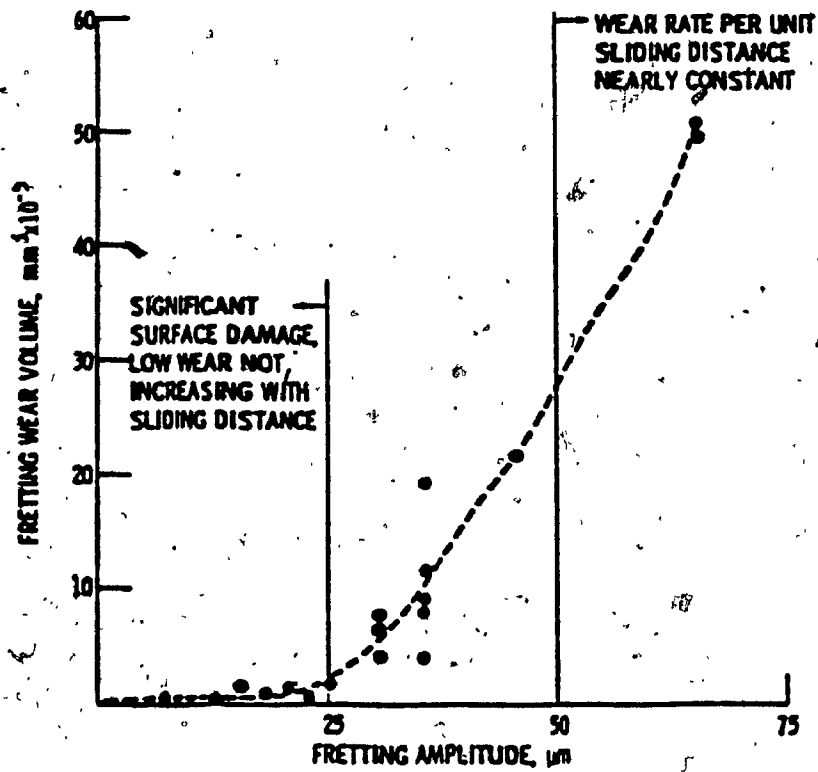


Fig. 17. Fretting wear volume versus amplitude for Aisi 9310 steel. 163 Hz, dry air, 10^6 cycles; 1.47 N normal load. After Bill (16).

contact area and collected around the periphery of fretted surface. The amplitude at which the transition occurs would likely depend on the contact geometry details.

2.3.3.2 FREQUENCY

Feng and Uhlig(41) reported decreasing fretting wear rates in mild steel as frequency increased up to about 20HZ. Beyond 20HZ, the frequency effect was not significant. They indicated that the frequency effect was associated with the rates of surface oxidation and available time for oxidation to occur between fretting cycles.

2.3.3.3 NUMBER OF FRETTING CYCLES

It is a universally accepted observation that fretting wear increases with the number of fretting cycles often in the manner shown in Fig. 18. There is an initial stage of fretting(not illustrated in Fig. 18.) persisting for 10^3 cycles during which fretting wear rates are high, and considerable adhesive transfer and plastic deformation to the surface occurs. The relative severity of this initial stage of rapid wear varies greatly depending on the materials. Following this initial stage of fretting, there is an "incubation" period during which wear rate is quite low lasting for 10^3 to 10^4 cycles. Beyond 10^4 cycles, a steady state condition is reached in which the wear rate increases. In general a critical number of fretting cycles (10^4 - 10^5) is required in fretting wear to initiate the onset of steady state wear.

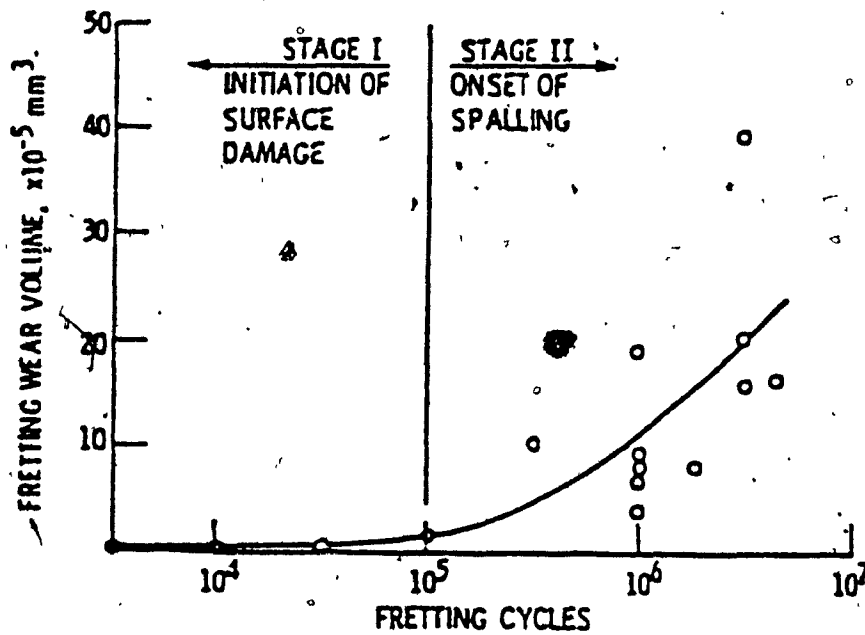


Fig. 18 . Fretting wear volume versus number of fretting cycles for Aisi 9310 steel 163 HZ.35um amplitude dry air, 1.47 N load . (After Bill(16)).

2. 3. 3. 4 ENVIRONMENT EFFECTS

Fretting wear experiments conducted on non-noble metals invariably showed substantially less wear in an inert environment such as argon or nitrogen than in air (81, 82) as shown in Fig. 19. There is reduced wear volume in spite of the substantially greater area of metallic contact, far less debris are evident, and micro-spall pit edges are much more clearly defined when fretting is conducted in inert environment.

2. 3. 3. 5 TEMPERATURE EFFECTS

Elevated temperature fretting wear experimental results indicate that fretting wear generally decreased with increasing temperature up to 816°C as shown in Fig. 20. Materials are usually affected by temperature in terms of change of mechanical properties and oxidation behaviour. For conditions under which rapid oxidation kinetics or selective oxidation of a certain alloy constituents, led to the formation of adherent, self protective oxide film, Handy (84) observed that the fretting wear was low. Wear scar features suggest that the primary role of the protective surface oxide film, during fretting is to reduce the incidence of metal to metal contact, thereby reduce fretting friction and surface damage in the form of micro-spalls. In the conclusion it can be claimed that elevated temperature has a beneficial effect on fretting wear.

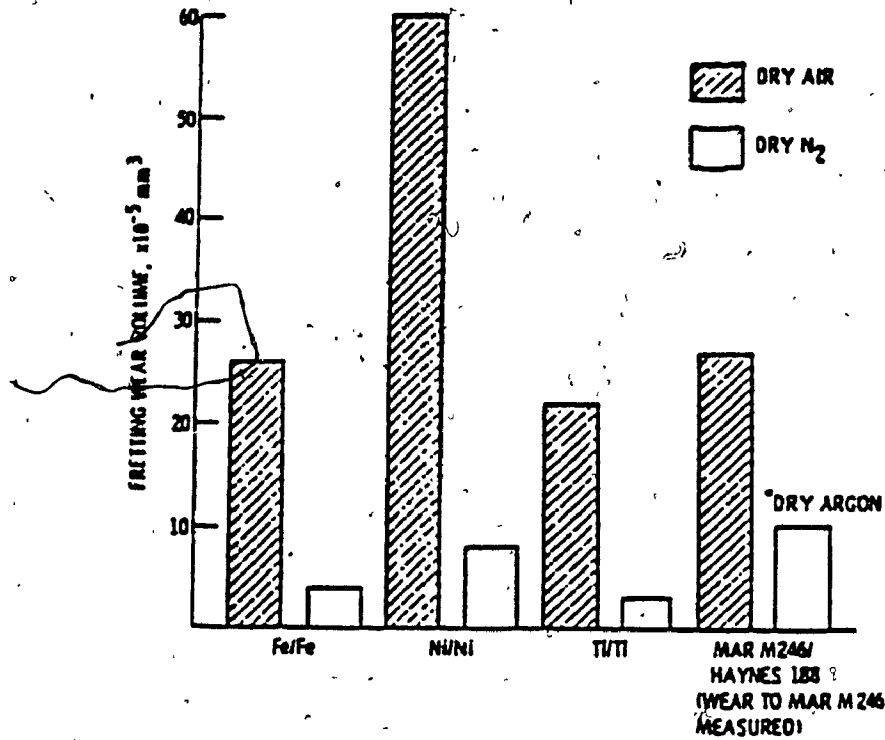


Fig. 19. Fretting wear volume of various metal combination in dry air and in an inert environment. 3×10^5 cycles, $50 \mu\text{m}$ amplitude, 80 Hz, room temperature, 1.47 N load. After Bill (81,82).

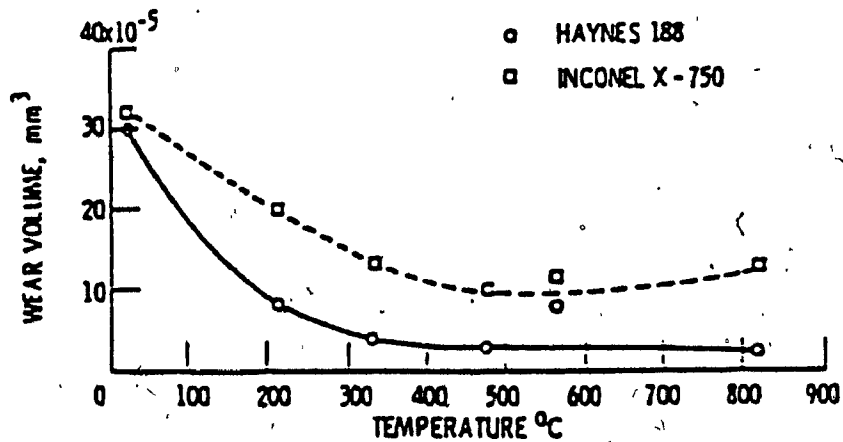


Fig. 20. Fretting wear volume versus temperature 80 Hz, 3×10^5 cycles, $75 \mu\text{m}$ amplitude, 1.47 load, 35 percent \pm ten percent relative humidity air. After Handy (84).

CHAPTER 3

THE ROLE OF ELASTIC STRESS ANALYSIS IN THE
INTERPRETATION OF FRETTING FATIGUE FAILURE

INTRODUCTION

Hertz had solved the problem of contact stress between two elastic bodies(42), considering the assumption of static contact under the action of a steady resultant force acting normal to the tangent plane at the point of contact. In practical applications of the theory neither of these conditions are fulfilled, particularly when friction and wear are involved. In such a case the two bodies in contact undergo some relative motion, either sliding or rolling or both, whilst the presence of friction ensures that the force tangential to the contact surfaces are transmitted between them. The introduction of sliding or rolling motion, together with various combination of transmitted forces, gives rise to a number of contact stress problems of considerable practical importance to which Hertz theory alone does not provide an adequate solution. In this chapter the contribution which elastic stress analysis can make to the understanding of fretting and fretting fatigue is discussed.

The chapter starts with a review of those configurations for which solutions have been found i.e the contact of spheres, cylinders and plates under a steady normal load and an alternating frictional shear load.

3.1 THEORETICAL MODELS

3.1.1 CONTACT OF SPHERES MODEL

The contact of two spheres or a sphere on a flat surface under a normal compressive force, and a shearing force (less than limiting friction force) has long been favoured by researchers into frictional phenomena, What is of particular importance in the present contact of spheres model evaluation context is the fact that the distribution of contact pressure is known by the Hertz theory and the development of that theory by Cattaneo(43) and Mindlin(44) make it possible to calculate the distribution of the interfacial shear traction.

3.1.1.1 SPHERE TO SPHERE CONTACT

Mindlin started by assuming that the interface had an infinite frictional capacity so that slip could not occur and demonstrated that shear traction rising to infinity at the edge of the contact region would then be required, as shown in Fig. 21 b. The solution was modified by assuming that the shear traction (q) at any point on the interface could never exceed limiting friction there; i.e. $q < \bar{\mu}p$ where $\bar{\mu}$ is a constant

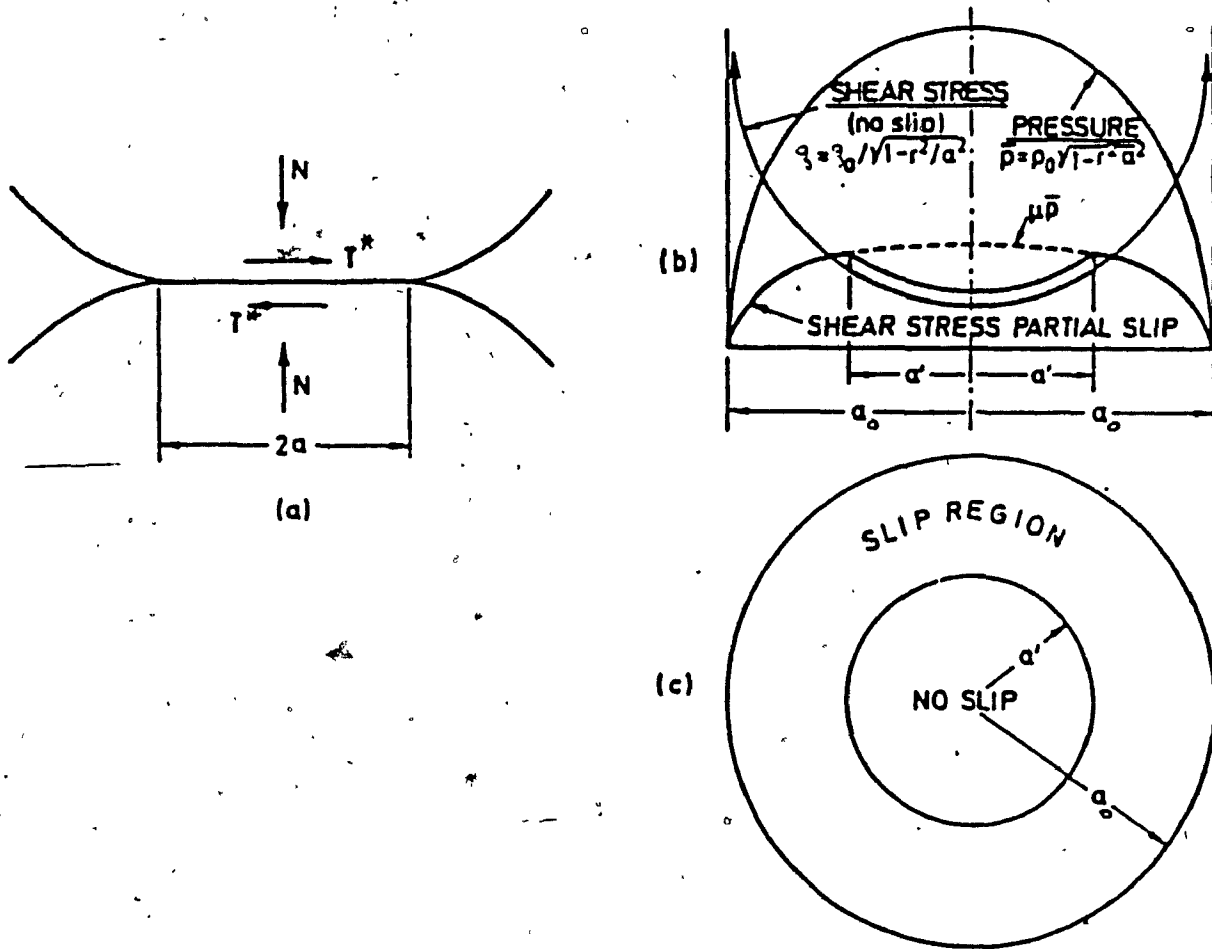


FIG. 21 (a) Contact of elastic spheres under normal and tangential forces. (b) Distribution of pressure on the contact surfaces according to Hertz. (c) Plan view of contact surface. Suppression of interfacial slip requires infinite shear traction at the edge of the contact region. A finite frictional capacity $\mu \bar{p}$ implies slip on the annulus $a' < r < a_0$ with the central region $r < a'$ remaining unslipped. After Mindlin (44)

coefficient of friction and \bar{p} is the Hertzian pressure. On the other hand, it is possible for a "relative slip" to take place between the surfaces over part of their area of contact without the initiation of overall sliding. It was found then that the interface is divided into two distinct regions, a circular region $0 < r < a'$ where the surface remain together and an annular region $a' < r < a_0$ extending to the edge of the contact area over which slip will occur (Fig. 21. c). The dimensions of the central locked region were given as :

$$\frac{a'}{a_0} = \left[1 - \frac{T^*}{\mu N} \right]^{1/3}$$

where:

N = The value of clamping force

T^* = The alternating shearing force

μ = the coefficient friction

a' = Minimum radius of no slip region

a_0 = Maximum radius of no slip region

when $\left(\frac{T^*}{\mu N} \right) \rightarrow 1$, the radius of the locked region

shrinks to zero and macroscopic sliding commence. If the shearing force (T^*) is caused to alternate between $\pm T^*$, $T^* < \mu N$ the region $r < a'$ remains locked but the direction of slip in

the annular region also alternate. Johnson(45) provided convincing experimental evidence in support of various aspects of this theory. The contact surfaces of metal spheres which had been clamped together by a steady load and subjected to alternating shearing forces were also divided into two regions, a central circular region where the surfaces remained undamaged and an outer annular region heavily fretted. The dimensions of these regions accorded well with Mindlin's results. O'Connor and Johnson(46) and Goodman et al. (47,57) found further evidence that the coefficient of friction grows with repeated alternating slip. Johnson(48) calculated the amplitude of slip through the annular region. The maximum value of the amplitude of slip(α) occurs at the edge of the contact area and has the value :

$$\frac{\alpha}{a} = \frac{\pi (2 - \nu)}{8} * \frac{\nu P_0}{G} \left\{ \left[1 - \frac{2}{\pi} \sin \left(\frac{a'}{a} \right) \right] \left[1 - 2 \left(\frac{a'}{a} \right)^2 \right] + \frac{2}{\pi} \left(\frac{a'}{a} \right) \left[1 - \left(\frac{a'}{a} \right)^2 \right]^{1/2} \right\}$$

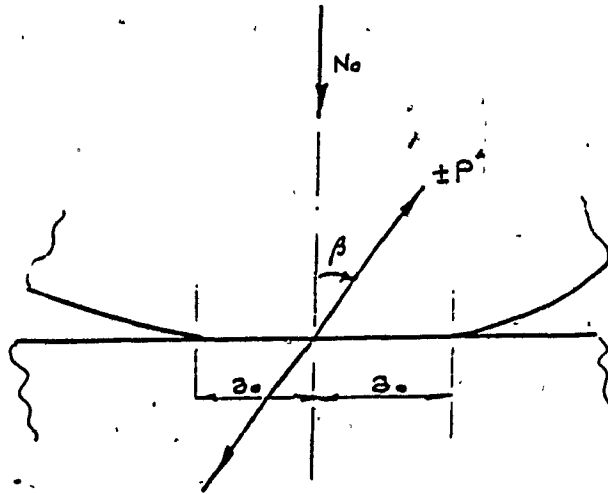
where :

$P_0 = 3N/2 \pi a^2 =$ The maximum Hertzian pressure

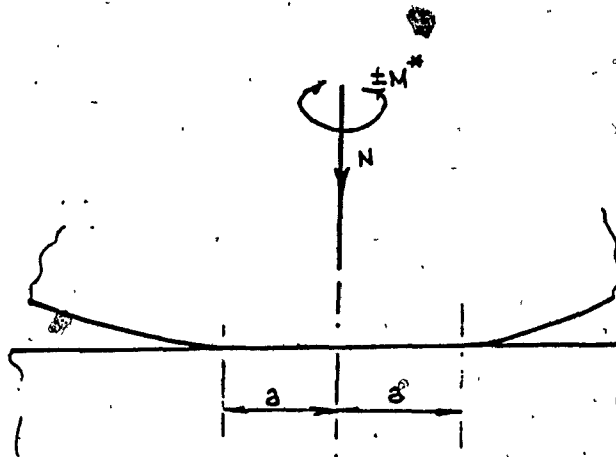
$G =$ Shear modulus of the material

$\nu =$ Poission ratio of the material

It should be noticed that the amplitude of slip (α) at the edge of the contact area increases with increasing the



(a)



(b)

Fig. (22) Spherical surfaces in contact subject to:
(a) An oscillating force of amplitude $\pm P^*$ at an oblique angle.
(b) An oscillating torsional couple of amplitude $\pm M^*$.
IDEALIZED FRETTING SITUATIONS . AFTER O'CONNOR (49) .

shearing force (T^*) until at the point of incipient sliding when

$$\left(\frac{T^*}{\mu N} \longrightarrow 1 \right) \text{ and } \frac{a'}{a} = 0 \text{ i.e.}$$

$$\frac{\alpha}{a} = \frac{\pi (2 - \nu)}{8} \frac{\mu P_0}{G}$$

Even at the point of incipient sliding, the maximum slip amplitude is several orders of magnitude smaller than the radius of the contact circle. It can be seen why some authors use the term 'micro-slip'. These results demonstrate the role which elastic stress analysis can play in the discussion of the fretting problem. As well as the elastic stress fields within the contacting solids, the extent of the slip region and the amplitude of slip can be determined. Mindlin's approach that contact surfaces slip, in order to relieve otherwise high concentration of shear stress on the interface, an effect entirely analogous to the onset of elastic deformation in ductile material. From this point of view, slip and fretting in clamped joints may be thought to have a beneficial effect. A further beneficial effect arises from the energy dissipated by friction. Such energy dissipation gives to the joint a damping capacity useful in controlling vibration and is an important source of structural damping.

3. 1. 1. 2 SPHERE ON FLAT MODEL

In this model Johnson and O'Connor (49) presented the contact of

spherical surfaces with a flat ones to study the frictional phenomena. Using this model it was possible to calculate the distribution of interfacial shear traction. The clamped joint is idealized as a spherical body pressed against a flat surface with a steady force (N_0) to give a circular area of contact of radius (a_0). The joint transmits either an oscillating force of amplitude $\pm p^*$ or an oscillating twisting couple M^* (as in Fig. 22 a and b respectively) by means of frictional traction acting at the interface. As the amplitude of the force or twisting couple was increased the region of micro slip spread inward until the two surfaces slide bodily, one over the other. The energy dissipated by friction in the fretting annular may be taken as a rough measure of the rate of surface damage that was measured by Johnson(48). Johnson's measurements of the energy dissipated per cycle as a function of the amplitude of the oscillating force were made for angles of inclination varying from 0° to 90° . The average angle of friction for the surface was about 29° ($\mu=0.56$). The experimental results are shown in Fig. 23. With $\beta = 0$, the oscillating force has the effect only of causing the normal pressure and area of contact to fluctuate. The measured energy dissipation (expressed as fraction of the maximum elastic strain energy of the cycle) exhibits a small constant value which represents the internal elastic hysteresis of the steel. The measurements with the oscillating force inclined at 10° and 20°

Johnson(48) Experimental result under:
 steady normal force $N_0 = 89\text{N. (20 lbs)}$
 Ball radius = 12.7 mm.
 Initial contact radius = 0.1956 mm.
 Frequency = 48 C/s .
 Ave. Coefficient of friction = 0.56.

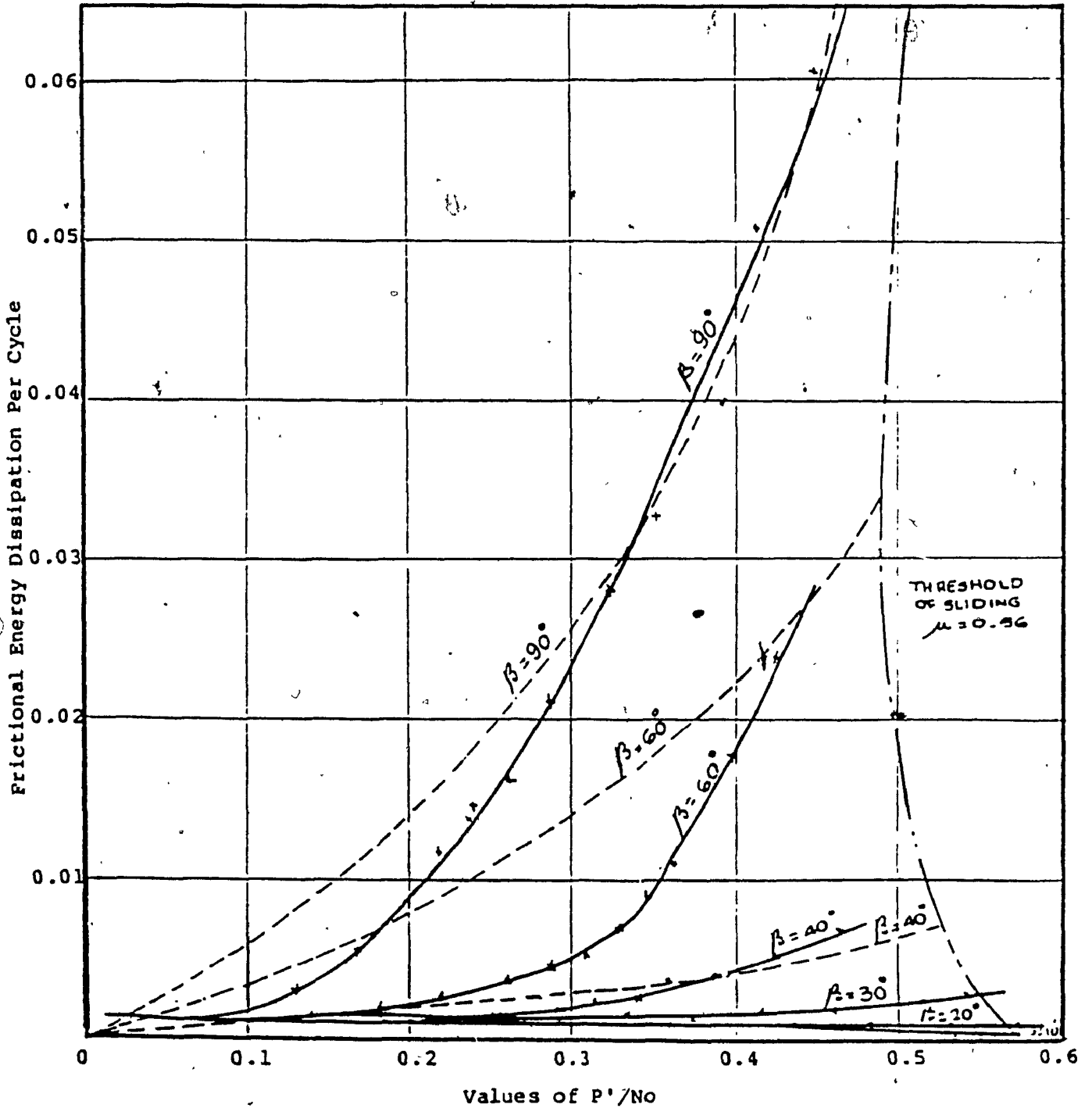
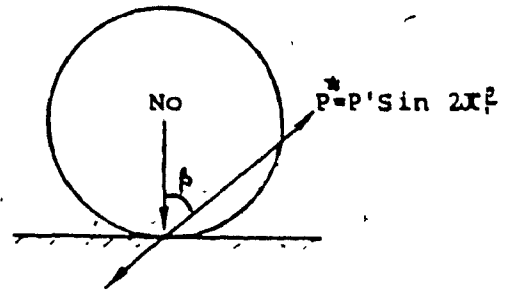


Fig.(23). Frictional energy dissipation at the contact of steel sphere and plate.

----- Theoretical curves (Mindlin and Deresiewicz 1953).
 ———— Experimental curves (Johnson (48) 1955).

to the normal are hardly distinguishable from those at 0° and no fretting of surfaces was detected. At 30° a ring of very small pits could be discerned and as the inclination of the force was increased a marked amount of fretting appeared until, at $\beta = 90^\circ$, the situation shown in Fig. 23 was obtained. It is evident that the prediction of slip resulting from the elastic theory was confirmed by the experiments.

3. 1. 2 CYLINDRICAL ON FLAT SURFACE MODEL

This model represents a cylindrical surface pressed in contact with a flat specimen carrying an alternating stress $\pm \sigma_{alt}$. As Fig. 24 indicates a Hertzian distribution of pressure (p) and frictional traction (q) result in a sharp finite stress concentration at C. For this case the distribution of shear traction $q(45)$ is given by the following relation:

$$q = q_0 \sqrt{1 - x^2/c^2} \quad 3. 1. 2. 1$$

where c = half width of contact between cylinder on a flat

x = variable width

The shear traction acting on the surface $|x| < c$, of a solid gives rise to a direct stress parallel to the surface (51):

$$\sigma_x = \begin{cases} -2q_0 \frac{x}{c} & , |x| < c \\ -2q_0 \left[\frac{x}{c} + \sqrt{x^2/c^2 - 1} \right] & , |x| < -c \end{cases} \quad 3. 1. 2. 2$$

Cylinders in contact over the interval $|x| < c$, when subjected

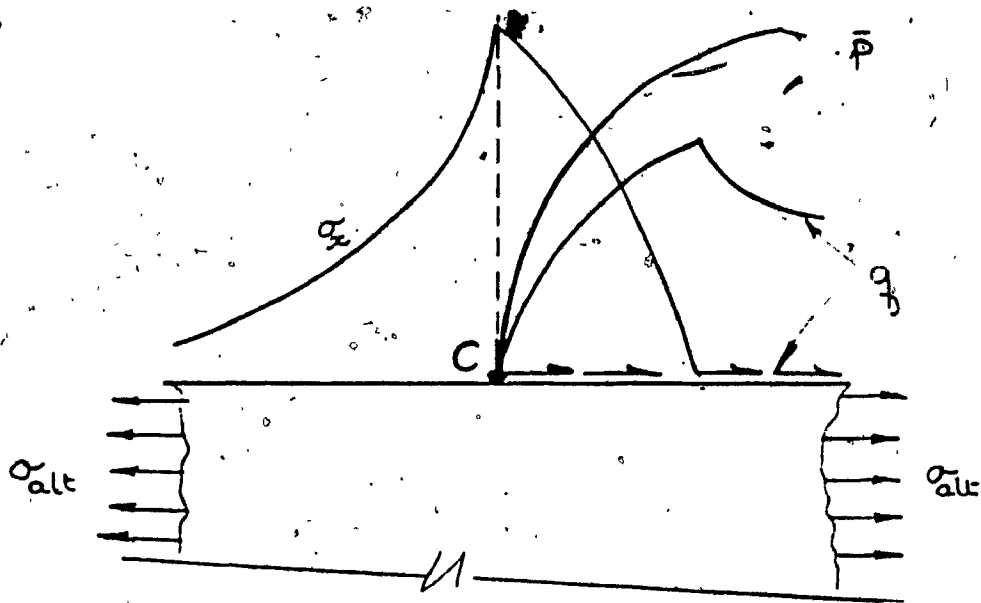


Fig. 24. Stress concentration at the edge of a micro-slip region. Shown a Hertzian distribution of pressure and frictional traction results in a sharp but finite stress concentration at C. After O'Conner(49)

to a tangential force $T < \mu N$ develop a surface shear traction q made up of :

$$q = q' = \mu p_0 \sqrt{1 - x^2/c^2}, \quad d < |x| < c \quad 3.1.2.3$$

$$q = \mu p_0 \sqrt{1 - x^2/c^2} - d/c \cdot \mu p_0 \sqrt{1 - x^2/d^2}, \quad |x| < d$$

3.1.2.4

where d is half width of adhesive region and is given by (52):

$$T/\mu N = 1 - d^2/c^2$$

Equation 3.1.3.2 is used to find the stress component σ_x , at the point C $(-c, 0)$, due to the surface traction given by the equations (3.1.2.3) and (3.1.2.4) thus:

$$\begin{aligned} |\sigma_x|_C &= (2 \mu p_0 \sqrt{1 - d^2/c^2}) \\ &= 2 \mu p_0 (T/\mu N)^{1/2}, \quad T < \mu N \quad 3.1.2.5 \end{aligned}$$

As it can be seen from equation 3.1.2.5, the peak contact stress adds to the alternating mean stress carried by the main member. Looking at the partial slip ($T < \mu N$), and remembering that p_0 is proportional to $N^{1/2}$, we see that the stress concentration at (A) increases with the value of μ and the amplitude of tangential force T , both raised to the $1/2$ power.

3.1.3 CYLINDER ON CYLINDER CONTACT MODEL

The system consists of two elastic cylinders with their axis parallel that are pressed together by a normal force N and transmits a shearing force T ($< \mu N$) by friction. The distribution of

surface shear traction (τ_{xy}) when the contact surfaces do not slip is given by the following relation (49):

$$\tau_{xy}(x) = q(x) = \frac{T}{2\pi a^n} \frac{1}{\sqrt{1 - x^2/a^{2n}}} \quad 3.1.3.1$$

where $q(x)$ is infinite at $x = \pm a^n$, so that slip is inevitable near these points. Now consider a film of thickness ($2t$), modulus of rigidity G_f is placed between the cylinders that are considered to be semi-infinite with contact on $y = \pm t$, $-a^n < x < a^n$ (see Fig. 25.). A normal force (N) and a tangential force (T) is applied to the system. Johnson and O'Conner (49) determined the distribution of shear traction $q(x)$ across the contact area as the thickness and rigidity of the film change. At the outset, both the surface displacements and traction at the interface are unknown. Let $u_f(x)$ be the tangential displacement of a point on the surface of the film relative to the plane of symmetry, $y = 0$, and let $u_s(x)$ be the tangential displacement of a point on the surface of the upper cylinder relative to an unstrained region of that cylinder, remote from the contact surface. The application of a tangential force (T) results in a relative tangential displacement (δ) between points in each cylinder remote from the contact surfaces. In case of the surfaces do not slip, the overall displacement was made of the sum of the elastic displacements of the solids and the film thus:

$$u_f(x) + u_s(x) = \frac{1}{2} \delta = \text{constant}, \quad |x| < a^n \quad 3.1.3.2$$

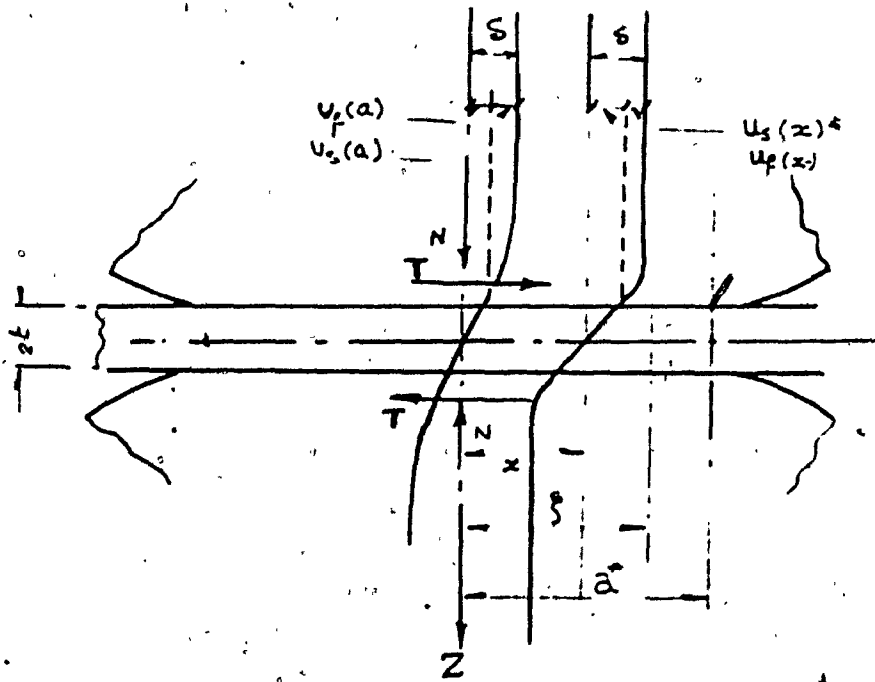


Fig. 25. Contact of two cylindrical solids separated by a thin elastic film. After O'Connor (49).

The stress boundary conditions on the interface ($y = \pm t$) are :

$$\begin{aligned} \tau_{xyf}(x) = \tau_{xys}(x) = q(x) & , |x| < a^n \\ = 0 & , |x| > a^n \end{aligned} \quad 3.1.3.3$$

As it was assumed in (49) the displacements u_f and u_s are functions denoted by F_f and F_s of the interface traction $q(x)$. Thus equation 3.1.3.2 becomes :

$$F_f(q, x, t, G_f) + F_s(q, x, G_s) = \partial/2 \quad , |x| < a^n \quad 3.1.3.4$$

Equation 3.1.3.4 is a formal statement of the problem of finding the shear traction on the interfaces in order to match displacements and stresses in the film and solids. Since the cylinders are assumed to be semi-infinite solids, then Boussinesq solution is applicable resulting in:

$$u_s(x) = \frac{1-\nu}{\pi G_s} \int_{-a^n}^{+a^n} \log |\xi - x| \cdot q(\xi) d\xi + \text{const} \quad |x| < a \quad 3.1.3.5$$

Substituting in eqn 3.1.3.4 and writing $X = \frac{x}{a^n}$, $\xi = \xi/a^n$

gives:

$$q(X) + \frac{1-\nu}{\pi} \cdot \frac{a^n G_f}{t G_s} \int_{-1}^{+1} \log |\xi - X| \cdot q(\xi) d\xi = \text{constant}, \quad |x| < a^n \quad 3.1.3.6$$

Eqn. 3.1.3.6 is Fredholm integral equation of second kind for $q(X)$. Exact solution to this eqn. is not yet available for the

values of $\omega = \frac{(1-\nu)}{\pi} \cdot \frac{a}{t} \cdot \frac{G_f}{G_s}$, however this equation was

examined in (49) to demonstrate the effect of the film on $q(X)$. For infinitely thin film, when $t/a^n \rightarrow 0$, $q(X)$ must have the form of equation 3.1.3.1 when t/a^n is large, the second term on the left-hand side of equation 3.1.3.6 will be compared to the first and hence:

$$q(X) = \text{constant} \qquad 3.1.3.7$$

It follows that when (t/a^n) has a small but finite value the surface traction will have a distribution somewhere between eqns. 3.1.3.1, 3.1.3.7. The distribution of $q(X)$ can therefore be modified between these limiting forms by suitable choice of (G_s/G_f) and (t/a^n) . The formulation of this problem demonstrated qualitatively the action of the film. In the contact of two cylinders without a film subjected to a tangential force, the condition of no slip requires that there be no vibration in the tangential displacement of points on the contact surface (eqn. 3.1.3.2 $u_f(x) = 0$). It is the requirement which leads to the shear stress concentration at the edge (eqn. 3.1.3.1). In composite contact deformation of the film, particularly near $x = \pm a^n$, reduces the tangential displacement on the cylinders near the edge of the contact area relative to the centre, so that the shear traction near the edge is decreased.

3.1.4 FLAT CIRCULAR CONTACT MODEL

The system consists of two large solid bodies, modulus of rigidity G_s in contact over a plane circular area of radius 'a'

on the surface ($z = \pm t$) of a film, modulus of rigidity G_f see Fig. 26. The approximate analysis of this model when a twisting moment (M) is applied has been developed by Johnson and O'Connor(49) and is summarized in this section. The cylindrical co-ordinates are used to describe the system which is symmetrical about the (z) axis the (z) = 0 plane. The displacement of a point is v, while $q(r)$ denotes surface traction (= $\tau_{\theta z}$ on $z = \pm t$). The displacement condition for no slip is given by:

$$v_f(r) + v_s(r) = \frac{\beta'}{2} r \quad |r| \leq a \quad 3.1.4.1$$

where : β' is the relative angle of twist of regions in the solids remote from the contact area. The stress boundary conditions on the interface remain the same, and the relation of displacement functions F_f and F_s (see eqn. 3.1.3.4) between surface traction and displacement were obtained by the following :

Let

$$q(r) = G_s \sum_{n=1}^N A_n \rho^{2n-1} \quad , \quad 0 < \rho < 1 \quad 3.1.4.2$$

$$= 0, \quad \rho > 1$$

where $\rho = \frac{r}{a}$ and A_n are coefficient to be determined with the assumption that the film deformed in simple shear, so that for F_f

$$v_f(\rho) = \frac{t}{G_f} \cdot q(\rho) = \frac{G_s t}{G_f} \sum_{n=1}^N A_n \rho^{2n-1} \quad 3.1.4.3$$

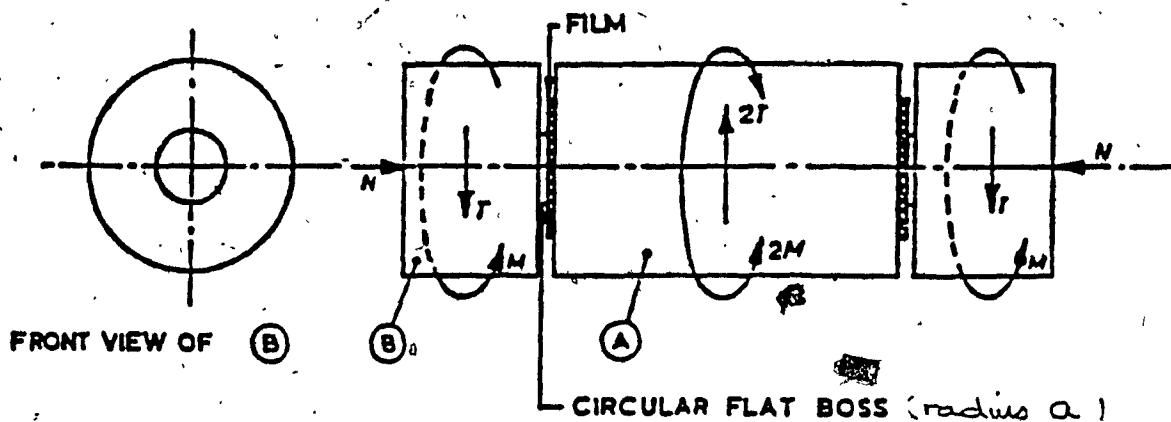


Fig. 26. Experimental arrangement of flat circular contact pressed together by a normal load N —the contact is then subject to either a tangential shear force T or a twisting couple M . After Johnson and O'Connor (49)

Consider the solid bodies to be semi-infinite, a general solution for the equations of elasticity for torsion problem (49) is :

$$v_s(\rho) = \frac{a}{G_s} \int_0^{\infty} \bar{q}(\xi) J_1(\xi\rho) d\xi \quad 3.1.4.4$$

where:

$\bar{q}(\xi)$ is function determined from the boundary conditions

$J_n(x)$ is Bessels functions. Then:

$$q(\rho) = \int_0^{\infty} \xi \bar{q}(\xi) J_1(\xi\rho) d\xi \quad 3.1.4.5$$

Note that $\bar{q}(\xi)$ is the Hankel transform of $q(\rho)$:

$$q(\xi) = \int_0^{\infty} \rho q(\rho) J_1(\xi\rho) d\rho \quad 3.1.4.6$$

$$= G_s \sum_{n=1}^N A_n \int_0^1 \rho^{2n} J_1(\xi\rho) d\rho$$

$$q(\xi) = G_s \sum_{n=1}^N A_n \sum_{m=1}^n (-1)^{\frac{m-1}{2}} \frac{(n-1)!}{(n-m)!} \frac{J_{m+1}(\xi)}{m} \quad 3.1.4.7$$

where v_s may be obtained from eqns. 3.1.4.5 and 3.1.4.7. The calculation involves evaluation of integral of the type:

$$\int_0^{\infty} (\xi)^{-m} J_{m+1}(\xi) J_1(\xi \rho) d\xi$$

which can be expressed in terms of the complete elliptic integrals $K(\rho)$ and $E(\rho)$. Substituting for v_f and v_s into eqn.

3.1.4.2 and reducing a set of linear simultaneous equations for the coefficients A_n are obtained:

$$\Omega \sum_{n=1}^N a_n \rho^{2n-2} + \frac{1}{(\rho)} F(a_n, \rho) = 1 \quad 3.1.4.8$$

where: $\Omega = \frac{G_s t}{G_f a}$, F is the function obtained by evaluation of

$v_s(r)$ and $a_n = \frac{A_n}{B_n}$ these equations have been solved for the

values of a_n for a range of values of Ω

Since $M = 2 \pi \int_0^a q(r) r^2 dr$, the relative torsional compliance

can then be calculated ($T = \beta/2M$). The value obtained by Mindlin for no film was considered in (49) as:

$$T_0 = \frac{3}{16 G_s a^3} \quad 3.1.4.9$$

Hence

$$T/T_0 = \frac{8}{3 \pi} \frac{1}{\sum_{n=1}^N \frac{n}{2n+2}} \quad 3.1.4.10$$

The solution for the tangential force is obtained in similar manner the same form of F_f is assumed, while F_s corresponding to a traction in the form of a series of even power of (r) is obtained by integrating Cerruti's solution for half space. The response of the film surface to a pressure distribution of the form:

$$P(\rho) = G_s \sum_{n=0}^{N1} \beta_n \rho^{2n} \text{ was obtained by using bi-harmonic}$$

stress function, polynomials in (r) and (z) , assuming the surface $(r = a)$ to be free of stress and ignoring the component C_{rz} on $z = t$ which of order (t/a) compared with $p(r)$. the film material is assumed to be incompressible. For further details see reference(53). The surface stress distribution obtained from each of these calculation are shown in Fig. 27, Fig. 28 and Fig. 29. It will be seen that increasing (Ω) rapidly reduces the severe stress concentrations at $(r = a)$. If transmitting an oscillating torque of amplitude M , it was found that the critical amplitude ratio at which fretting would first be observe is given by :

$$\frac{M^M}{M_s} = \frac{\sum_{n=0}^{N1} b_n}{\sum_{n=0}^{N1} \frac{b_n}{2n+3}} \times \frac{\sum_{n=1}^N \frac{a_n}{2n+2}}{\sum_{n=1}^N a_n} \quad 3.1.4.11$$

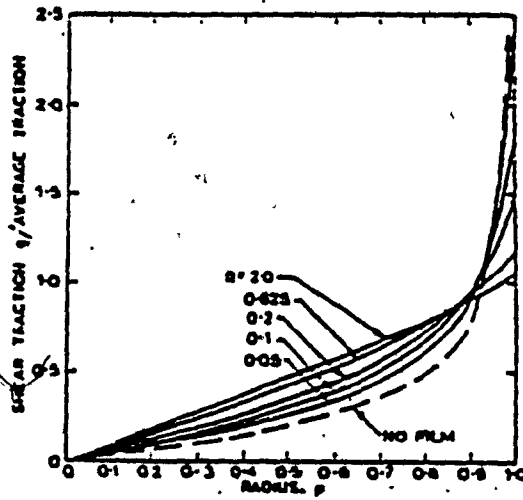


Fig. 27. Distribution of shear traction on flat circular contact subject to a twisting moment M

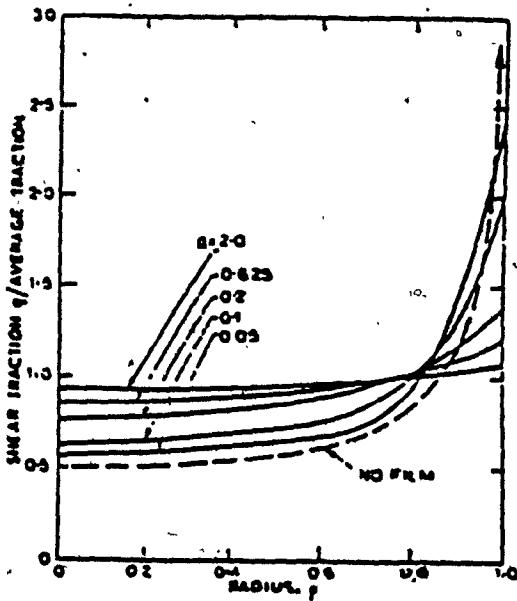


Fig. 28. Distribution of shear traction on flat circular contact subject to a tangential force T

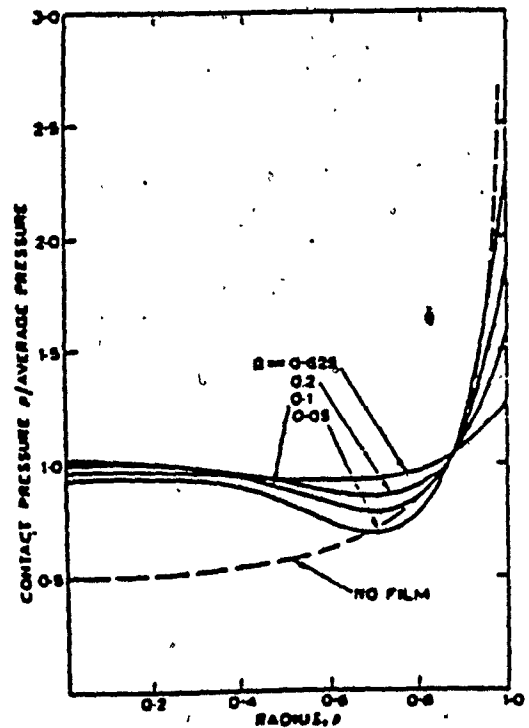


FIG 29. Distribution of normal pressure on flat circular contact

where M_s is the torque required to produce sliding and a_n, b_n are the coefficients obtained from the torsion and normal load calculated respectively. When $\Omega = 0$ and the stress distribution

exhibits singularities at $r = a$, i. e. $\frac{M^*}{M_s} = \frac{8}{3\pi} = 0.85$ when Ω is large and the stress distribution approach their limiting shapes,

$$\frac{M_n}{M_s} \rightarrow 0.75$$

these results are compared with experiment in Fig. 29.

In conclusion the analysis yields the distribution of contact stress and values of tangential and torsional compliance of the contact for variation in the parameters $\Omega = G_s t / G_f a$. In the contact subjected to a normal force N and a twisting couple M , the value of the critical friction ratio M^* / M_s (M_s is the torque required to cause bodily sliding), at which slip and fretting would first occur, was also found.

3. 1. 5 FLAT ON FLAT MODEL

J. S. Chung, et al. (54) carried out the analysis of specific physical system consists of a rectangular plate and two smaller fretting pads of a unit thickness, which exert on each other pair of equal and opposite transverse forces, N^* as shown in Fig. 30. The plate is fixed along one end and subjected to a cyclic axial force Q_0 acting at the other end. Under the action of cyclic load, the plate elongates and shortens as a function of time, and frictional force develop between the plate and the fretting pads. The investigators specifically analyzed the stress produced in the

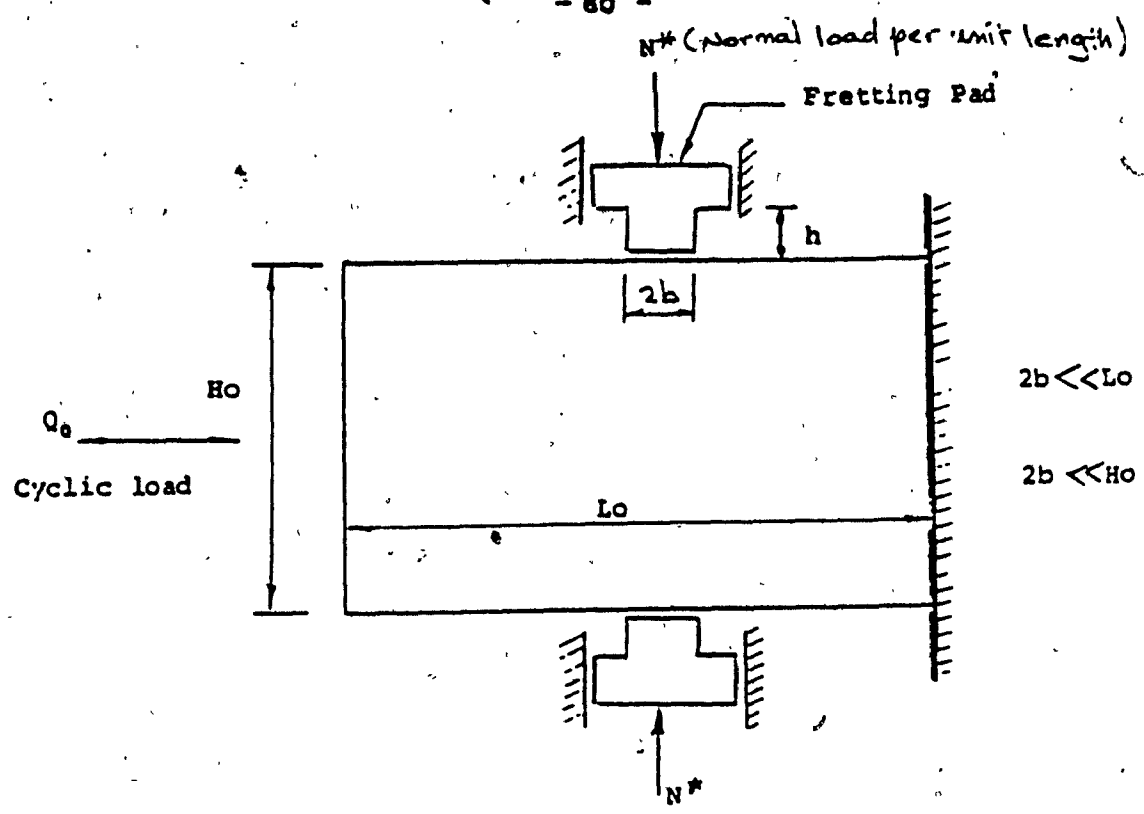


Fig. 30 . Physical system analyzed.
After Hoepfner et al (54) .

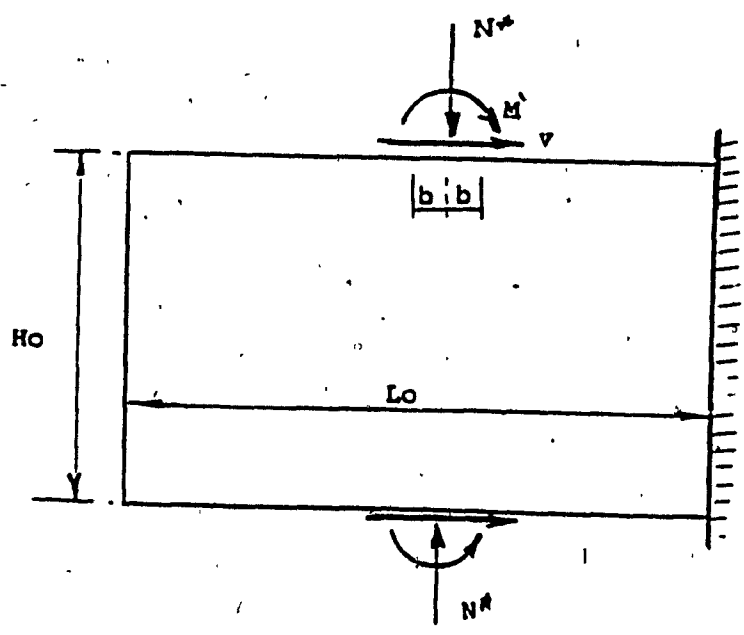


Fig. 31 . Load used in flat on flat model.
After Hoepfner et al (54) .

plate by the combined action of the cyclic axial load, and the normal and frictional forces that occur between the plate and the fretting pads. The analysis was presented with the following assumption:

- 1 - The material is homogeneous, isotropic and linearly elastic.
- 2 - The frequency of the cyclic load is much lower than the lowest natural frequency of the plate, thus it does not involve any substantial dynamic effect.
- 3 - The plate is thin. So that the problem can be approximated as a "plane stress" problem.
- 4 - The length of the contact area is much smaller than the dimensions of the plate i.e. $2b \ll L_0$, $2b \ll H_0$ as indicated in Fig. 30.
- 5 - Letting N^* , V and M' denote the stress resultants exerted by the fretting pad see Fig. 31, thus:

$$V = \mu N^* \quad 3.1.5.1$$

$$M' = \frac{Vh}{2} \quad 3.1.5.2$$

where :

μ = friction coefficient.

h = outstanding height of the fretting pad

Eqn 3.1.5.2 was based on the assumption that the fretting pad behaves essentially as a column prevented against rotation at both ends

- 6 - The distributed normal stress q_N^* and q_M' associated with N^* and

M vary in accordance with the ordinary theory of beams, thus:

$$q_N''(x) = \frac{N''}{2b} \quad 3.1.5.3$$

$$q_M'(x) = \frac{M'x}{I} = \frac{3 \mu N'' h}{4 b^3} x \quad 3.1.5.4$$

where I = is the moment of inertia.

The coordinate system (x, y) is as shown in Fig. 32. q_N'' and q_M' are considered positive when compressive. It is further assumed that no separation occurs between the plate and the fretting pads. i. e.

$$q_N'' + q_M' > 0 \quad 3.1.5.5$$

at all contact points. Since slippage is considered to have taken place in few cycles of loading it was considered to be reasonable to express the friction stress distribution (S) as follows (54):

$$S = \mu (q_N'' + q_M') \quad 3.1.5.6$$

except near the corner of the fretting pads where $S = 0$ from theoretical consideration. The classical solution for the case of a semi-infinite plate subjected to a concentrated normal load N'' is shown in Fig. 33a. The stress distribution is given by (42).

$$\sigma'_r = \frac{2 N'' \sin \theta}{r} \quad 3.1.5.7a$$

$$\sigma'_\theta = 0 \quad 3.1.5.7b$$

$$r'_\theta = 0 \quad 3.1.5.7c$$

In case of a tangential force (T) as known in Fig. 33b. The corresponding expression is :

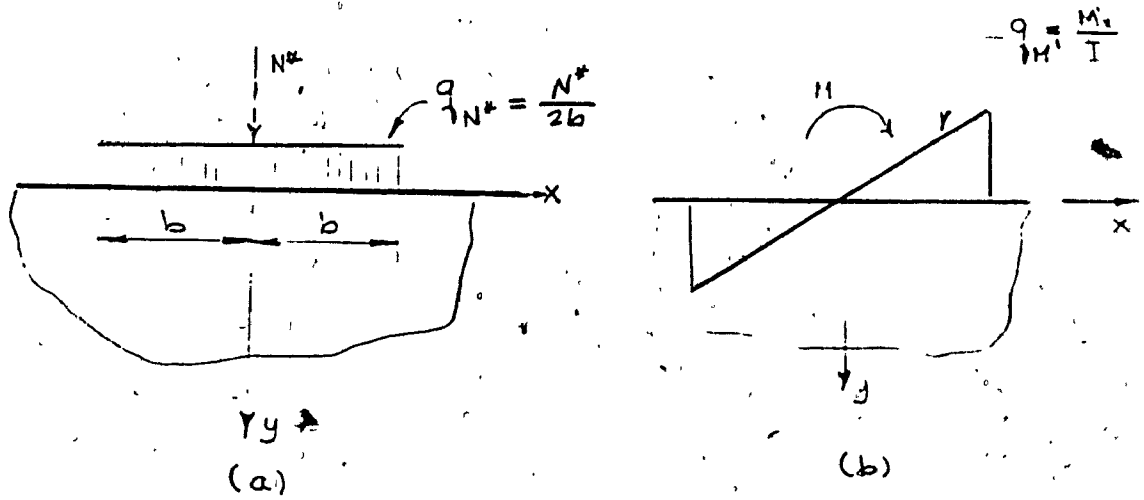


Fig.32. Distribution of contact loads.

(a) Effect of N^* (b) Effect of M'

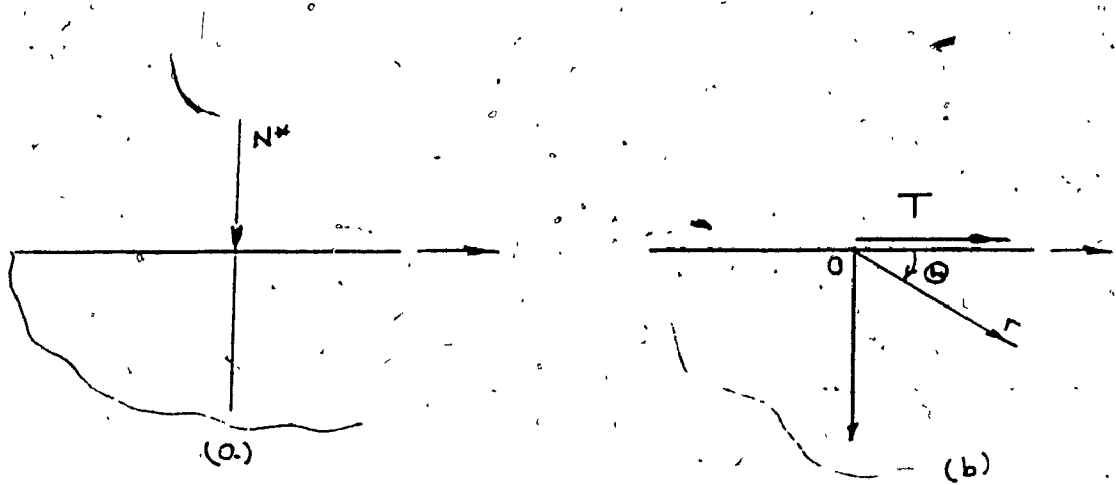


Fig.33. Classical solution

(a) Normal Force (b) Tangential Force

After Chung et al (54).

$$\sigma_{\theta}^{\prime} = - \frac{2 T}{\pi} \frac{\cos \theta}{r} \quad 3.1.5.8a$$

$$\sigma_{\theta}^{\prime} = 0 \quad 3.1.5.8b$$

$$\tau_{\theta}^{\prime} = 0 \quad 3.1.5.8c$$

These two classical solutions, used in conjunction with the principle of superposition, based on all the analytical results were presented by Chung et al. (54). It was concluded that the stresses produced in the plate by N^{\prime} , M^{\prime} and V were decreased rapidly as the distance from the contact area increases. It follows that in analyzing the stresses in general vicinity of a particular fretting pad, the contribution of other fretting pad can be neglected without introducing any substantial errors (54).

The overall stress at an arbitrary point of interest can thus expressed as:

$$\sigma_x = (\sigma_x)_0 + (\sigma_x)N^{\prime} + (\sigma_x)M^{\prime} + (\sigma_x)V$$

$$\sigma_y = (\sigma_y)_0 + (\sigma_y)N^{\prime} + (\sigma_y)M^{\prime} + (\sigma_y)V$$

$$\tau_{xy} = (\tau_{xy})_0 + (\tau_{xy})N^{\prime} + (\tau_{xy})M^{\prime} + (\tau_{xy})V$$

$$\text{In which : } (\sigma_x)_0 = \frac{Q_0}{H_0}$$

$$(\sigma_y)_0 = 0$$

$$(\tau_{xy})_0 = 0$$

The above equations present the stress produced by the maximum tensile value of the cyclic load Q_0 . Numerical solutions (54) were obtained for the physical system shown in Fig. 30 to verify the role of the coefficient of friction (μ) as it is vary with the

number of cycles for specific cases i.e when $\nu = 0, 0.2, 0.4, 0.6$ and 0.8 and $\alpha' = 0, 1, 5$ and 10 , where :

$$\alpha' = \left(\frac{Q_0/H_0}{N^*/b} \right) = \left(\frac{\sigma_0}{N^*/b} \right),$$

$\frac{Q_0}{H_0}$ = maximum value of axial cyclic stresses, and

N^*/b = twice the average normal contact load under fretting pad

The fretting pad height (h) was assumed to have a fixed value,

$h = 0.2b$. For each set of values of the problem parameters the

state of stress was determined numerically (54) at a total number

of 861 points in the general vicinity of each fretting pad,

namely at all points of a grid system defined by $\Delta x, \Delta y =$

$b/10$ in the region : $-2b \leq x \leq 2b$, $0 \leq y \leq 2b$.

The principle stresses and the maximum shear stresses were

obtained for each point (54) by treating the problem as two

dimensional one from the equations:

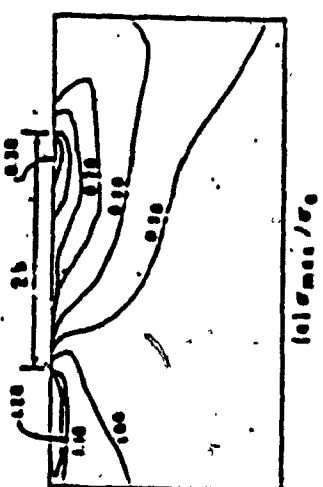
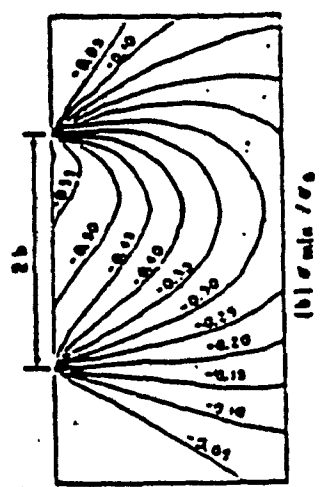
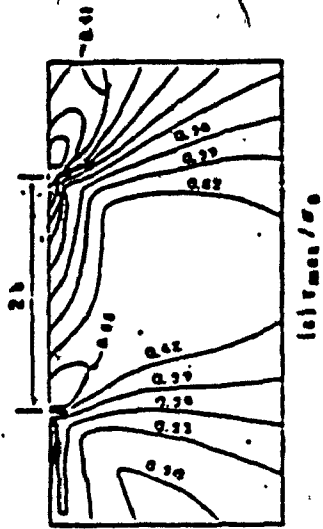
$$\sigma_{\max} : \sigma_{\min} = \frac{\sigma_x + \sigma_y}{2} \pm \left[\left[\frac{\sigma_x - \sigma_y}{2} \right]^2 + \tau_{xy}^2 \right]^{1/2}$$

$$\tau_{\max} = \left[\left[\frac{\sigma_x - \sigma_y}{2} \right]^2 + \tau_{xy}^2 \right]^{1/2}$$

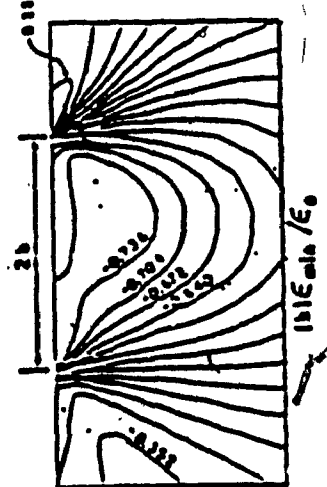
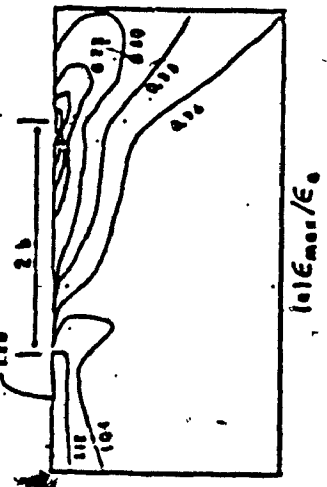
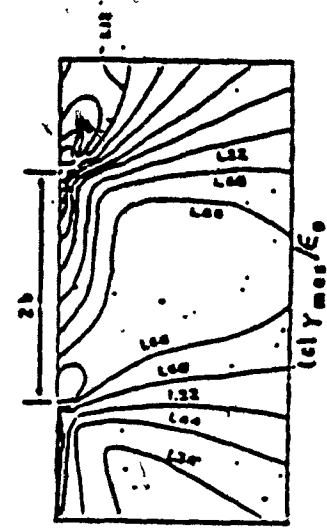
Stress and strain contour diagrams were constructed for σ_{\max} ,

σ_{\min} , ϵ_{\max} , ϵ_{\min} and τ_{\max} . Examination of figures (34-36) show that

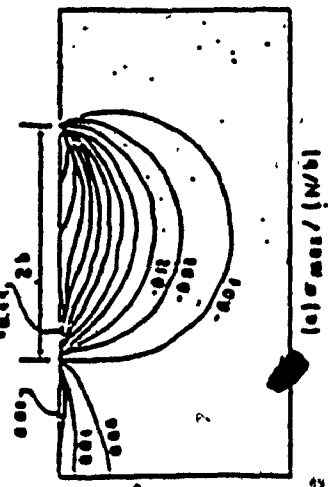
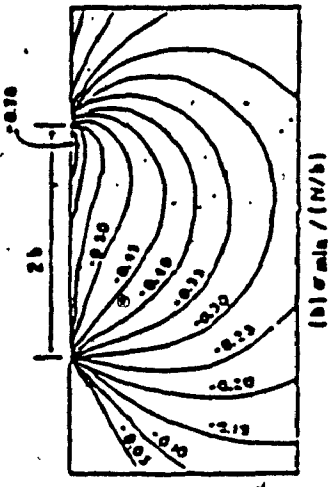
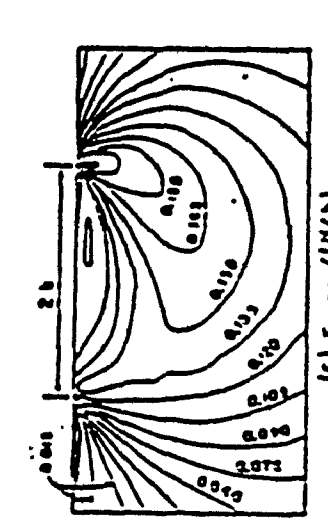
the stress produced by the load N^*, M', V represent essentially



34A - Stress Contour Lines ($\alpha = 0.1, \mu = 0.4, \lambda/\beta = 0.3$)



34B - Strain Contour Lines ($\alpha = 0.1, \mu = 0.4, \lambda/\beta = 0.3$)



34C - Stress Contour Lines ($\alpha = 0.1, \mu = 0.4, \lambda/\beta = 0.3$)

After. Chung et al (54).

localized phenomenon provided $2b \ll L_0$ and $2b \ll H_0$. The conclusion was that the maximum region of tensile stress occurs on the plate immediately outside the contact area, whereas minimum region of tensile stress occurs on the plate immediately inside the contact area (Figs. 34A, C-36). The maximum shear stress varies substantially from one case to another. In most cases the shear stress reaches local maximum in different points some of which lie on the surface near the edge of contact and under the fretting pad for a depth of $y \approx b$ (Figs. 34A, C-36). Some shear stresses were below the surface of contact under the fretting pad (Fig. 35 B, C). It is important to recall in this connection that τ_{max} in Figs. 34-36 refer to maximum shear stress in the plane stress sense. When σ_{max} , σ_{min} have the same sign, τ_{max} in the three dimensional sense would have to be obtained as one half the numerically greater principal stress. According to the linear theory analysis the question of crack initiation and propagation would normally be most critical on the edge of the plate immediately outside of the contact area because of:

- (1) The maximum values of the principal stresses and strains occur in that region.
- (2) The surface abrasion associated with the fretting action which would conceivably produce additional stress concentration, which was not included in this analysis.

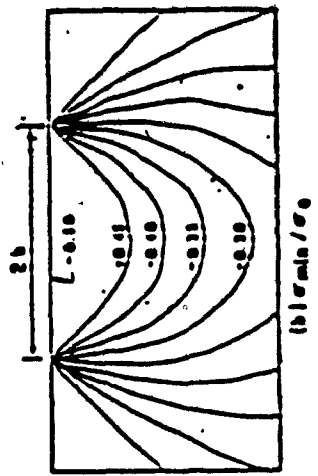
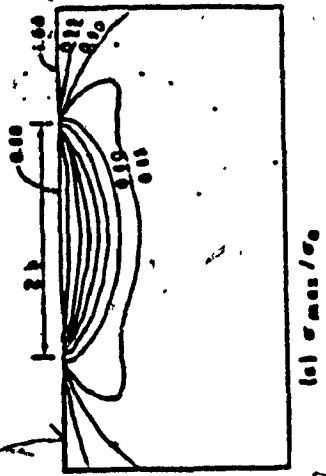


Fig. 35A. — Stress Contour Lines ($\mu = 0.1$; $\nu = 0.6$; $\lambda/b = 0.3$)

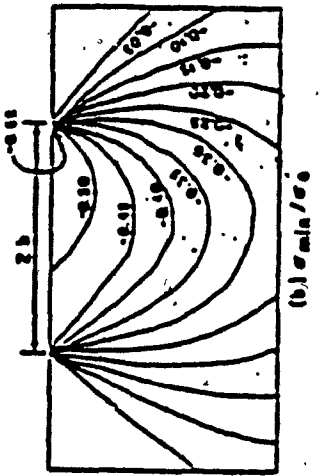
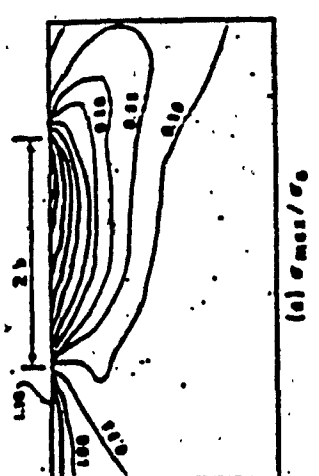
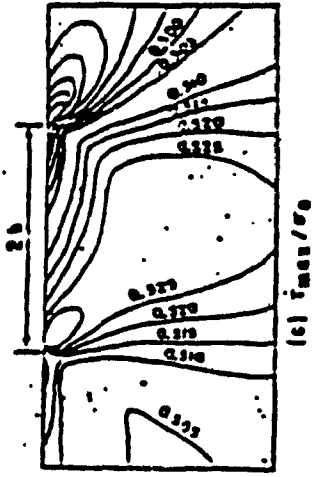


Fig. 35B. — Stress Contour Lines ($\mu = 0.1$; $\nu = 0.7$; $\lambda/b = 0.3$)

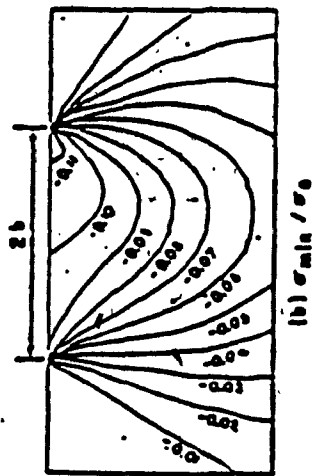
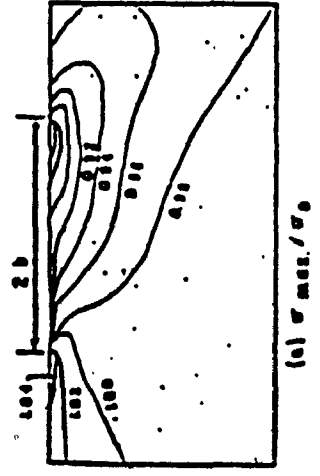
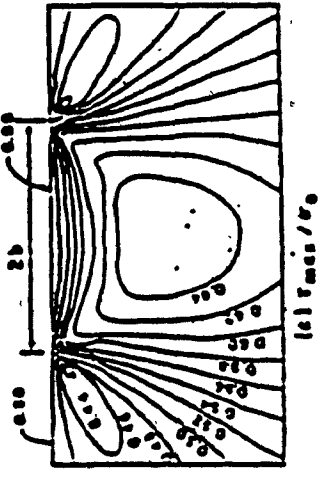
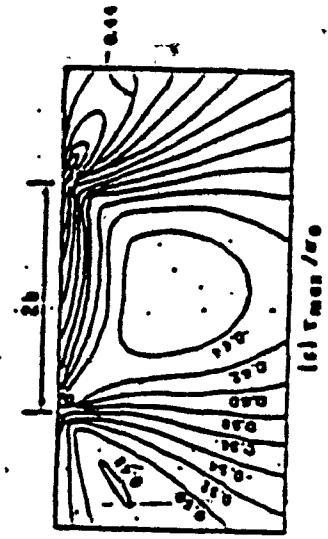
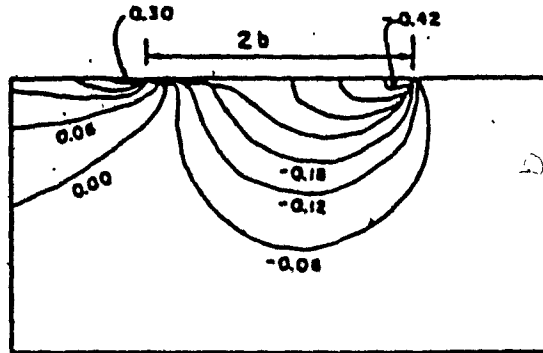


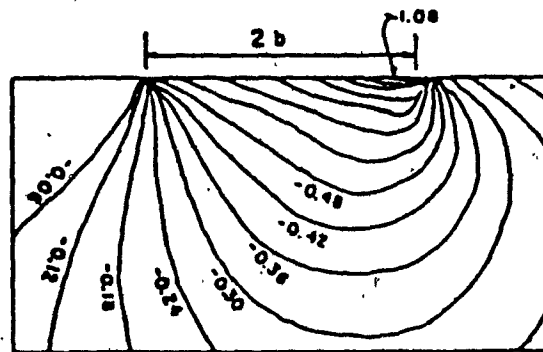
Fig. 35C. — Stress Contour Lines ($\mu = 0.1$; $\nu = 0.3$; $\lambda/b = 0.3$)



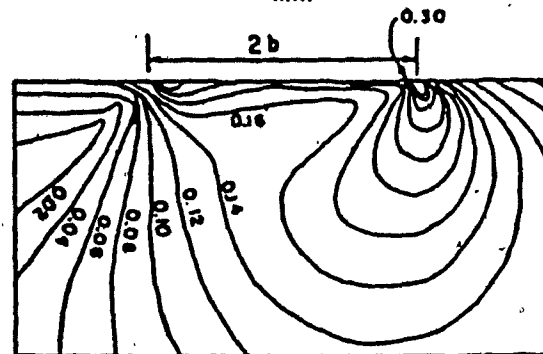
After. Chung et al (54).



(a) $\sigma_{max} / (N/h)$



(b) $\sigma_{min} / (N/h)$



(c) $\tau_{max} / (N/h)$

FIG 36 — Stress Contour Lines ($\alpha = 0; \mu = 0.4; \lambda/b = 0.2$)
After. Chung et al (54).

This observation is consistent with the experimental results reported by various investigations(65,66). It is conceivable, that the cracks could also be initiated at some subsurface points as a result of various contributing factors such as(1) stress concentration associated with localized discontinuities or(2) deviations from the linear stress distribution presented here which is due to residual stress or due to nonlinearity in stress behaviour.

3.2 JUSTIFICATION OF THE THEORETICAL MODELS

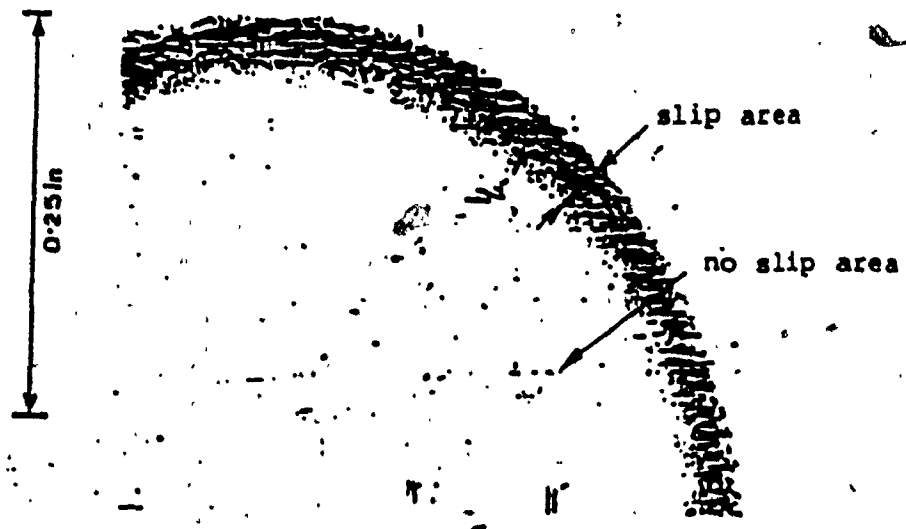
This section examines the available experimental results reported in the literature to confirm or deny some of theoretical models presented in section 3.1

3.2.1 SPHERE ON SPHERE MODEL EXPERIMENT

An experimental investigation of the torsional arrangement was first made by Tomlinson, Theorp and Gough(56). In the experiments work carried out by Johnson(45,48), the fretted specimens were subjected to an oscillating force, first with the force acting tangential to the contact surface(45) and later with an oblique force(48). Further careful experiments have been made by Goodman and Brown(57). A wide variety of material have been tested by Klint(58). With the exception of an oscillating force inclined at a small angle to the normal, all of these experiments revealed a similar pattern of micro-slip and fretting damage. The contact circle was divided quite sharply into the central circular region which was undamaged and an annular area in which

central circular region which was undamaged and an annular area in which oscillating micro-slip produced the familiar form of surface damage and corrosion shown in Fig. 37. It was observed that as the amplitude of the force or twisting couple was increased the region of micro-slip spread inward until the two surfaces slid bodily, one over the other. The measurements of the energy dissipated by friction in the fretting annulus taken by Johnson (46,49) Mindlin, Deresiewicz and others (59-61) confirmed the theory of elastic contact stress of spheres in contact subjected to oscillating force and twisting couple.

The experiments have demonstrated the necessity of micro-slip in an annular region under the action of the smallest forces, or couples, otherwise the interface would be called upon to transmit an infinite shear traction at the periphery of the contact circle. On the assumption that the shear traction in the slip region takes on a limiting value $q = \mu p$, where μ is a constant coefficient of friction, the theory predicts the compliance of the joint and the rate of frictional energy dissipation. A special case arise when the line of action of the oscillating force p^N lies within the cone of friction i. e when $\tan \beta < \mu$. Here Mindlin and Deresiewicz (60) showed that no micro-slip or energy dissipation would be expected. The experiments reported in references (45, 48, 56- 58) supported the theoretical picture on almost all accounts. It should however



Fig(37) Annular region of micro-slip showing fretting damage at the contact of steel spheres produced by an oscillating tangential force. (Areas are divided into slip and no slip according to Mindlin's theory). After Johnson(45).

be noted that the measurements of energy dissipation, particularly those made by Johnson(45, 48), depart from the theoretical predictions in one significant respect. At moderate force amplitude (i.e about a half the limiting friction force) the measured energy losses decrease with repeated oscillation to a value appreciable less than would be expected by theory. This effect was attributed to a change in the effective coefficient of friction brought about by repeated slip due to the effect of surface asperities.

3. 2. 1. 2 SPHERE ON FLAT EXPERIMENT

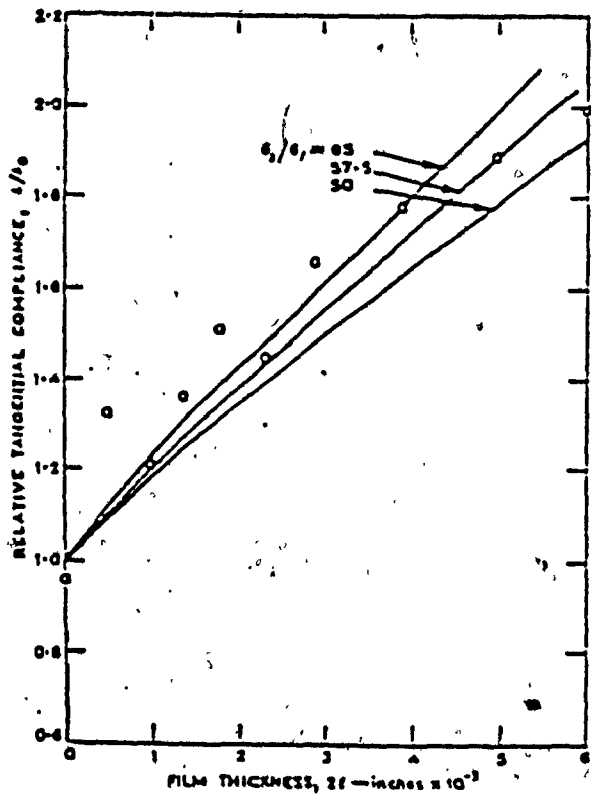
Experiments on the contact of hard steel sphere with a plane surface Johnson(45) has produced a striking evidence of fretting over an annular area as the elastic theory predicts. Measurements of the energy dissipated per cycle as a function of the amplitude of the oscillating force for angles of inclination of the oscillating force varying from 0° to 90° are shown in Fig. 23 (45).

The figure shows that when the oscillating force exceeds about 0.5° ($\mu = 0.56$) the surface slides as a whole. Below this value, the energy dissipated per cycle becomes a measure of the area over which slip takes place. At 30° inclination, a ring of very small pits could be discerned and at 90° the situation shown in Fig. 23 was obtained. The annular region of contact confirms that described by Tomlinson, Theorp and Gough (56). All investigators have chosen situations represented by the right-hand region of

Johnson's diagram, that is when bulk sliding takes place. This is because fretting damage is best studied quantitatively when sliding conditions are adjusted to produce gross slip at the contacting surfaces of such a magnitude that the elastic discrete scuff marks appeared that rapidly developed into almost continuous failure. The friction force rose slowly with the load during the early part of the test, the initial scoring being accompanied by sharp pressure peaks that grew progressively until erratic friction indicated gross damage by scuffing. This examination had enabled a definite sequence of evidence during the passage of a single contact across the surface to be established. At the lighter loads the surfaces are improved by smoothing of the asperities remaining from grinding. As the load increased the higher temperatures at the point of contact cause burnishing of the surfaces, accompanied by metallurgical change in local area of the material.

3.2.2 CIRCULAR FLAT CONTACT EXPERIMENT

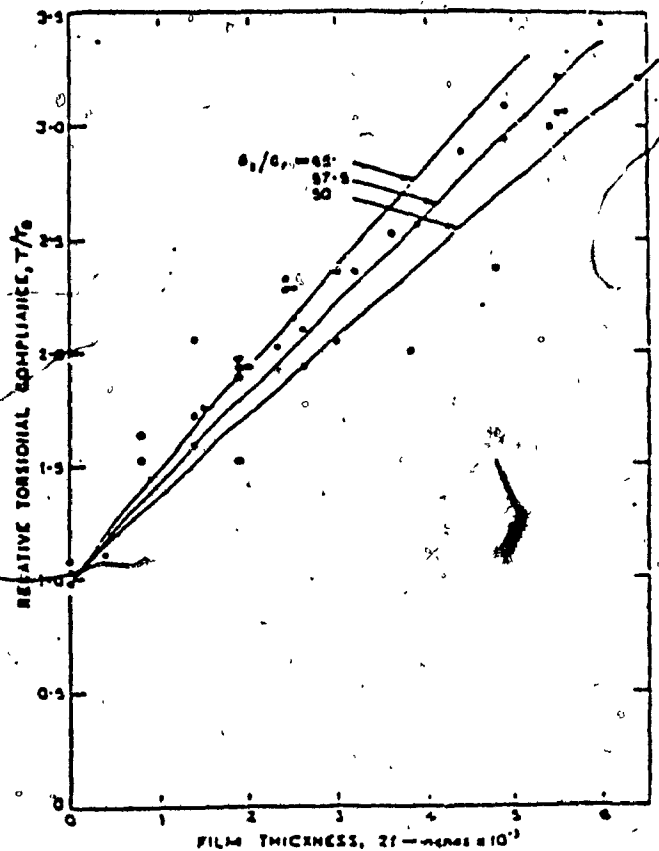
The system in section 3.1.4 has been described in (62) and is shown in Fig. 26. Measurements for the tangential and torsional compliance of the contact were made for films of thickness from 0 to 0.15mm by taking slope at zero load of the deflection curve. The compliance of the contact with no film present ($t = 0$) agreed reasonably well with Mindlin's theory for both tangential and torsional loads. The results are shown in Fig. 38 and Fig. 39. In



$a = 0.24$ in.

Theoretical compliance with no film, $\delta_0 = 1.56 \times 10^{-6}$ in./ton.

Fig. 38. Variation of tangential compliance of flat circular contact with film thickness: theoretical and experimental



$a = 0.26$ in.

Theoretical compliance with no film, $T_0 = 0.382$ sec lb in.

Fig. 39. Variation of torsional compliance of flat circular contact with film thickness: theoretical and experimental

both instances the compliance is shown as multiple of the theoretical value. These measurements were made to check the accuracy of the predicted compliance (eqn. 3.1.4.11 in the theory of circular contact). A direct comparison using an independently determined value of G_S/G_f was not made. The film material could be cast only in very thin layers which did not permit a simple independent measurement of elastic modulus. For the purpose comparison, the three solid lines shown in Fig. 38 and Fig. 39 are the predicted compliance values for the three values of G_S/G_f . It appeared that the two sets of experiments are consistent with each other and with the theory if $G_S/G_f \approx 57.5$

CHAPTER 4

FRACTURE MECHANICS FOR PREDICTING FRETTING FATIGUE

4.1 INTRODUCTION

Any discussion of fatigue must be related to the movement of dislocations under the influence of applied stress. The threshold stress to cause a dislocation to move is very small; it can be the so-called Peierls-Nabarro force and therefore cycling stress well below the elastic limit will involve oscillating the dislocations (65). It is only at the yield point that Frank-Read sources begin to operate and results in a massive increase in the number of dislocations and the consequent plastic deformation. The observations of Forsyth were explained in terms of the movement of dislocations on parallel or intersecting slip planes. Two examples are shown in Fig. 40. The type of dislocation structures formed during fatigue depends on the Stacking-Fault energy of the material. A low Stacking-Fault energy makes cross-slip from one slip system to another difficult by dislocation and intersecting planar arrays of dislocations are formed. At high Stacking-Fault energy, cross slip occurs leading to the formation of cellular structures. The relation between type of dislocations array and Stacking-Fault energy as a function of the number of cycles to failure is shown in Fig. 41.

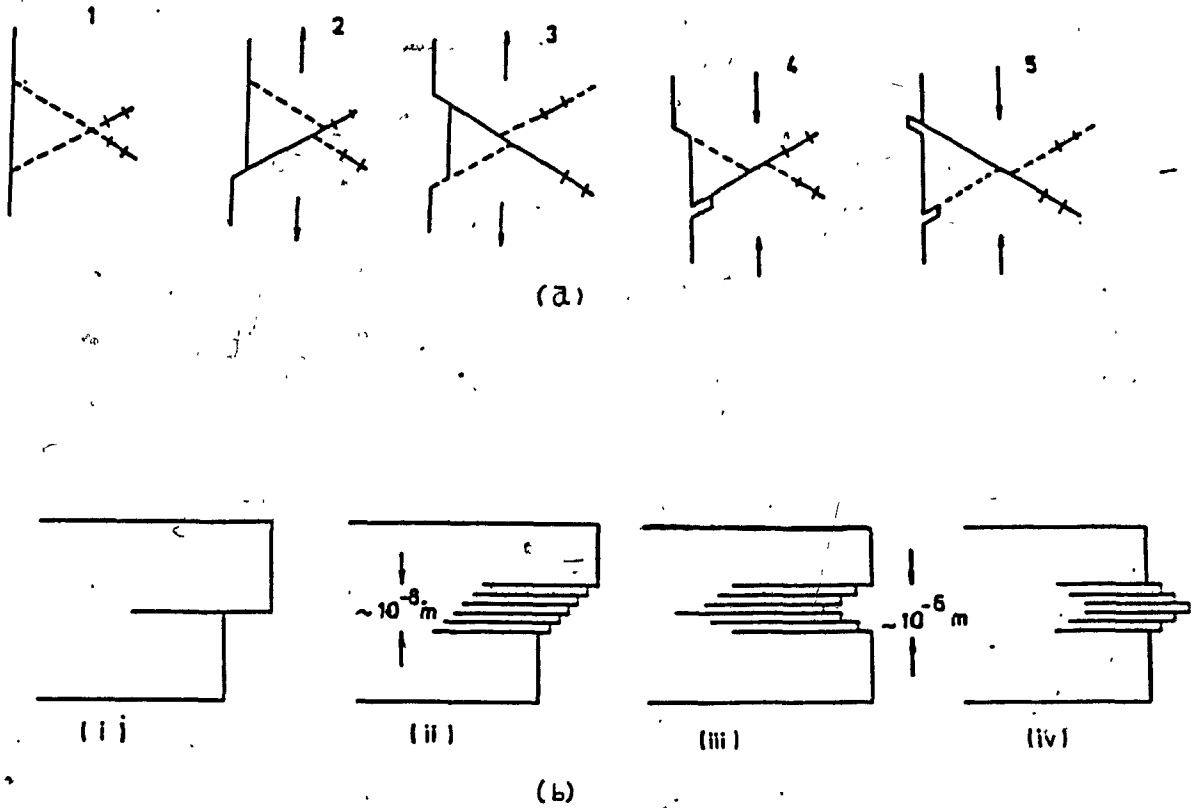


FIG. 40. Possible mechanisms for the formation of persistent slip bands on the surface of a test-piece. (a) intersecting slip systems; (b) parallel slip systems. After Waterhouse (65).

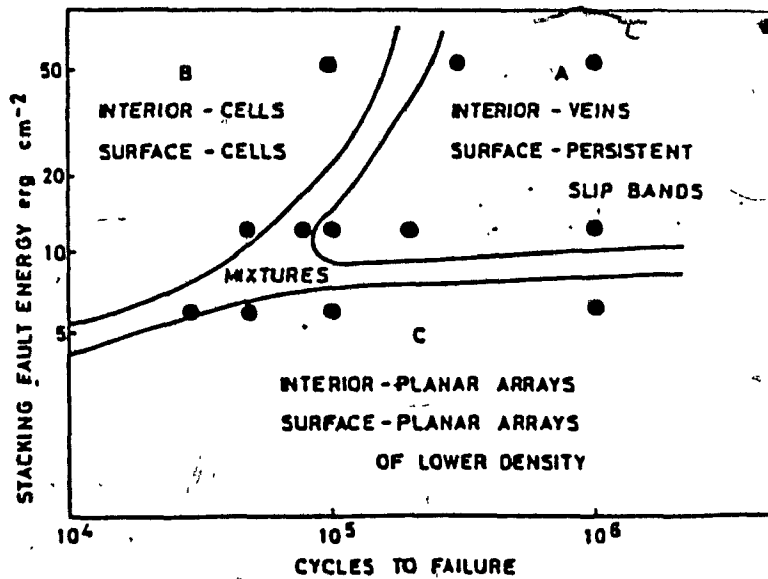


FIG. 41. Dislocation arrangements near the surface and within the material in a face-centred cubic metal as a function of stacking fault energy and stress amplitude—high stress amplitude = low number of cycles to failure.¹⁴ After Waterhouse, (65).

Initially the nucleated fatigue crack grows in the shear mode, i. e. at an angle of 45° to the applied principal stress, designated as stage I. This is because the slip occurs on the slip system where the resolved shear stress is maximum, i. e. on the slip plane most nearly at 45° to the direct stress (Fig. 42). The length of stage I crack depends on the stress level and the environment. Low alternating stress and corrosive atmosphere encourage stage I crack growth. In stage II, the growth of the crack is dominated by tensile stresses at the crack tip and the crack therefore proceeds in a direction perpendicular to the applied stress. The change over from stage I to stage II is often at a grain boundary where the crack enters crystals of different orientation to the one in which it was initiated. In fretting fatigue, the alternating shear applied to the surface by the fretting action usually encourages stage I growth to such an extent that a pronounced lip is formed on one fracture surface with a corresponding chip on the other. Examination of fracture surface reveals that although the stage II crack surface may seem relatively smooth in appearance, there are striations which correspond to the crack with each cycle of stress. Each striation contains a portion of ductile failure and cleavage failure, the relative amount depending on the overall ductility of the material and also the environment. The stress intensity factor arising from a crack of length a and an applied stress of σ is given by $K = \sigma \sqrt{\pi a}$. Fig. 43 shows a typical crack growth curve indicating a

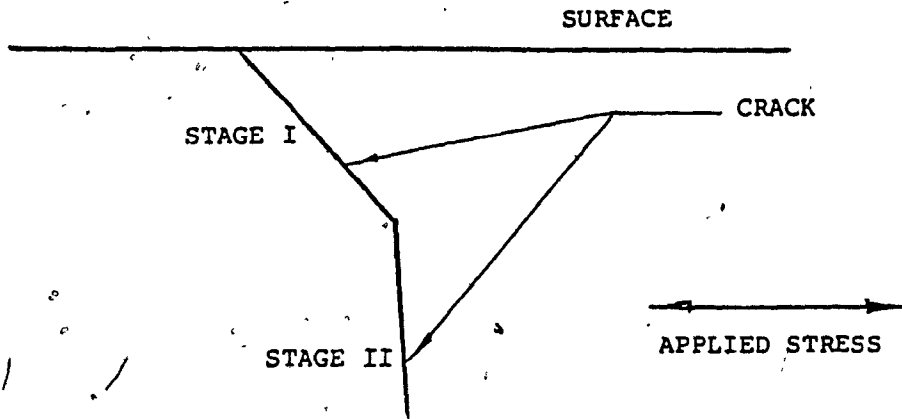


Fig. 42. Stage I and stage II development of a propagating crack After Waterhouse (65)

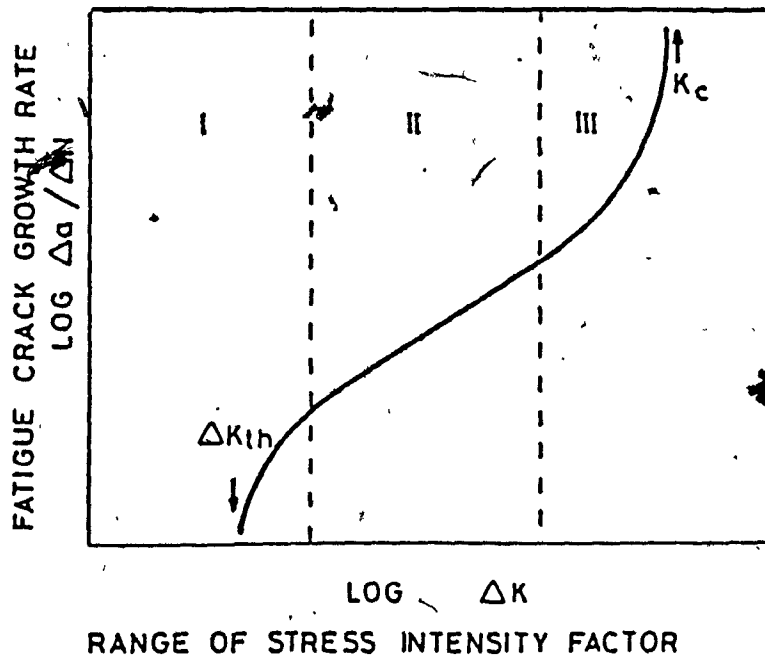


FIG. 43 . Typical crack growth curve indicating a threshold value of stress intensity factor ΔK_{th} . After Waterhouse (65).

threshold value of stress intensity factor. The first region(I) is corresponding to the threshold value of ΔK (defined as the variation between the stress intensity factors K_{min} and K_{max} at the tip of the crack, both dependent on the length of the crack) that could be as small as 10^{-8} or 10^{-9} mm per cycle at frequency of 1 Hz or less. The second linear region(II) is the part of the curve to which the empirical Paris-Erdogan relation applies

$$\frac{\Delta a^n}{\Delta N'} = (c' \Delta K)^n$$
 where a^n is the crack length, N' is the number of cycles and c', n are constants. The application of this graph is applied namely when the fracture mechanics to fatigue is concerned with the growth of the crack under cycling stress.

4.2 THE S-LOG N CURVE

The S-log N curve represents the end result of the initiation and propagation of a fatigue crack. Some observations however can be made concerning the influence of the external factors such as environment or fretting on the fatigue curve. Fig. 44 shows that any factor which lowers the fatigue limit from A to A' is having an influence on the initiation of the crack since at applied stresses between A and A' a crack is formed which propagation to failure, whereas in the absence of the factor no failure would occur. Any factor which shifts the upper part of the curve to the left, i. e. from B to B' is having an effect on the propagation of the crack since the life is shorter at any given stress. In practice, both parts of the curve are often affected and the

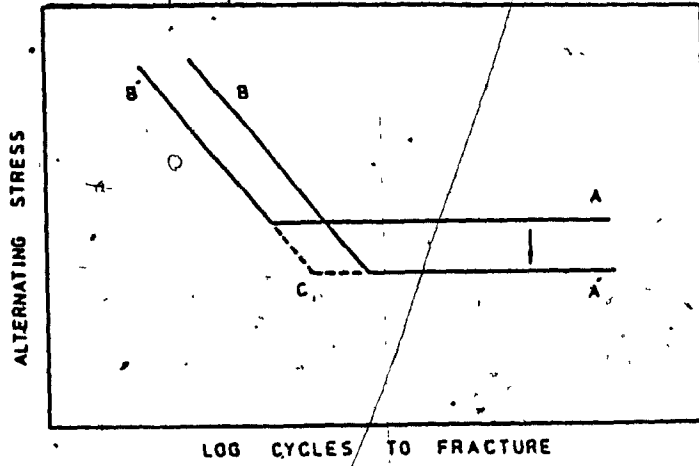


Fig. 44 . Schematic representation of the S-log N curve. After Waterhouse (65).

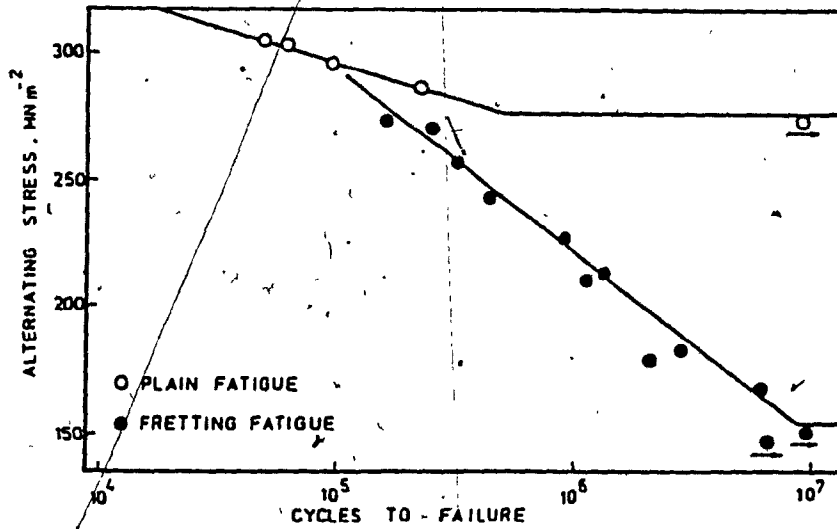


Fig. 45 . Effect of fretting on the fatigue behaviour of an austenitic steel. At stresses just above the fatigue limit, the fatigue life is similar for plain fatigue and fretting fatigue, indicating that when a crack is initiated, whether by fretting or not, its propagation rate is approximately the same in both cases. After Waterhouse, (65) .

result is the curve B'CA'. fretting is particularly effective in initiating a fatigue crack but once it has grown out of the immediate region of the surface where the additional shear stress is acting, the propagation rate will be little influenced. This is illustrated in Fig. 45 which shows the effect of fretting on the fatigue behaviour of an 18Cr10Ni austenitic steel (65).

4.3 STRESS INTENSITY FACTORS

Fretting fatigue crack is initiated very early in the fatigue life of metals and fatigue life is dominated by the propagation of small cracks. These characteristics of fretting fatigue crack are analyzed by using the stress intensity factors at the tip of the crack growing from the contact edges. The stress intensity factor is assumed to be made up from three individual contributions (19). First is the contribution due to the body stress in the specimen which would have been the only contribution had there been no fretting pads. Second is the contribution due to the alternating frictional loads. The third contribution is that due to normal pad loads (this contribution was static and compressive). Stress intensity factors were therefore evaluated in (66) for a range of assumed distributions of pad load as shown in Fig. 46, which included the extreme cases of all the loads concentrated either at the front or back portion of the fretting pad foot. It was assumed that the actual stress intensity factor involved a distribution of pad load somewhere between these two extreme

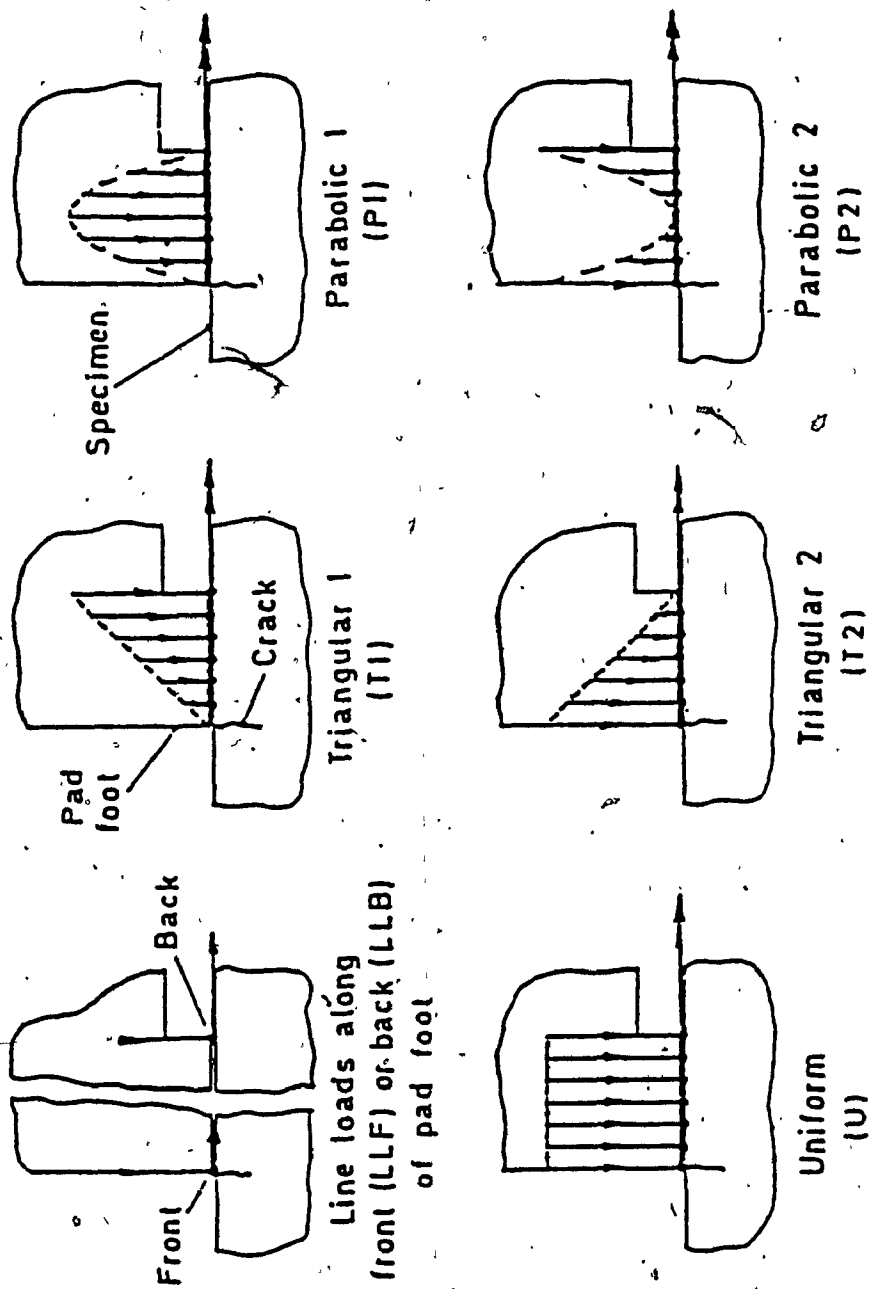


FIG. 46 . Assumed distribution of frictional and normal pad loads.
After Eason (1957)

2

conditions. Fig. 47 and Fig. 48 show the stress intensity factors K_{fp} and K_{np} for the range of assumed pad load distributions due to frictional and normal loads respectively. As can be seen from Fig. 47 the stress intensity factor due to frictional forces is split into two components K_{fp1} which varies with the assumed pad load distribution and K_{fp2} which is negative and accounts for the fact the specimen alternating body stress is lower under those pads because some loads are diverted through the pads.

4.4 THE FRACTURE MECHANICS MODEL

4.4.1 STRESS INTENSITY FACTORS DUE TO LINE LOADS

The method for calculating stress intensity factors developed by Rooke and Jones(66) involves the calculation of stress intensity factor(K) for an extended edge crack in a half plane subjected to a localized load Fig. 49. Opening mode(K_I) and shear mode (K_{II}) stress intensity factors were evaluated for the tangential force (T) and normal force(N) acting on the crack.

Their least squares polynomial fits to the results are given as follows:

(K_I) Opening mode due to normal loading(N)

$$K_I = \frac{N}{\sqrt{\pi a}} (1 - r^2) \left[0.8240 + 0.0637r - 0.8430r^2 + 15.41r^3 - 53.38r^4 + 59.74r^5 - 21.82r^6 \right] \quad 4.1$$

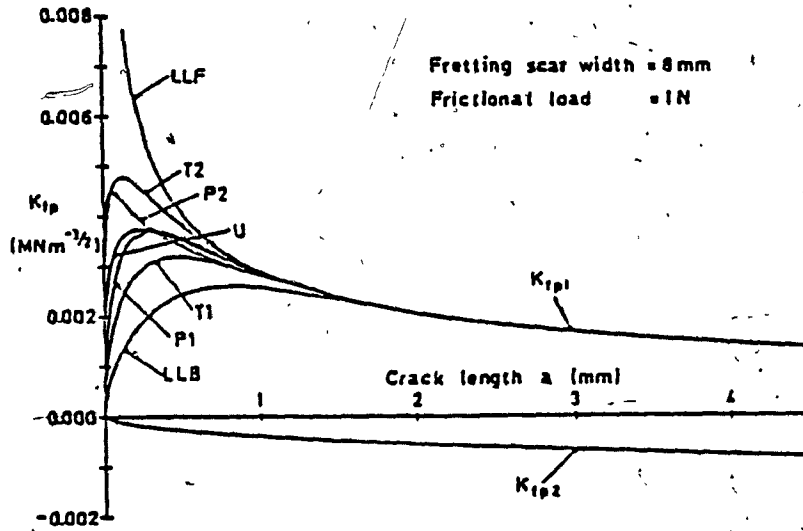


FIG. 47. Stress intensity factors for different distributions of frictional pad load.

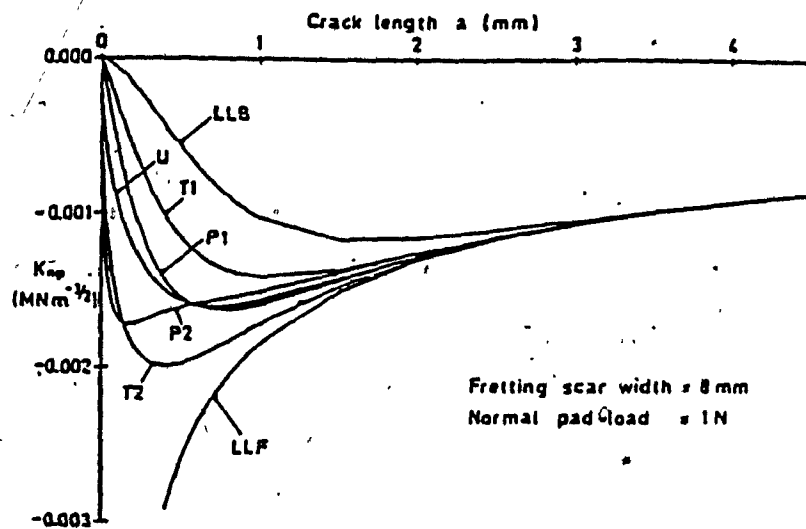


FIG. 48. Stress intensity factors for different distributions of normal pad load.
After. Rooke et al. ('66).

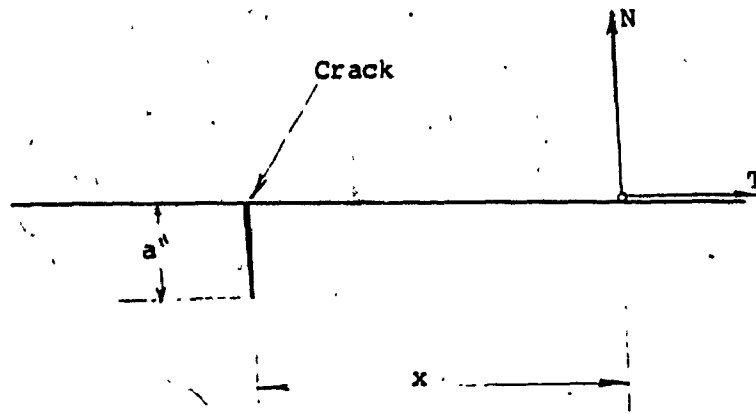


Fig.4.9. Crack Plate Subjected to Contact Forces

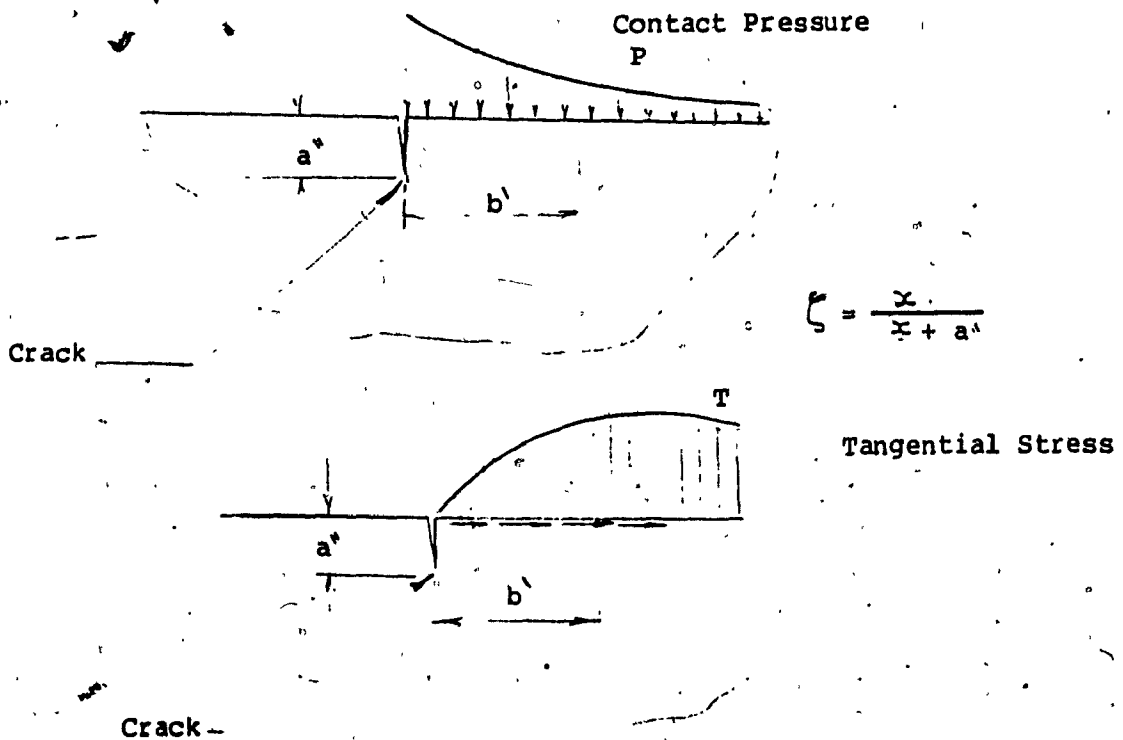


Fig (50) Crack Plate Subjected to distributed contact stresses

After, Hattori, et al. (67).

(K_I) Opening mode due to tangential loading(T)

$$K_I = \frac{T}{\sqrt{\pi a^n}} (1 - \xi^2) \left[1.2949 + 0.0044\xi + 0.1281\xi^2 + 10.89\xi^3 - 22.14\xi^4 + 10.96\xi^5 \right] \quad 4.2$$

K_{II} Shear mode due to normal loading(N)

$$K_{II} = \frac{-N}{\sqrt{\pi a^n}} (1 - \xi^2) \left[1.294 - 1.184\xi + 5.442\xi^2 - 28.14\xi^3 + 41.8\xi^4 - 22.38\xi^5 + 3.162\xi^6 \right] \quad 4.3$$

(K_{II}) Shear mode due to tangential loading(T)

$$K_{II} = \frac{-T}{\sqrt{\pi a^n}} * \frac{K_I}{(N / \sqrt{\pi a^n})}$$

where : $\xi = \frac{x}{(x + a^n)}$ 4.4

4.4.2 STRESS INTENSITY FACTORS DUE TO DISTRIBUTED LOADS

In the case when the edge crack is subjected to distributed contact pressure(P) and distributed tangential stresses(Tⁿ) instead of point forces(N) and (T), the stress intensity factors can be obtained by integrating eqns. (4.1) to (4.4) along the x direction as follows

(see Fig. 50):

from eqn. 4.1 $K_{I(P)} = \int K_{I(P)}(\xi) d\xi \quad 4.5$

from eqn. 4.2 $K_{I(T^n)} = \int K_{I(T^n)}(\xi) d\xi \quad 4.6$

from eqn. 4.3 $K_{II(P)} = \int K_{II(P)}(\xi) d\xi \quad 4.7$

from eqn. 4.4 $K_{II(T^n)} = \int K_{II(T^n)}(\xi) d\xi \quad 4.8$

4.4.3 MEAN AND ALTERNATING STRESS INTENSITY FACTORS

UNDER FRETTING CONDITIONS

Both opening and shear mode stress intensity factors can be calculated using the above method. However the influence of shear loading on fatigue crack growth is not yet established, hence mode II effects can not be included in the analysis at this stage (67). Since the specimen alternating body stress is lower under the pads because some load is diverted through the pads. (19, 68) the component K_{fp2} shown in figure 47 has a negative value:

$$K_{fp2} = - 1.12 \frac{F_f}{A} \sqrt{\pi a''} \quad 4.9$$

where F_f = maximum frictional force in stress cycles on each pad foot

A = cross section area of specimen

The alternating stress intensity factor K_a is given by the components due to alternating body stress σ and a frictional force F_f (19)

$$K_a = 1.12 \sigma_a \sqrt{\pi a''} + \frac{0.008}{e} F_f K_{fp1} - 1.12 \frac{F_f}{A} \sqrt{\pi a''} \quad 4.10$$

and the mean intensity factor given by :

$$K_m = 1.12 \sigma_m \sqrt{\pi a''} + \frac{0.008}{e} F_n K_{np} + K_d \quad 4.11$$

where : F_n = normal force on each pad foot

K_d = the crack length correction stress intensity factor

(19, 68, 69, 70)---

e : is the fretting scare width

Both mean and alternating stress intensity factors were multiplied by the finite width correction of Harris(71) for an edge crack in a specimen with end restrained in bending. This takes the form of a function of $(\frac{a''}{w})$:

$$f\left(\frac{a''}{w}\right) = \frac{5}{1.12\sqrt{(20 - 13\frac{a''}{w} - 7(\frac{a''}{w})^2)}} \quad 4.12$$

Where : w = the distance between fretted surface (specimen depth).

The above finite width correction was found to be the most appropriate one to use following some residual static strength tests on a part-fatigued specimen(72).

4.5 CALCULATION OF CRACK RATES

At specified values of crack length, the mean stress intensity factors K_m can be calculated(67) from eqn. (4.11) together with the appropriate range of alternating stress intensity factor K_a from eqn. (4.10) corresponding to the alternating r.m.s (root mean square) stress (σ_r) applied. Equation 4.10 requires values of frictional force to be measured. Edwards' analysis(19) indicated that only one value of K_a per crack length is required for constant amplitude loading, together with K_m and computer subroutine (75) cited in reference(19) to obtain the crack rate $\frac{da''}{dN}$ from Pearson's(76) crack rate data. For variable amplitude loading at each crack length, crack rates are to be calculated for K_m and

the range of values of K_a appropriate to the magnitudes of the individual cycles in the spectrum. The final rate is to be obtained by a linear summation of these rates weighted according to the probability of occurrence of K_a within each variable amplitude sequence.

$$\frac{da''}{dN'_{\text{random}}} = \int_0^{\infty} P(K_{a''}) \frac{da''}{dN'} (K_{a''}) dK_{a''}$$

where : $P(K_{a''})$ = probability distribution of $(K_{a''})$.

$$\frac{da''}{dN'} = \text{crack rate.}$$

$K_{a''}$ = semi-range alternating stress intensity factor.

4.6 FRACTURE MECHANICS PREDICTIONS

An experimental investigation of fracture mechanics predictions is described in(19), using the model shown in Fig. (51). In all the cases presented in this section (19), it was assumed that the distribution of normal loads had the same shape as the distribution of frictional loads (see Fig. 46.).

4.6.1 EFFECT OF INITIAL FLAW SIZE AND LENGTH CORRECTION

ON PREDICTED LIFE

All fracture mechanics analyze have to assume an initial flaw size for the crack to propagate. Examination of fracture surface of the fretted specimen(77) showed that by the time cracks had reached a depth of 0.02mm, the majority were propagating in stage

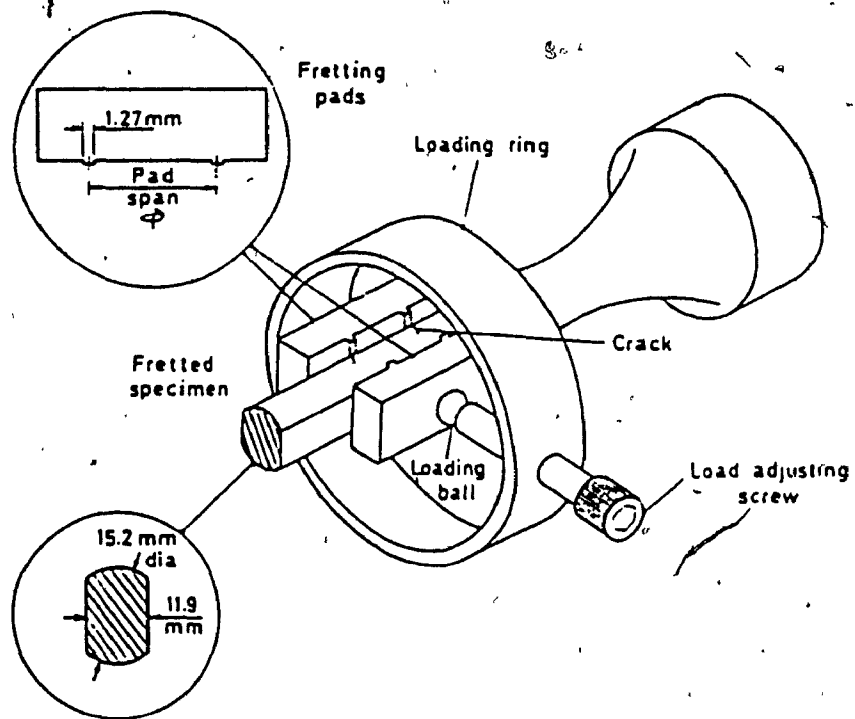


FIG. 51. Fretted specimen assembly
After Edward (19)

II manner, although they tended to slant slightly so as to grow under fretting pads. Fig. 52 compares experimentally achieved lives of standard fretted specimen under constant amplitude loading with those predicted assuming uniform pad load distributions and initial flaw sizes of 0.02 and 0.1mm with and without the length correction. The predicted fatigue limits were due to initial flaw not propagating, whereas experimental evidence (77) showed that the fatigue limit was due to cracks stopping at round 0.2mm. Considering the predictions using the length correction, it can be seen that the fatigue limits were more accurately predicted and in fact the predicted fatigue limit was in this case due to cracks stopping after an initial period of propagation. However, at the highest stress levels the predicted lives were too short by a large factor. Figures 53 and 54 show the effect of initial flaw size on the life prediction of standard fretted specimens under variable amplitude loading without, and with the length correction, respectively.

Fig. 55 shows predicted variable amplitude S-N curves for plain specimens assuming a range of initial flaw sizes and using length correction. Experimental test points for standard fretted and plain specimens are shown for reference. Comparison with the equivalent predictions for standard fretted specimens, Fig. 54 shows that in the latter case the effect of initial flaw size was for less marked. The reason for this less critical behaviour for

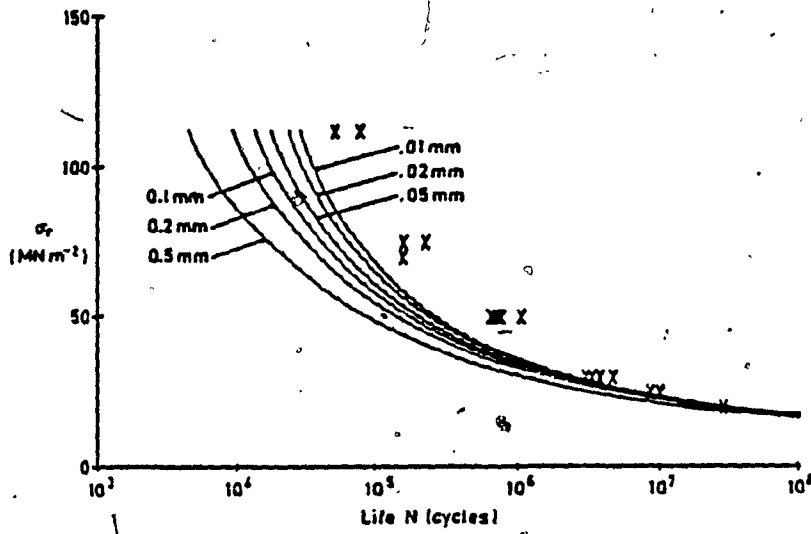


FIG. 54. Effect of initial flaw size on predicted life—variable amplitude; length correction used.

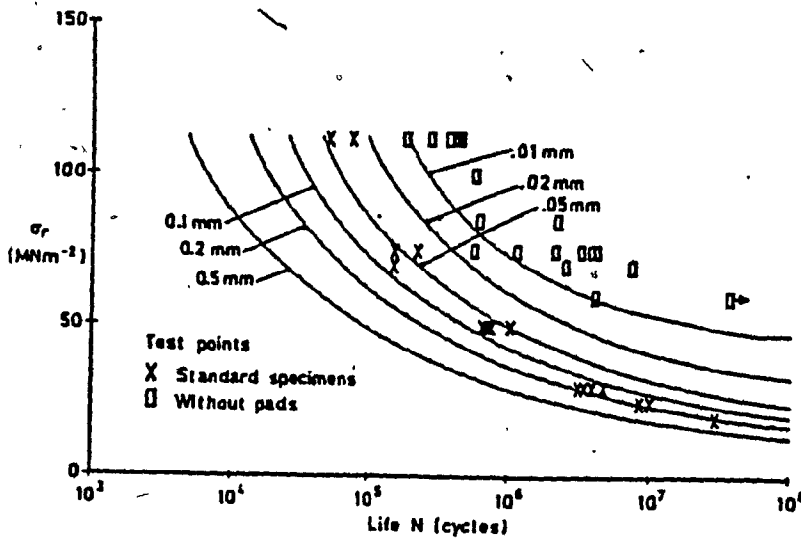


FIG. 55 Effect of initial flaw size on predicted life—no pads; variable amplitude; length correction used.

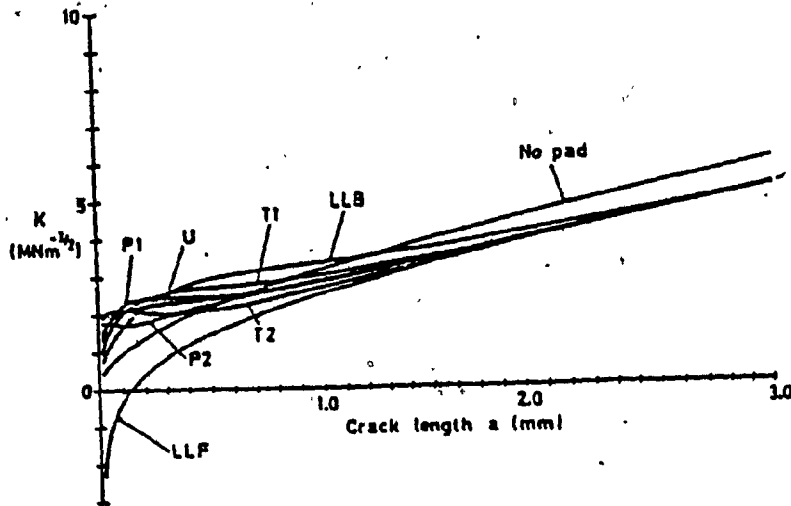


FIG. 56 Peak stress intensity factors for a range of pad load distributions. After Edward et al (77).

for less marked. The reason for this less critical behaviour for specimens with pads was that in this case the stress intensity factor, and hence the crack rate, were more nearly constant over the fatigue life Fig. 56. The same was found to apply for constant amplitude loading.

4. 6. 2 PREDICTED AND MEASURED CRACK PROPAGATION CURVE

Fig. 57 shows predicted crack propagation curves for constant amplitude loading on fretted specimens, while Fig. 58 shows variable amplitude loading on fretted specimens. In both cases a uniform distribution of pad loads were assumed with an initial flaw size of 0.02mm. The crack length is plotted against fraction of life it lasted so that the shapes of the crack propagation curves could be compared at different stress levels. As it can be seen in both these figures, the predictions in which the length correction was used, varied distinctively in shape with alternating stress level. One curve predicted without the length correction is plotted for each loading for an rms stress level of 50MNm^{-2} and is labeled(NLC). Finally, a measured crack propagation curve for each loading action at an rms 50MNm^{-2} was plotted in Fig. 57 and Fig. 58. These curves were constructed by fatigue testing specimens to different percentage of the expected life, breaking them statically and measuring the size of any fatigue crack thus revealed(68). As it can be seen from Fig. 57 the

predicted curves using the length correction were more nearly in accordance with the measurements. Fig. 57 which corresponds to variable amplitude loading indicates that although the prediction using the length correction is in better agreement with the measured curve than without, the agreement at the early part of life was not good. In particular neither of the predictions indicated the observed fact that the crack curve would start off at relatively fast rate and then slow down. Fatigue crack propagation takes place relatively fast out of the region in which pad loads give a big contribution to the stress intensity factor and then slow down. It was confirmed that the shapes of the measured crack propagation curves involved acoustic emission traces obtained on standard fretted specimens under both types of loading (72). Under variable amplitude loading there was an initial period of acoustic emission activity which could have been associated with an early period of relatively fast crack growth. For constant amplitude loading this was not the case. It would appear that a fracture mechanics model, which was reasonably accurate in predicting the shape of the crack propagation curve under constant amplitude loading, was very inaccurate under variable amplitude loading. Therefore, either the stress intensity factors calculated for variable amplitude loading were much less accurate than for constant amplitude

loading or the cumulative damage model used was inaccurate.

Note that the cumulative damage model used was linear summation of constant amplitude crack rates weighted according to the probabilities of occurrence of alternating stress intensity factors within each variable amplitude sequence (78).

4. 6. 3 EFFECT OF ASSUMED DISTRIBUTION OF PAD LOAD ON FATIGUE LIFE

Fig. 59 shows predicted and achieved lives for standard fretted specimens under a constant amplitude loading with an assumed initial flaw size of 0.02mm and a range of assumed pad load distribution. As can be seen, all the distributions which were symmetrical about the middle of the fretting pad foot predicted lives that were similar to those for uniform pad load distribution. The assumption that the pad loads were more concentrated towards the back of the pad foot improved the predicted life at the higher stress levels. Thus the stress intensity factor at short crack length was primarily the result of two large components; namely frictional and normal forces that tended to oppose each other and a small percentage change in one component could give a large change in the resultant stress intensity factor. Fig. 60 shows the same set of predictions as Fig. 59, but for variable amplitude loading. It can be seen that, apart from the curve for assumed line load at the front of the pad foot, the pattern of predictions were similar to that under constant amplitude

loading. At the higher stress levels however the predictions tend to be more accurate. The most appropriately predicted curve would be expected to be between triangular 1 (Fig. 46) and the left hand group of curves representing symmetrical distribution. Allowance for retardation of the crack due to high loads in sequence(79) would have increased predicted life. It can be summarized that, the variable amplitude predictions were more accurate than the corresponding constant amplitude predictions. This was a rather surprising result in view of the error indicated by a comparison of predicted and measured crack curves in section 4.7.2.

4.7.4 PREDICTION FOR A RANGE OF PAD SPANS

In the experimental study carried out in(69), showed that the pad span ϕ was taken as a variable distance between the contact of fretting pads and specimen for the range $2.0 < \phi < 34.35\text{mm}$. Fig. 61 and 62 show predictions for the constant and variable loadings applied to specimens having the full range of pad spans at pad load = 2.5KN. The predictions were all made on the same basis, i. e. using the length correction, an initial flaw size of 0.02mm and triangular 1 pad distribution (see Fig. 46). This assumption was regarded as reasonable compromise to illustrate the way the model predicts the effect of pad span on fatigue life. As it can be seen from Fig. 61 and 62 the relative variable

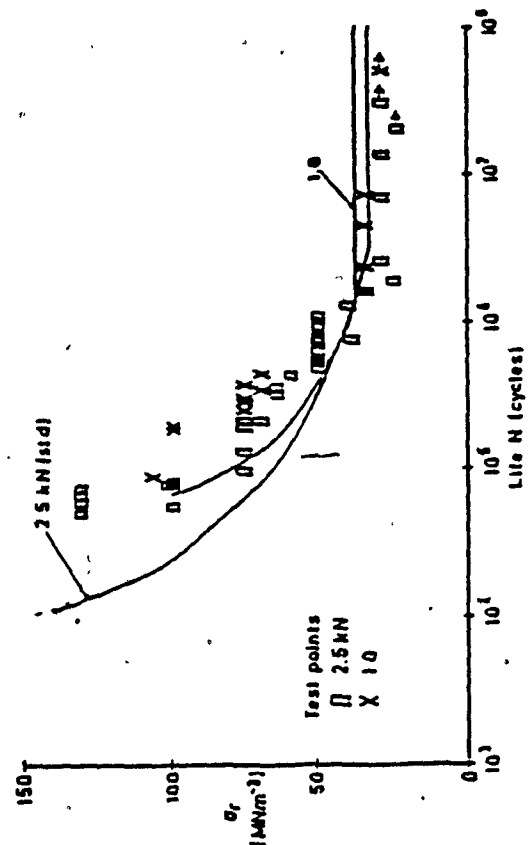


FIG. 63 Predicted and achieved lives for two pad loads—pad span = 16.5 mm; constant amplitude.

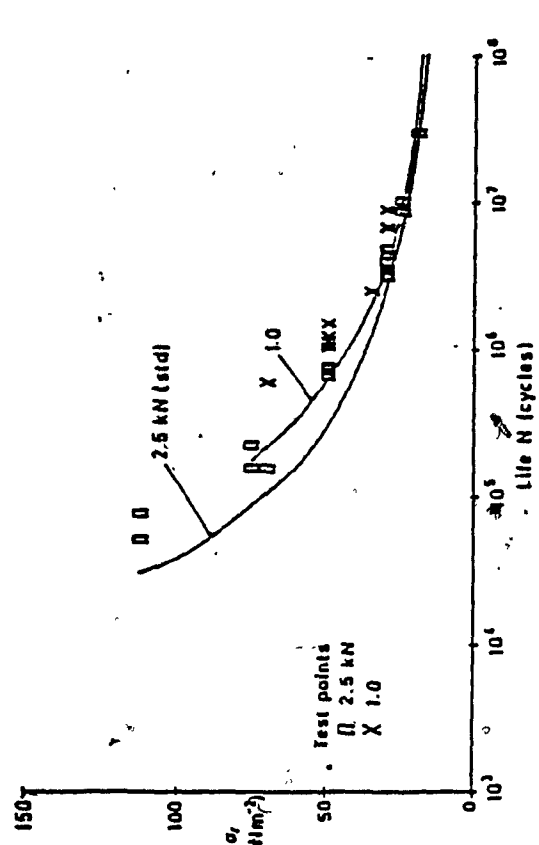


FIG. 64 Predicted and achieved lives for two pad loads—pad span = 16.5 mm; variable amplitude.

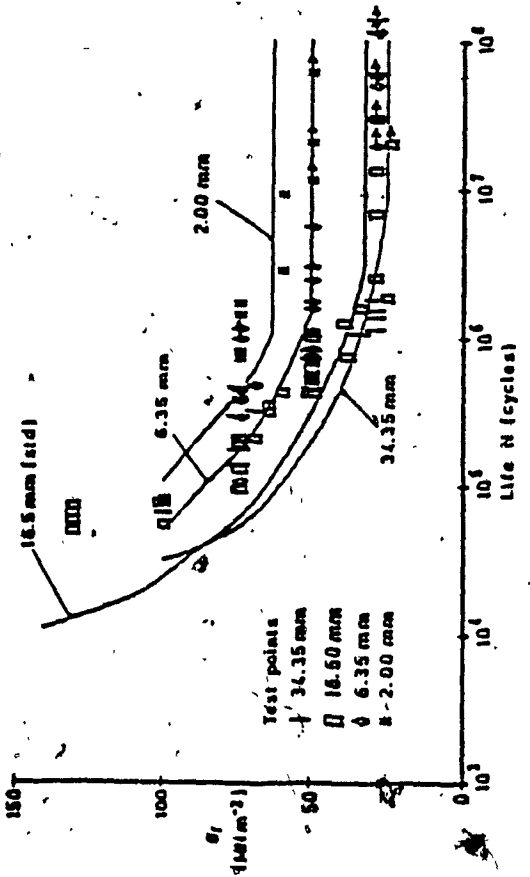


FIG. 61 Predicted and achieved lives for a range of pad spans—constant amplitude.

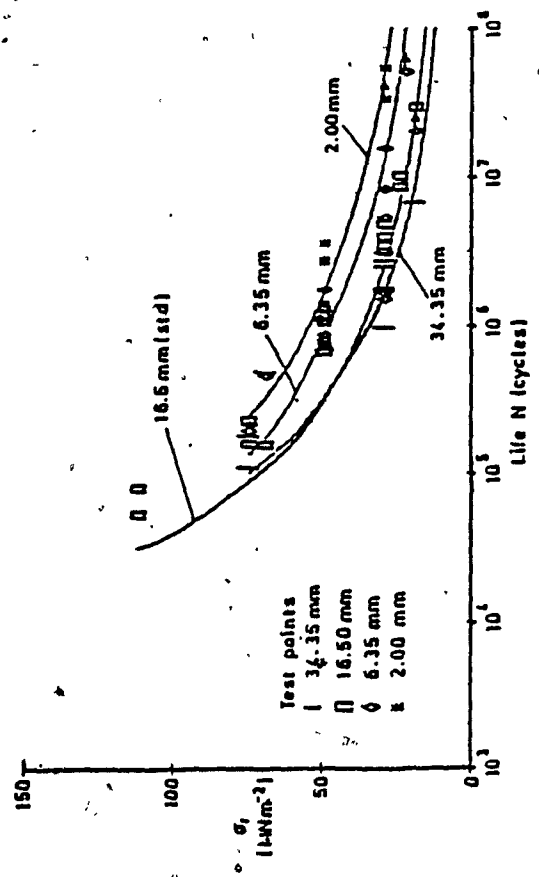


FIG. 62 Predicted and achieved lives for a range of pad spans—variable amplitude. After. Edward et al (77).

of fatigue life relative to pad span was predicted very well for constant amplitude and variable amplitude loading. This predicted variation in life with pad span was contributed entirely to the associated changes in frictional force and related stress intensity factor. Predicted lives were, however, consistently more accurate under variable amplitude loading.

4.6.5 PREDICTIONS AT TWO PAD LOADS

Fig. 63 shows experimental and predicted lives for specimens with pad span of 16.5mm and two values of pad load, 1 KN and 1.5KN, under constant amplitude loading. Fig. 64 shows the same for variable amplitude loading. Predictions were made with the same assumptions regarding initial flaw size. As it can be seen from the figures 63 and 64 that the most accurate life predictions were for variable amplitude loading. It can also be noticed that the effect of pad load on predicted and achieved fatigue life was small at the lower stress levels. This may appear surprising in view of the relatively large difference in frictional force recorded between the two pad loads. As revealed before, an important fact, however, there were two factors which offset this. The first one being the fretting scar width was less at the low pad load. Secondly the more important was the fact that reducing the normal pad load reduced the magnitude of its associated stress intensity factor. This tended to offset the reduction in the damaging stress intensity factor associated with the frictional

loads. The net effect was that the predicted lives could go up or down with the pad loads. As can be seen from Fig. 63, at different stress levels it was predicted that the life would generally increase with decrease in pad load, except over a small range of alternating rms stresses around 40 MNm^{-2} where a small decrease was predicted. It can be concluded for fracture mechanics predictions, that the accuracy of the predictions under both constant and variable loading was consistent particularly for variable amplitude loading. The most inaccurate predictions were made for constant amplitude loading at the highest alternating stresses. The effect on fatigue life of changing pad span and load was predicted well. A crack length correction was assessed which empirically took account of the fact that short cracks having the same alternating stress intensity factor as long cracks tend to propagate faster. It was found that the use of the length correction factor gave very good predictions of the fatigue limit, and, overall, gave the best predicted S-N curve shapes. The most serious failure of the fracture mechanics model was that it did not predict the observed fact that under variable amplitude loading there was an initial relatively fast rate of crack propagation after which it slowed down.

CHAPTER 5

PRACTICAL APPLICATION

5.0 INTRODUCTION

As it was indicated before, fretting fatigue failure takes place when repeated loading on a structure causes a sliding movement at metallic interface and results in the development of high stress intensity and thus the initiation of fatigue cracking. This chapter is therefore devoted to discuss more of the circumstances under which fretting fatigue failures arise in service and to description of diagnostic features that can be observed in real situations. After describing how to identify true fretting fatigue, some commonly observed cases are depicted. This will be followed by consideration of more specific engineering situations where failures still commonly occur, but where the fretting aspect is at least recognised. Remedial measures for counteracting the fretting fatigue failures are outlined. Then measures include improved design, surface treatment, surface coating, surface finish, lubrication and the proper selection of material.

5.1 THE IDENTIFICATION OF TRUE FRETTING FATIGUE

The rubbing together of clean metallic surfaces soon produces what are frequently described as scars at some of the surface.

asperities. These scars characteristically reveal the direction in which the rubbing action has been taken place by being streaked and elongated in this direction. The scar generally has a rough appearance although in some instances it may be also compacted as to form a glaze. Scars on steels have a characteristic red-brown colour, black on aluminum alloys and they may also vary from a compacted glaze to a powdery deposit. The roughening of the metal surface itself that is associated with the fretting product may vary from patches of microscopic pits to large, shallow abraded areas. Fretting product may be compacted in the mouth of the crack, although such a feature is not by itself evidence of fretting-induced cracking. This raises the important point of cause and effect, bearing in mind that the loosening of a joint by fatigue can by itself cause considerable fretting. This may mask the actual evidence of pre-crack fretting i. e. true fretting fatigue.

5.2 EXAMPLES OF FRETTING FATIGUE FAILURE IN PRACTICE

There are two clearly distinguishable classes of fretting fatigue related to fastened joints:

1 - Flanges, i. e. flat faces in contact subjected to varying shear loads which, depending on the normal closure loads on the faces, may suffer some degree of slippage.

2 - Loaded, filled holes, i. e. pins or fasteners bearing on the bores of holes subjected to some interface sliding.

Fastener closure itself can cause appreciable dishing around

the holes that results in non-uniform contact. These various situations are illustrated in Fig. 65. It is also common to find asperities in the form of burrs around holes that result from drilling. In these situations the paint barrier may be broken and metal to metal contact points are formed as illustrated in Fig.

66. With unpainted parts, such features would be very likely to result in fretting and painted surfaces may be abraded away as shown in Fig. 67. Other features that present fretting hazards are shown in Fig. 68 and relate to washers or fastener heads that, either because of distortion in assembly, or because of incorrect geometry, do not seat uniformly. Another example, Fig. 69, will be recognised as a fairly common case where misalignment and side loads are applied in a fork fitting. In lap joints where fretting may lead to fatigue failure the crack will form in the member where the fatigue stresses is highest. This one part will act as a fretting pad to the other. In some instances it is perfectly possible for cracks to appear in both parts. The same situation can arise in pin and lug joint. The interface between a pin or fastener and the bore of the hole in which it is situated clearly represents a case where fretting might occurs. In such a loaded hole the normal and sliding loads are inter-related and it is likely position of the fretting scars. Whereas fasteners are not expected to rotate, pin may well do so. In some cases pin failures may be experienced and in other cases, depending on the stresses

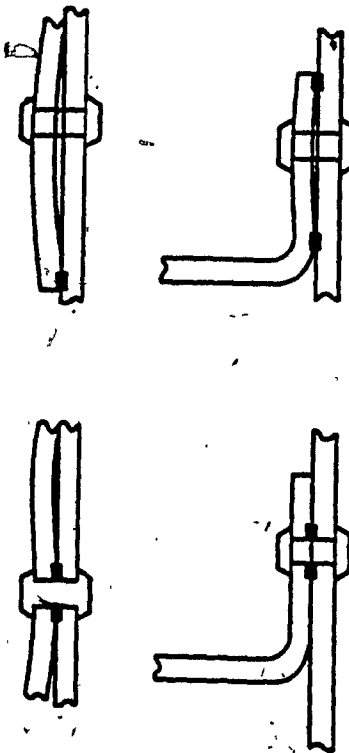


FIG. 65. Schematic diagrams of thin sheet joints illustrating commonly occurring fretting points. Danger points indicated thus ■.

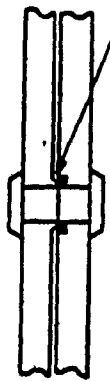


FIG. 66. Schematic diagram illustrating how drilling burrs cause fretting points. Danger points indicated thus ■.



FIG. 68. Schematic diagram illustrating the positions of frequently observed fretting damage. Danger points indicated thus ■.

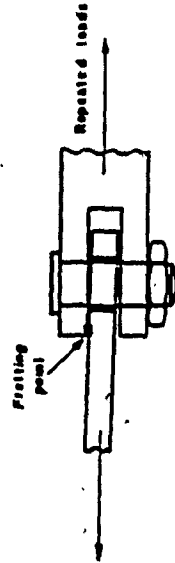


FIG. 69. Schematic diagram illustrating how misalignment of a fork end fitting can cause fretting fatigue problems. Danger points indicated thus ■.



FIG. 67. An anodized and painted aluminum alloy surface where fretting abrasion has penetrated to cause metal-to-metal contact. x 4.

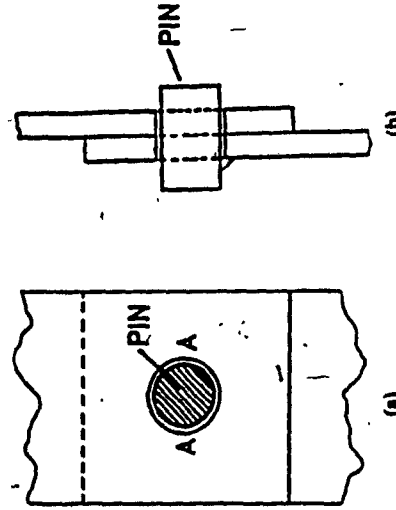


FIG. 70 (a) Front elevation of single pinned joint; (b) Side elevation of single pinned joint.

present, fretting fatigue may occur in the lug, or body in which the pin operates. When a pin loaded joint, Fig. 70, is tested in fluctuating tension, fretting occurs at the diametrically opposite sides of the hole, A-A, and a fatigue crack is initiated which propagates through the reduced section to failure.

Other mechanical components in which fretting fatigue is commonly observed, are wire ropes or cables, spring washers of various forms, leaf springs, coil springs, keys in keyways on shafts and splines, wheel bosses on shafts and collars and bushes, roller bearings, rivet heads, press fitted hub on axle, reactor rod fuel elements assembly, etc.

5.3 DESIGN APPROACH TO PREVENT FRETTING FATIGUE

The design engineer has to familiarize himself with the methods (80) required to alleviate or to eliminate fretting fatigue in structures which are dependent on the exact situation and are empirically oriented. The common schemes are lubrication of the interface, component plating, judicious selection of material, shimming, alternation of the clamping pressure, reduction or elimination of cyclic stress, provision for the escape of debris and treatment of contacting surfaces including the introduction of residual stress. The lubricants decrease the coefficient of friction, exclude the corrosive influence of environment and carry away some of the abrasive particulate sloughed from the surfaces. Viscous lubricants are generally effective over a

limited life, while the effectiveness of solid lubricants (e. g molybdenum disulphide, zinc oxide) are situation oriented. Plating is another effective method of reducing fretting damage. Such coating are usually about 2-100µm thick and are produced by spraying, dipping or electrodeposition. The most common metallic coatings are cadmium and chromium. Cadmium is a soft compliant metal which can be used when the slip amplitude is small and plating of this type shears with the movement, thus tending to avoid the sliding motion. In contrast, chromium is a hard abrasive resistant metal which resists microwelding at the points of contact. Other processes which have more limited application are anodization, phosphatization and the use of bonded coatings. The selection of compatible pairs of different materials often alleviates fretting difficulties. Many considerations, however, are involved in selecting the bonded coated materials and the choices are usually empirical. The use of compliant shim stock often acts to eliminate relative movement. Some successful materials are lead, rubber and silver. For metallic materials however the selection must avoid the creation of a galvanic cell in any deleterious environment. As previously mentioned, the increase in the clamping pressure can reduce fretting damage, at higher pressure, relative motion can be arrested entirely if the elements can tolerate this elevated stress level in ordinary fatigue. Lower clamping pressures usually permit larger amplitude

sliding, and fracture can be avoided if the clamping pressure threshold is not exceeded. A roughened surface have also been found to be beneficial in removing debris from the fretted area. However, the stress concentration associated with this approach may be prohibitive. Many surface treatments which lead to the increase in the resistance to crack initiation are available. Most of these treatments alter the hardness of one or both of the components (e. g nitriding, carburizing, induction hardening). Another approach is to induce residual compressive stresses. Various forming operations have proved successful (e. g drop forging, surface rolling and shot peening). Some other preventative measures which have been used to reduce or eliminate fretting include (80) the following :

- (a) Elimination of the vibration.
- (b) Prevention of slip.
- (c) Exclusion of atmosphere.

Methods of eliminating vibration should be considered, although generally these may not be practical. A simple design change or relocation of a mechanism, however, may dampen vibration sufficiently to eliminate slip or at least to reduce the length of the slip path sufficiently enough to minimize damage. For the lip to be prevented, the normal load or the closeness of fit can be increased, although increasing the normal pressure

may increase fretting if relative motion is not completely eliminated. Slip may also be prevented, by raising the coefficient of friction by plating or by bonding elastic material to surfaces. As for the exclusion of the atmosphere, some investigations believe that one of the major function of a lubricant is to exclude air from the contacting surface.

CHAPTER. 6

CONCLUSIONS AND RECOMMENDATIONS FOR FURTHER WORK


6.1 CONCLUSIONS RELATED TO THE MAIN PARAMETERS INFLUENCING
THE FORMULATION OF FRETTING FATIGUE/WEAR PROCESS

Among numerous variables, it was concluded that there are eight basic variables that play an important role in controlling the fretting wear/fatigue process. These are: the amplitude of relative motion, the magnitude and distribution of the contact pressure, the state of stress (including magnitude, direction and relative variation with respect to time), the number of cycles of fretting, the type of material of the member, the frequency of the relative motion, the temperature in the region and the atmospheric environment.

6.2 CONCLUSIONS RELATED TO THE MECHANISM OF
FRETTING FATIGUE/WEAR

1. Fretting fatigue failures are consistently occurring near the edge of the contact area or near slip-non slip boundaries.
2. The main factor in producing a fretting fatigue failure was the additional alternating shear stress in contact areas arising from frictional stress between the surfaces.

3. The microstructure of the material has an influence on fretting fatigue: the fine structure is more resistant to damage than the coarser annealed structure.
4. The fretting resistance of a joint is increased by increasing the coefficient of friction. Large coefficient of friction allow large shear traction to be transmitted without slip; this leads to a higher stresses at the edge of the contact bodies.
5. The length of the crack in stage one(I) depends on the stress level and environment. In stage two(II) the growth of the crack is dominated by the tensile stresses at the crack tip and the crack therefore proceeds in a direction perpendicular to the applied stress.
6. A critical number of fretting cycles (10^4 - 10^5) was required in fretting wear to initiate the onset of steady state wear, and in fretting fatigue to initiate damage ultimately leading to failure. The critical number of cycles corresponds to the number of cycles associated with the accumulation of low cycles fatigue damage.
7. Elevated temperature had a beneficial effects on both fretting wear, and fretting fatigue. Surface oxide films that can readily form at elevated temperatures reduce interfacial adhesion and plastic flow, thereby reducing fretting wear rates and increasing fretting fatigue lives.
8. Available data on the effect of fretting amplitude, number of



fretting cycles, and fretting frequency showed both fretting wear and fretting fatigue to be influenced in a consistent manner. That is condition that tend to accelerate fretting wear also tend to accelerate fretting fatigue failures.

6. 3 CONCLUSIONS RELATED TO THE ELASTIC STRESS ANALYSIS IN THE INTERPRETATION OF FRETTING FATIGUE FAILURES

1. The conditions of slip and fretting were less severe if the oscillating force transmitted by the joint can act nearly at right angles to the interface (sphere on sphere model).
2. Elastic stress analysis can be used to predict the incidence of interfacial slip in clamped joints under the conditions of alternating load. The predicated slip regions are compared well with observed regions of fretting damage.
3. Interpretation and prediction of the results of fatigue tests have been achieved through the calculation of the stress field in clamped joints on similar configurations.
4. Accurate prediction of the reduction in fatigue strength due to fretting necessitates the microscopic distribution of stress within the joint to be known.
5. The energy dissipated by friction in fretting annulus may be taken as a rough measure of the rate of surface damage.
6. Stress analysis, supported by experimental verification shows that shear stress concentration at metallic interface and micro-slip could be eliminated by introducing an elastic layer at the interface.

6.4 CONCLUSIONS RELATED TO APPLICATION OF FRACTURE

MECHANICS FOR PREDICTING FRETTING FATIGUE

1. Contact pressure and tangential stress distributions obtained by the conventional stress analysis methods are used to calculate the stress intensity factor for cracks at the contact edges.

2. The contact pressure loading near the crack causes the crack to close and therefore makes the stress intensity factor negative. The tangential stress working near the crack makes the stress intensity factor high especially in the small crack region.

3. The accuracy of predicted lives using fracture mechanics models was good, particularly for variable amplitude loading.

The most inaccurate predictions were made for constant amplitude loading at the highest alternating stresses.

4. The use of the length correction in fracture mechanics results in a more accurate prediction of the fretting fatigue limit, the shape of the S-N curve and the crack propagation curve.

5. The draw back of the fracture mechanics model, which is demonstrated in predicting the initial rates of crack propagation under variable amplitude loading, is contributed to the stress intensity factor and or possible the model configuration itself.

6.5 CONCLUSIONS RELATED TO PRACTICAL APPLICATIONS

Remedial measures for counteracting fretting fatigue failures include improved design (recommended wherever possible), surface

treatment, surface coating, and lubricants.

6.6 FURTHER WORK

1. No firm conclusions have been reached on the correlation of coating effectiveness in fretting wear and fretting fatigue, based on available data. More research work is therefore, recommended in which a similarity in fretting contact conditions for fretting wear and fretting fatigue is to be maintained.
2. Some specific areas that would benefit from further attention include varied frequency experiments conducted in an inert environment, details of the influence that contact geometry has on the effect of various fretting parameters and results from more comprehensive list of materials than that currently predominate in the literature.

BIBLIOGRAPHY

1. Eden, E. H., N. W. Rose, L. E. Cunningham, "The Endurance of metals: Experiments on Rotation Beams at University College, London" proceeding of the institution of mechanical engineers, London, England, Vol: 4, October, 1911, pp 839-880.
2. Tomlinson, G. A. "The Rusting of Steel Surface in Contact," proceeding of the Royal Society of London, series A, Vol. 115, no" 771, July 1, 1927, pp. 472-483.
3. Fink M et al., "Neue Ergebnisse auf dem Gebiete der Verschless for schung" Organ Fortschritte Eisenbahnwesens, Bd. 84, nr. 20, October 15, 1929, pp. 405-412.
4. Uhlig, H. H., M. I. Feng, D. W. Tierney, and A. McCleelan "A Fundamental Investigation of Fretting Corrosion," NACA Technical note, 3029, December, 1953.
5. Waterhouse, E. B. "Fretting Corrosion," The institution of Mechanical Engineers, London, England, 1955.
6. Nishioka K., and K. Hirakawa, "Fundamental Investigation of Fretting Fatigue. part 1, 2, 3, 4 and 5" Bull. J. S. M. E 1969.
7. Godfrey, D. and M. J. Bailey., "Coefficient of Friction and Damage to contact area during the early stage of fretting, in glass, copper, or steel against copper," NACA technical note 30 11, Sept, 1953.
8. Godfrey, D. "Investigation of Fretting by Microscopic Observation," NACA report no. 1009. 1951 (Formerly TN 2039, Feb. 1950.
9. Uhlig, H. H. "Mechanism of Fretting Corrosion," Journal of applied Mechanism, Transactions, ASME, Vol. 76, 1954 pp 401-407.
10. Feng, I. M. and G. B. Rightmire "The Mechanism of Fretting," lubrication Engineering, Vol, 9, June 1953 pp. 134 ff.
11. Feng, I. M. "Fundamental Study of the Mechanism of Fretting" final report, Lubrication Laboratory, Mass. Ins. of Tech. Cambridge. Mass., 1955.

12. Bill, C. R. "Fretting Wear and Fretting Fatigue. How they are related" Transactions of the ASME, Vol. Dec. 1981.
13. Collins, A. J. "Fretting Fatigue Phenomenon with Emphasis on Stress Field Effects," Ph. D. thesis. the Ohio. State University, 1963.
14. Waterhouse, R. B. , "Fretting fatigue", Applied science, Esses, England, pp 145. 1981.
15. Chivers, T. C. , S. C. Gordeldr "A Literature Review of Palliatives for Fretting Fatigue," paper presented at 4th International Tribology Conference, Paisley, England, Sep. 1979.
16. Bill, R. C "Fretting Wear and Fretting Fatigue-how they are related," paper presented at the ASLE. ASME joint. Lubrication Conference. N. O. LA. Oct. 1981.
17. Niskioka, K. and Hirakawa, K. , "Fundamental Investigation of Fretting Fatigue. III. some phenomena and mechanics of surface crack" Japan S. M. E, Bulletin. Vol 12. no. 51, June 1969 pp 397-407.
18. Waterhouse, R. B. , "Fretting Corrosion", Pergamon Press, Oxford, 1972, pp 130-162.
19. Waterhouse , R. B. , "Fretting Fatigue", Applied science, Esses, England pp 205-210, 68-96. 1981.
20. Wright, G. P. , "Studies in Fretting Fatigue", D. Ph. Thesis, Oxford University, England (1970).
21. Lui, H. W. , T. H. Corten and M. G. Sinclair, "Fretting Fatigue Strength of Titanium Alloy RC 130B." Proc. ASTM, 57, 623 (1957).
22. Nishioka, K. and Hirakawa, K. "Fundamental Investigation of Fretting Fatigue. Part 5 the effect of relative slip amplitude", Bull. J. S. M. E. 12-692-7, 1969.
23. Brainard, W. A. , Buckley, D. H. , "Adhesion Friction and Wear of a Copper Bicrystal with (111) and (210) Grains" NASA TND-7232, 1973.
24. Gual, D. J. , and Duquette, J. "The Effect of Fretting and Environment on Fatigue Crack Initiation and early propagation in Quenched and Tempered steel 4130 steel" Metallurgical Transaction A, Vol 11A, Sept. 1980 pp 155-1561.

25. Hoepfner, D.W, G.C. Salivar, and D.L. Creighion, "Effect of Frequency and Environment on Fatigue Crack propagation of SA33B-1 steel" engineering fracture mechanics,
26. Hoepfner, D.W. and L.G. Goss, "A Fretting Fatigue Damage Threshold Concept" wear, Vol. 27, Jan. 1974 pp. 61-70.
27. Bill, R.C. and A.D. Rohn, "Influence of Fretting on Flexural Fatigue of 304 Stainless Steel and Mild Steel" NASA TP-1193-1978.
28. Poon, C., and D. Hoepfner., "The Effect of Environment on the Mechanism of Fretting Fatigue" wear, Vol. 52, Jan. 1979 pp 175-191.
29. Hamdy, M.M., and Waterhouse, R.B. "The Fretting Fatigue Behaviour of a Nickel Based Alloy (Inconel 718) at elevated Temperature" wear of materials, 1979, ASME, N.Y 1979 pp 351-335.
30. Bowden, F.P., and D. Tabor, "The Friction and Lubrication of Solids, part 11," Oxford Clearedon press, 1964, p51.
31. Feng, I.M. and G.B. Rightmine, "An Experimental study of fretting" Proc. Inst. Mech. Engrs, London, 170, 1055-60 (1956).
32. Godfrey, D. "Investigation of Fretting Corrosion by Microscopic observation," NACA Technical note 2039, Feb. 1950.
33. Godfrey, D. "Study of Fretting Wear in Mineral Oil," Lubrication engineering, 12, Jan. Feb, 37-42 (1956).
34. Godfrey, D. and M.J. Bailey, "Coefficient of Friction and Damage to contact area during the early stages of fretting. I. Glass, copper or steel against copper," NACA Technical note 3011, Sept. 1953.
35. Godfrey, D. and M.J. Bailey, "Early Stages of Fretting of Copper Iron, and Steel," Lubrication Engineering, 10, May-June. 155-9 (1954).
36. Godfrey, D.E., E. Bisson, "NACA Studies of Mechanics of Fretting (Fretting Corrosion) and Principle of Mitigation," Lubrication Engineering, 8, Oct. 241-3 (1952).
37. Uhlig, H.H. "Mechanism of Fretting Corrosion" ASME Journal of Applied Mechanics, 21, Dec. 401-7 (1954).
38. Uhlig, H.H., M.I. Feng, et al, "Fundamental Investigation of Fretting Corrosion," NACA Technical note 3029 (1953).

39. Halliday, J. S. and W. Hirst. "The Fretting Corrosion of Mild Steel" Proc. Roy. Soc. London, 236A, 411-25. Aug. 1956.
40. Waterhouse, R. B. "Fretting Corrosion", Proc. Inst. Mech. Engrs, 169, 1159-72 (1955).
41. Feng I. M and H. H. Uhlig, "Fretting Corrosion of Mild Steel in Air and Nitrogen", ASME Journal of Applied Mechanics Vol. 21 no. 4 Dec. 1954 pp. 395-400.
42. Timosenko. P. S., J. N. Goodier, "Theory of Elasticity", McGraw Hill. 3rd edition pp 409-420. (1970), pp 97-100.
43. Cattaneo. C. , "Sull'ontantio di due Coproi Elasi-Distribuzione local degli sforzi". Rend. d'Acad. Naz. Dei Lincei, 27, series, p6, pp 342, 434, 474 (1938).
44. Midlin, R. D, "Compliance of Elastic Bodies in Contact", J. Appl. Mech. Trans. ASME, series E, 16, 259 (1949).
45. Johnson, K. L. "Surface Interaction between Elastically Loaded Bodies under Tangential Forces", Proc. Roy. Soc. London A. 230-531 (1955).
46. O'Connor, J. J. and L. K. Johnson, "The Roll of Surface Asperities in Transmitting Tangential Forces between Metals", wear, 6, 118 (1963).
47. Hamilton, M. G. and E. L. Goodman, "The Stress Field Created by a Circular Sliding Contact", J. Appl. Mech. (Trans. ASME series E), 33, 371 (1966).
48. Johnson K. L. "Energy Dissipation at Spherical Surfaces in Contact Transmitting Oscillating Forces", J. Mech. Eng. Sci, pp 314-362 (1961).
49. Johnson K. L. and J. J. O'Connor, "Mechanics of Fretting", Proc. Ins. Mech. Engr. Vol 178. pt. 33, 1964.
50. Smith, J. O. and K. C. Liu, "Stress due to Tangential and Normal Loads on an Elastic Solids", J. App. Mech. Trans. A. S. M. E 1953, 75, 157.
51. Poritsky, H. "Stress and Deflection of Cylindrical Bodies in Contact", *ibid.*, 1950, 72, 191.

52. Sneddon, I. N. "Fourier Transforms", McGraw-Hill, N. Y and London p. 503, 1951.
53. O'Connor, J. J. "Forces between Bodies in Contact", Ph. D dissertation Cambridge University, (1961).
54. Ching, J. S, C. Oranc, M. ASCE, and W. D. Hoepfner, "Elastic Stress in Fretting Fatigue". J. Mech. Engrs. Sci, pp 387-403, (1981).
55. Chung J. S "Fretting Fatigue Stress Simulation", thesis presented to university of Missouri-Columbia Mo. in 1979 in partial fulfillment of the requirement for the degree of master of science, (1979).
56. Tomlinson, G. A, L. P Thrope, and J. H. Gough, "An Investigation of the Fretting Corrosion of Closed Fretting Surfaces", Proc. Instn. Mech. Engrs. London. 1939p. 141-233.
57. Goodman L. E, B. C Brown, "Energy Dissipation in Contact Friction Constant Normal and Cyclic Tangential Loading", J, Appl. Mech. Trans. ASME 84, series E, 17, 1962.
58. Klint, R. V. "Oscillating Tangential Forces on Cylindrical Specimens in Contact", Trans, Amer. Soc. Luric. Engrs. 3, 225, (1961).
59. Mindlin, R. D, P. W Mason, F. T Osmer, and H. Deresiewicz, "Effect of an Oscillating Tangential Force on the Contact Surfaces of Elastic Spheres", Proc. Ist U. S. Nat. Cong. App. Mech. ASME, 203, 1952.
60. Mindlin, R. D and H. Deresiewicz, "Elastic Spheres in Contact under Oblique Forces", J. App. Mech. Trans. ASME 75, 237, (1953).
61. Deresiewicz, H. "Contact of Elastic Spheres under an Oscillating Torsional Couple", *ibid*, 76, 52, (1954).
62. O'Connor, J. J. "Forces between Bodies in Contact", Ph. D, Dissertation Cambridge University, 1961.
63. Endo, K and H. Goto, "Initiation and Propagation of Fretting Fatigue Cracks", wear, Vol. 38, pp 311-324 (1976).
64. Waterhouse, R. B and E. D. Taylor "The Initiation of Fatigue Cracks in 0.7% Carbon Steel by Fretting", wear Vol, 17, pp139-147, (1971).
65. Waterhouse, B. R. "Fretting Fatigue", Applied science, Essex, pp. 14-19, England, 1981.

66. Rooke, P. D' and A. D. Johnes "Stress Intensity Factors in Fretting Fatigue", MHSO, London. UK. (1977).
67. Hattori, T, M. Nakamura, and T. Watanabe, "Fretting Fatigue Analysis by using Fracture Mechanics", ASME. WAM/DE-10, (1984).
68. Edwards, P. R, J. R. Ryman, and R. Cook. "Fracture Mechanics Prediction of Fretting Fatigue under Constant Amplitude Loading", RAETR 77056, (1977).
69. Edwards, P. R, J. R. Ryman, and R. Cook "Fracture Mechanics Prediction of Fretting Fatigue", Proc, Ninth ICAF symposium Darmstadt (1977).
70. Forst, N. E, P. L. Pook, , and A. K. Denton "Fracture Mechanics Analysis of Fatigue Crack Growth data for Various Material", NEL/A2/1/69 (1969).
71. Rook. D. P. and J. D. Cartwright. "Compendium of Stress Intensity Factors", MHSO, London, UK. (1974).
72. Ryman, R. J. and P. M. Blackwell, "An Acoustic Emission Investigation of the Initiation and Propagation of Fretting Fatigue Cracks in ESL65 Aluminum Alloy under Constant and Random Amplitude Loading", Testwell Ltd, report FAT/130 issue 2 (1978).
73. O'Connor, J. J. and L. K. Johnson, "The Role of Surface Asperities in Transmitting Tangential Force between Metals", wear, 6, 11-39 (1963).
74. Field, J. E, M. D. Natters, "Fretting Fatigue Strength of EN26 Steel, Effect of Mean Stress, Slip and Clamping Conditions", NEL report 275 (1967).
75. Edwards, P. R, "A Computer Program for the Interpolation and Extrapolation of Crack Propagation Data", RAETR 76115 (1976).
76. Pearson, S. "Initiation of Fatigue Cracks in Commercial Aluminum Alloy and Subsequent Propagation of very small Cracks", RAETR 72236 (1973).
77. Edwards, P. R, and J. R. Ryman, "Studies in Fretting Fatigue under Service Loading Conditions", Proc. Eight ICAF Symposium, Lausanne (1975)
78. Elber, W. "Fatigue Crack Closure under Cyclic Tension", Engineering Fracture Mechcs. , 2, pp. 37-45 (1970).

79. Slippel, K. O, and D. Weisgerber. "Flight by Flight Crack Propagation Test, Results with General Load Aspects and Comparison with Calculation according to different models", Proc. Ninth ICAF Symposium, Darmstadt (1977).

80. Hoppner, D. W, F. L. Gates, "Fretting Fatigue Consideration in Engineering Design", wear, Vol. 70. pp 155-164 (1981).

81. Bill, R. C., "Study of Fretting Wear in Titanium Monel-400, and Cobalt-25 Percent Molybdenum using SEM", ASLE, Transactions. Vol 16, no. 4, pp. 286-290, Oct. 1974.

82. Bill, R. C., "The Role of Oxidation in the Fretting Wear Process", NASA TM-81570, AVRADCOM-TR-80-C-15, 1980.

83. Endo, K., Goto, H., and Nakamura, T., "Effects of Cyclic Frequency on Fretting Fatigue Life of Carbon Steel", Japan Society of Mechanical Engineers, Bulletin, Vol. 12, no. 54, pp 1300-1308 (1969).

84. Nix, K. J. and T. C. Lindley., "The Application of Fracture Mechanics to Fretting Fatigue", Fatigue Fracture Engineering Mater. Struct. Vol. 8, no. 2, pp 143-160, (1985).

85. Control of Fretting Fatigue, NASPubl. NMAB-333, 1977 (National Academy of Sciences, Washington, D. C).